Branch-restricted localization of phosphatase Prl-1 specifies axonal synaptogenesis domains

Urwyler, Olivier ; Izadifar, Azadeh ; Vandenbogaerde, Sofie ; Sachse, Sonja ; Misbaer, Anke ; Schmucker, Dietmar

Abstract: Central nervous system (CNS) circuit development requires subcellular control of synapse formation and patterning of synapse abundance. We identified the <jats:italic>Drosophila</jats:italic> membrane-anchored phosphatase of regenerating liver (Prl-1) as an axon-intrinsic factor that promotes synapse formation in a spatially restricted fashion. The loss of Prl-1 in mechanosensory neurons reduced the number of CNS presynapses localized on a single axon collateral and organized as a terminal arbor. Flies lacking all Prl-1 protein had locomotor defects. The overexpression of Prl-1 induced ectopic synapses. In mechanosensory neurons, Prl-1 modulates the insulin receptor (InR) signaling pathway within a single contralateral axon compartment, thereby affecting the number of synapses. The axon branch–specific localization and function of Prl-1 depend on untranslated regions of the <jats:italic>prl-1</jats:italic> messenger RNA (mRNA). Therefore, compartmentalized restriction of Prl-1 serves as a specificity factor for the subcellular control of axonal synaptogenesis.

DOI: https://doi.org/10.1126/science.aau9952

Title: Prl-1 phosphatase directs compartmentalized control of InR/Akt signaling during CNS synapse formation

Authors: Olivier Urwyler[1,3,*], Azadeh Izadifar[1,2], Sofie Vandenbogaerde[1], Sonja Sachse[1], Anke Misbaer[1,2], Dietmar Schmucker[1,2,*]

Affiliations:

[1] VIB Center for Brain & Disease Research, Leuven, Belgium
[2] KU Leuven, Department of Neurosciences, Leuven, Belgium
[3] Institute of Molecular Life Sciences, University of Zurich, 8057 Zurich, Switzerland.
* corresponding authors

Abstract:

CNS circuit development requires subcellular control of synapse formation and patterning of synapse abundance. Using genetic single-cell analyses, we identified the *Drosophila* membrane-anchored phosphatase "protein of regenerating liver" (Prl-1) as an axon-intrinsic factor that promotes synapse formation in a spatially restricted fashion. Loss of Prl-1 in mechanosensory neurons reduced the number of CNS pre-synapses that are localized on a single axon collateral and organized as a terminal arbor. Homozygous flies lacking all Prl-1 protein had locomotor defects. Overexpression of Prl-1 induced ectopic synapses. In mechanosensory neurons Prl-1 modulates the Insulin Receptor (InR) signaling pathway within a single contralateral axon compartment thereby affecting the number of synapses. Axon branch-specific localization and function of Prl-1 depends on UTR-sequences of the *prl-1* mRNA. Therefore, compartmentalized restriction of Prl-1 serves as a specificity factor for subcellular control of axonal synaptogenesis.

One Sentence Summary:

Intracellular signaling mechanisms promote synaptogenesis specifically in one subcellular compartment of a Drosophila CNS axon.

Main Text:

Central nervous system (CNS) function relies on controlled axon branching and synapse formation during development. Establishment of neuronal circuits requires matching of pre- and post-synaptic neurons, determination of synapse locations and numbers, and specification of diverse synapse types (*1*, *2*). Formation of multiple axon branches allows single CNS neurons to innervate several different target areas and target cells thereby increasing output complexity (*3*, *4*). However, for each axon branch, the quantity of synapses formed determines the number of potential postsynaptic partners and the strength of connectivity to each of them. Branch-specific control of synapse numbers is therefore essential for correct and complex circuit formation. While synapses can be formed *en passant* on primary axon branches, formation of terminal arborizations allows for more synapses in a particular location (*5*). In developing axons of both vertebrates and invertebrates, localization of pre-synaptic proteins, as well as axonal RNAs and mitochondria, is associated with emergence of filopodial protrusions and their stabilization into nascent branches (*5-9*), including stabilization of arbors by synaptic adhesion complexes (*10*). Thus, terminal arborization and synaptogenesis together lead to formation of local synapse-dense axon terminals.

Cell-surface receptors mediate cell-cell communication and sensing of environmental cues during axon guidance, branching, and synapse formation (*3*, *11-13*). For example, “neuritic adhesion complexes” containing Neuroligin and Neurexin, and pre-synaptic proteins Syd1 and Liprin-α, locally stabilize filopodia establishing distinct axon arborizations (*10*). Less is known about cell-intrinsic factors that locally control terminal arborization and synaptogenesis *in vivo* (*4*). Here, we use a genetic single-cell

approach in *Drosophila* to identify a factor that functions in formation of dense, synapse-rich terminal arbors specifically in one collateral of a CNS axon.

We found differences in arborizations and synapse numbers formed by individual axon collaterals of single mechanosensory neurons in the *Drosophila* CNS. We focused on two types of mechanosensory neurons that innervate large sensory bristles on the dorsal thorax of the fly (scutellar (SC) and dorsocentral (DC) bristles, Fig. 1A). These mechanosensory neurons form three main central axonal projections, to innervate anterior, posterior, and contralateral CNS target areas, respectively (Fig. 1B). In DC neurons, *en passant* synapses that form directly on the axon shaft are predominant in the main anterior projection, which in addition forms a few variable higher-order processes that sprout from the main branch and contain terminal synapses (Fig. 1D). The posterior projection has few terminal or side-arbors and only forms a few *en passant* synapses at an intermediate and distal position (Fig. 1D and see also (*14*)). The contralateral projection of DC neurons is rich in both *en passant* and terminal synapses that form on an extensive network of arborizations across the region of the CNS midline and contralaterally (Fig. 1D, H). The extensive synaptic arborizations are only present in DC neurons (aDC, pDC) and not in the closely related SC mechanosensory neurons, although their target areas overlap almost perfectly (Fig. 1B-C). Therefore, mechanosensory neurons provide an *in vivo* model for studying mechanisms underlying the quantitative and subcellular restriction of pre-synapse formation.

Prl-1 function regulates formation of synapse-dense terminal arbors

Reversible phosphorylation cascades often regulate cellular signal transduction. We therefore targeted the kinome / phosphatome of *Drosophila* to scan for signaling factors that control synaptogenic regulatory mechanisms. RNAi constructs (*15*) were driven in a restricted set of peripheral mechanosensory neurons as described (see Experimental Procedures and (*14*)). We assessed phenotypes caused by cell-autonomous depletion of the target gene products in mechanosensory neurons. Among a set of synaptogenic candidates we found that knockdown of *phosphatase of regenerating liver* (*prl-1*) eliminated the terminal arbor and reduced numbers of synapses in the contralateral projecting axon

collateral (Fig. 1E, I), while *en passant* synapses along the axon shaft, and synapses in the other two main axon collaterals, were unaffected (Fig. 1E, I). Terminal arbor and bouton formation at *Drosophila* neuromuscular junctions appeared unaffected (see Fig. S8). The *Drosophila* genome encodes a single *prl* gene; three *Prl* genes (Prl-1-3) are found in vertebrates (*16*, *17*). We generated *prl-1* loss-of-function alleles by CRISPR/Cas9-mediated gene editing. In six mutant alleles (Fig. S1A, B) the stop codons are close to the start ATG and no Prl-1 protein can be detected by antibody staining (Fig. S1C). We consider these six alleles to be protein null mutants. *prl-1* null flies are viable and fertile, albeit hatching is delayed (Fig. S1D). Consistent with the RNAi knock-down, synaptic arborizations were lost from the contralateral mechanosensory neuron axon collateral in *prl-1* mutant animals (Fig. 1F, J, M, N). Neither cell body morphology, axon caliber (Fig. S3), nor axon growth and guidance to the CNS were affected. Projections of the related SC mechanosensory neurons were normal (Fig. S4). The DC neuron mutant phenotype was fully rescued by introduction of a *prl-1* BAC transgene (bacterial artificial chromosome; Fig. 1G, K). Anterior and posterior branches of the mechanosensory neuron arbor did not show any morphological defects in the mutants, indicating that *prl-1* is specifically required for formation of dense synaptic terminal arborizations in one out of three main mechanosensory neuron axon collaterals. We estimated numbers of pre-synaptic active zones by quantifying puncta of the active zone marker Bruchpilot (Brp; (*18*, *19*)), and found an approximate decrease by 65% of synapses in the contralateral branch, while synapse numbers were not altered in the anterior branch (Fig. 1O, P; Fig. S5). Consistent with a role for Prl-1 in only the axon compartment of the contralateral branch, HA-tagged transgenic Prl-1 specifically expressed in DC neurons is enriched in this axon collateral compartment (Fig. 1Q). Correlative light and electron microscopy confirmed labelling of pre-synapses by the markers (see also (*14*)). No defects were apparent in the structure of remaining synapses in the mutant (Fig. S6).

Homozygous *prl-1* mutant adults are normal in size and morphology (Fig. S1E,F), but occasionally show a “held-up” wing phenotype (see Movie S1). The mutant flies however display locomotor defects and cannot fly (Fig. S7A-C; Movie S1). Our analysis of the morphology of NMJ synapses shows no defect, suggesting that *prl-1* is not required for NMJ formation (Fig. S8). In contrast,

analysis of the brain and CNS revealed altered synaptic connectivity in several circuits in homozygous *prl-1* mutant flies (Fig. S7, S9, S10). First, two distinct brain neuropils related to olfaction and olfactory related learning, the antennal lobes and mushroom bodies, respectively, were disorganized, with evident axonal or synaptic defects (Fig. S7E, G, and Fig. S9). For example, we find changes in size and organization of synaptic termination zones of odorant receptor neurons in their respective target area, the glomeruli of the antennal lobe (Fig. S7E, G, I). Second, while cell numbers of the sensory neurons (Fig. S7D, F, H) as well as neurons of the ventral nerve cord (VNC; Fig. S10D, E) are unaltered, the size of the CNS neuropile (i.e. region of densely packed axons, dendrites, synapses) is reduced in *prl-1* homozygous adult flies (Fig. S10A-C). We noted a size reduction particularly of the metathoracic neuropile in the VNC, which is smaller in homo- or hemizygous *prl-1* null mutants than in wild-type flies or *prl-1* null mutants rescued with the BAC transgene.

To test if an increase of Prl-1 function (i.e. gain-of-function) could promote ectopic synapse formation, we overexpressed Prl-1 in mechanosensory neurons, in otherwise wild-type animals (Fig. 2). Indeed, we found an aberrant increase in Syt1 puncta in ectopic proximal regions of the main axon, a region that rarely contains pre-synapses in controls (Fig. 2A, B, E-H). In addition, axon terminals of Prl-1 overexpressing neurons appeared less mature than controls, and resembled axonal protrusions occurring during synapse formation at developing stages (see Fig. 5). Small protrusions were observed on the main branch (Fig. 2F), and even longer ones in terminal regions (Fig. 2D). These filopodial protrusions cannot be detected in control samples (Fig. 2C, E). Ectopic protrusions were associated with Syt1 marker puncta, which were located either at the base or within the protrusion (Fig. 2F''). These findings suggest that Prl-1 is capable of inducing ectopic synapses. However, an increase of synapses is not seen throughout the entire axonal arbor indicating constraints in the synaptogenic function of Prl-1. Formation of ectopic synapses by gain of Prl-1 is not linked to an increase in ectopic branches or terminal arbors. This suggests the possibility that Prl-1 is involved in synapse formation or stabilization, rather than terminal arbor formation (i.e branching).

Prl-1 function involves modulation of Insulin Receptor (InR) to Akt signaling

In our attempts to identify regulators or targets of Prl-1 phosphatase, we conducted a secondary candidate screen and discovered that cell-autonomous inhibition of multiple Insulin Receptor (InR) signaling components resulted in *prl-1* like phenotypes (Fig. 3). RNAi-based knock-down of InR in mechanosensory neurons, or expression of a dominant negative form of the InR, led to pronounced reduction of terminal synapses on the contralateral axon compartment of DC neurons (Fig. 3B, top panels). The same was observed for knockdown of Chico (encoding a *Drosophila* InR substrate), of PI3 kinase (by targeting either the p110 or the p60 subunit), of Akt, and of the mTORC1 complex subunit Raptor (Fig. 3B, D, E; Fig. S11; Fig. S12). Consistent with the finding that knockdown of PTEN, a negative regulator of the pathway, increases terminal synaptic arborizations on the contralateral branch, expression of a membrane-targeted, constitutively active form of Akt (*20*) led to hypertrophy of synaptic terminals (Fig. 3A, B, D). We also tested knock-down of Pdk but found no synaptic defect, suggesting that Pdk does not participate in this presynaptic signaling cascade (Fig. S13). All the above-mentioned manipulations affected the contralateral projecting axon collateral but not the main axon shaft or other collaterals of DC neurons (Fig. 3A; Fig. S12).

As loss of *prl-1* leads to the same loss of terminal synapses as reduction in InR/Akt signaling, we performed three experiments to test for genetic interactions and epistasis. First, we knocked down PTEN in *prl-1* heterozygous mutant animals and observed a suppression in exuberant arborizations observed upon PTEN knockdown alone (Fig. 3C, D; Fig. S11; Fig. S12). Second, we expressed constitutively active Akt in mechanosensory neurons of *prl-1* null animals. This led to a rescue of terminal synapses in the contralateral branch (Fig. 3C, D, Fig. S11; Fig. S12). Third, and conversely, we tested whether loss of Akt retained dominant defects over UAS-Prl-1 expression. UAS-Prl-1 expression showed no rescuing effect in mechanosensory neurons depleted of Akt (Fig. 3D), consistent with Akt being downstream of Prl-1.

All our genetic studies are also consistent with previous findings of high-throughput screens targeting the kinase/phosphatase signaling networks *in vitro*. Combined genome-wide RNAi and

proteomics screens in *Drosophila* cells suggested that activity of Prl phosphatases might be linked to InR signaling (*21*), and several vertebrate cell-culture studies provided evidence for a role of Prl phosphatases in PI3K – PTEN / Akt signaling (*22*, *23*).

Thus we suggest that compartmentalized *prl-1* activity regulates a spatially specific mode of synaptogenesis in terminal arbors via modulation of the InR pathway likely upstream of Akt.

Targeting phosphoinositide levels affects terminal arbors

Prl phosphatases have various potential protein targets such as the ERM protein Ezrin or a Rho-GTPase-activating protein (*16*), although RNAi based knock-down of several proposed protein targets provided no evidence of their involvement in Prl-1-related functions in synapse formation (Fig. S14). Vertebrate Prl phosphatases can dephosphorylate phospholipids *in vitro:* human Prl-3 has a PI(4,5)P2 (phosphatidylinositol 4,5-bisphosphate) 5-phosphatase activity, dephosphorylating PI(4,5)P2 to PI(4)P (phosphatidylinositol 4-phosphate) (*24*). Moreover, phospholipids directly regulate Akt signaling (Fig. 3E). Akt is recruited to the plasma membrane and activated by PI(3,4,5)-trisphosphate and PI(3,4)P2 (*25*, *26*). PTEN is itself activated by PI(4,5)P2 (*27*).

We therefore tested whether dephosphorylation of PI(4,5)P2 could be relevant *in vivo* during synapse formation of DC neurons. We reasoned that a loss of Prl-1 activity could cause an increase of local PI(4,5)P2 levels and that an increase of PI(4,5)P2 levels in DC neurons could also be achieved by promoting phosphorylation of PI(4)P by a PI(4)P specific kinase. The *Drosophila* PI(4)P 5-kinase Skittles (Sktl) catalyzes PI(4)P phosphorylation to PI(4,5)P2 (*28-30*). Therefore, Sktl overexpression in DC neurons might be equivalent to loss of Prl-1. We found that Sktl overexpression in DC neurons leads to a reduction of terminal arborizations, phenocopying *prl-1* loss-of-function (Fig. 4A-C). Moreover, co-expression of Prl-1 together with Sktl suppresses the Sktl gain-of-function phenotype (Fig. 4A,C). This result provides support for the idea that the Prl-1 phosphatase and Sktl kinase can carry out opposing functions and is consistent with the hypothesis that PI(4,5)P2 levels could be decreased by Prl-1 function *in vivo*.

In amino acid sequence, *Drosophila* Prl-1 shares features with human Prl-3 that are thought to affect activity toward phosphoinositides (Fig. S15). The point mutation G129E in human PTEN and the mutation A111S in human Prl-3 abolish phosphatase activity toward phosphoinositides, but not toward phosphoproteins, of these related phosphatases (*24*, *31*). We, therefore, generated transgenes with the corresponding mutants in *Drosophila* Prl-1 (G114E and A116S, respectively), and tested their ability to rescue the *prl-1* null phenotype in DC neurons. While a mechanosensory neuron specific expression of a wild-type transgene rescued the loss of terminal arborizations (Fig. 4D,E), the G114E mutant transgene did not (Fig. 4D,E; Fig. S16). In this experiment only mechanosensory neurons express the rescue constructs and the VNC target tissue remains mutant with reduced neuropile size (Supplementary Fig. S16). In the case of the A116S mutant, we were unable to observe axonal projections of labeled mechanosensory neuron clones, suggesting a dominant effect of this mutant transgene that prevents axon growth or induces apoptosis or axon degeneration.

To further substantiate that Prl-1 leads to dephosphorylation of PI(4,5)P2 *in vivo*, and to determine whether synapse loss in mechanosensory neurons of *prl-1* null mutants is due to increased PI(4,5)P2 levels, or, conversely, decreased PI(4)P levels, we used constructs expressing the PH domain of phospholipase Cδ fused to GFP (PLCδPH.GFP (*32*)). PLCδPH.GFP binds to PI(4,5)P2 and prevents interactions of PI(4,5)P2 with cellular binding partners, thereby reducing functional PI(4,5)P2 levels (*33*). Expression of PLCδPH.GFP, but not of a mutant form that does not bind to PI(4,5)P2 (*32*), rescued loss of terminal arborizations in *prl-1* mutants (Fig. 4F-H). We therefore conclude that the *prl-1* null phenotype is a consequence of elevated PI(4,5)P2 in the mutant, and that PLCδPH.GFP expression can restore terminal synapse formation by blocking excessive PI(4,5)P2.

Together, our results provide evidence that Prl-1 promotes DC neuron axon arborization in a specific target area by locally influencing the phosphoinositide-dependent PI3K-PTEN signaling loop.

Prl-1 affects synapse stabilization

To gain insights into the cellular processes that cause reduced terminal synapse and arbor formation specifically in one target area of mechanosensory neurons in *prl-1* null flies, we visualized the cellular differentiation of single DC neuron compartments during development (Fig. 5). In wild-type flies, we identified three distinct stages of terminal arbor and synapse formation. In a first phase (45-70 hrs after pupariation, apf), the contralateral growing axon collateral extends many filopodial protrusions in all directions including the growth direction. All these protrusions extend from the main axon shaft (Fig. 5A, top left) but are most prominently formed on the contralateral projecting axon collateral. In a second phase (60 – 75 hrs apf), in which the main branch has reached the contralateral target area, filopodial protrusions are most numerous at an axon segment stretching across the midline. At this stage, new cellular processes that contain Syt1 marker protein have formed and contain additional filopodia protrusions (Fig. 5A middle left, 5C middle and bottom; Fig. S18A). These satellite growth cones (*34*) are likely precursors of terminal synapse-bearing arborizations observed in adult animals. Finally, in a third phase (after 75 hrs apf), immature filopodial protrusions and satellite growth cones disappear, and are transformed into terminal synapse-bearing arbors (Fig. 5A, bottom left panel; Fig. S18B). In *prl-1* null flies in stage 1 and in part in stage 2, the developing axon collaterals and filopodial protrusions form like in wild type controls (Fig. 5A, top right panels). Filopodial protrusions are extending into different directions in normal abundance (Fig. 5B, left plot). Likewise, satellite growth cones with filopodia, some of which having Syt1-positive puncta, are also formed in *prl-1* mutants, and filopodia originate from them (Fig. 5D; Fig. S18A). However, the number of satellite growth cones per axon segment is reduced in mutant animals, and satellite growth cones extend less filopodial protrusions, both leading to a net reduction in the total number of filopodial protrusions (Fig. 5B). In contrast to a reduction of filopodia originating from satellite growth cones, we did not observe a reduction of filopodia emanating from the main branch (Fig. 5B, right panels). These results indicate that early stages of arborization at the midline, i.e. formation of filopodial protrusions and satellite growth cones, is not affected upon loss of *prl-1*. In contrast, formation or stabilization (or both) of a sufficient amount of satellite growth cones, is defective in *prl-1* mutants. Because Syt1 marker accumulates in satellite growth cones, and filopodia extend from

Syt1 positive locations, these processes could be dependent on accumulation of synaptic material or formation of synapses in emerging axonal processes. Finally, in stage 3 in *prl-1* mutant axons most of the protrusions and satellite growth cones have disappeared. This suggests that in *prl-1* mutants stabilization or consolidation of the terminal arbors as well as nascent synapses failed and are being aberrantly retracted (Fig. 5; Fig. S18B). Thus Prl-1 function is necessary for stabilization or maturation of terminal synapse-bearing arbors but not initiation or branching of axons at terminal arbors.

Compartment-specific Prl-1 enrichment

How does signaling by Prl-1 and the InR / Akt signaling activity get spatially restricted in DC axons? The branched morphologies of neurons bring many opportunities to compartmentalize subsections of the neuron. For mechanosensory neurons additional genetic screens and characterization of other molecular pathways are required to study relevant mechanisms. However, by studying the localization of Prl-1 protein in mechanosensory neurons itself we found that (i) epitope-tagged Prl-1 expressed from a transgene is enriched in the contralateral axon collateral, and also present to a lesser degree in midline-proximal branches (see above, Fig. 1Q). (ii) the subcellular localization as well as the rescuing activity are dependent on regulatory sequences in long 5'- and 3'- untranslated regions (UTRs) of *prl-1* messenger RNAs (Fig. S19). These long UTRs are essential for Prl-1 function in local synaptic arbor formation as only HA-tagged Prl-1 proteins expressed from a transgene containing both the 5'- and 3'-UTRs (HA.*prl-1*.UTRs^{plus}) were able to substantially rescue synaptic defects of *prl-1* mutant neurons (Fig. 6F; Fig. S16). Anti-HA stainings showed that the epitope tagged protein localized to distal axons of mechanosensory neurons and was enriched in contralateral projecting branches (Fig. 6B,D; Fig. S20). In contrast, a transgene without UTRs (HA.*prl-1*.UTRs^{minus}) led to weaker Prl-1 signal in mechanosensory neuron axons in the CNS (Fig. 6B; Fig. S20). Nevertheless, without UTRs, the compartmentalized enrichment of Prl-1 is still visible in wildtype or heterozygous neurons (Fig. 6B,C). Given that Prl proteins form homotrimers (*35*, *36*) we reasoned that formation of complexes between Prl-1 expressed from the endogenous locus,

and HA.Prl-1 expressed from transgenes, could lead to a trapping of HA.Prl-1 protein at sites of endogenous Prl-1 enrichment (see schematic, Fig. 6E). Indeed, we found that the contralateral branch enrichment of protein expressed from HA.*prl-1*.UTRs^{minus} was lost in a *prl-1* null mutant background, and HA.Prl-1 localized ectopically and evenly to all axon branches of mechanosensory neurons (Fig. 6B,C). In contrast, localization of HA.Prl-1 expressed from the transgene with UTRs remained compartmentalized even in the absence of endogenous protein (Fig. 6B,D). Comparisons of protein levels in diverse wild type and mutant backgrounds by use of fluorescent intensity is challenging. It is further complicated by the reduction of axon arbors in mutant and partially rescued samples, which thereby could indirectly contribute to a reduced fluorescence intensity. However, the fact that in null mutants the HA.prl-1 protein (when expressed from transgene lacking UTRs, i.e. HA.*prl-1*.UTRs^{minus}) is redistributed ectopically and thereby leads to an increased intensity in ipsilateral axon collaterals (unaffected in mutants), and lack of changes in distribution of the general membrane marker CD8.Cherry in mutants (Fig. S21), provide clear evidence that Prl-1 is endogenously enriched in the contralateral projecting axon of pDC axons. Consistent with its role in formation of terminal arbor synapses, a tagged InR protein was also localized to the contralateral projecting pDC collateral at mid-developmental stages (Fig. S22).

Collectively, these results reveal a role of the *prl-1* UTRs in axon compartment specific localization of the Prl-1 protein and that this subcellular enrichment is likely essential for the functional specificity of Prl-1 in neurons.

Concluding remarks

Here we identified cell-intrinsic presynaptic mechanisms that contribute to subcellular control of synapse type and numbers in *Drosophila* CNS axons. Compartment-specific regulation of the InR signaling by Prl-1, likely by targeting the PI3K-PTEN-dependent phosphoinositide cycle, enables the spatially restricted formation of a synapse-rich terminal arbor. This is supported by several complementary experiments. First, genetic interactions show that loss of a single copy of *prl-1* can

suppress PTEN knock-down dependent synapse defects (Fig. 3; Fig. S11). Second the genetic epistasis analysis, where activated Akt can rescue *prl-1* mutant defects but not vice versa, suggests that Prl-1 functions upstream of Akt (Fig. 3D; Fig. S11). Third, the targeted manipulation of PI(4,5)P2 levels by overexpressing the PI(4)P 5-kinase Skittles in mechanosensory axons phenocopies loss of Prl-1 (Fig. 4A-C). Fourth, reducing the level of accessible PI(4,5)P2 by expressing a PI(4,5)P2 specific binding domain (PLCδPH.GFP) can suppress the Prl-1 synapse formation defects (Fig. 4F-H). All these experiments are consistent with the model that Prl-1 targets the PIP2 levels in presynaptic axon segments. However, we cannot rule out that Prl-1 might only indirectly lead to dephosphorylation of PI(4,5)P2 through an as of yet unknown target in neurons. Nevertheless, this study shows that distinct lipid/phosphoinositide domains in developing axons and their likely dynamic changes contribute to spatial specificity of CNS synapse formation.

While enrichment of Prl-1 protein and activity in a distinct axon branch defines this compartmentalization, it is unclear whether the localized enrichment is due to protein trafficking, protein retention, or local translation. We consider local translation a particularly attractive scenario because our data showed that the UTR sequences of *prl-1* mRNA are functionally required. Moreover, the InR pathway, which is affected by Prl-1, itself is a potent regulator of translation (*37*). The identification of regulatory UTR sequences in the *prl-1* mRNA that direct axon branch specific protein localization will be a decisive tool for future studies in order to define the responsible cellular mechanisms.

Vertebrate Prl-1-3 phosphatases affect cell division or growth as well as metastasis of tumor cells (*17*, *38*, *39*). Analogous to Drosophila Prl-1, the expression of vertebrate Prl-3 in cancer cell lines is regulated at the translational level through the RNA-binding protein PCBP1 and a GC-rich motif in the 5'UTR of the *prl-3* mRNA (*40*). However, roles for Prl proteins in CNS development have not been reported. Yet Prl-1, Prl-2, and Prl-3 are broadly expressed in the vertebrate CNS (Allen Brain Atlas (*41*)). Prl phosphatases are therefore poised to function in vertebrate brain development in ways similar to the effects we have shown here on assembly of neuronal circuits and synapses in *Drosophila*.

References and Notes

1. S. Yogev, K. Shen, Cellular and molecular mechanisms of synaptic specificity. Annu Rev Cell Dev Biol. 30, 417–437 (2014).
2. M. E. Williams, J. de Wit, A. Ghosh, Molecular mechanisms of synaptic specificity in developing neural circuits. Neuron. 68, 9–18 (2010).
3. D. A. Gibson, L. Ma, Developmental regulation of axon branching in the vertebrate nervous system. Development. 138, 183–195 (2011).
4. H. Schmidt, F. G. Rathjen, Signalling mechanisms regulating axonal branching in vivo. Bioessays. 32, 977–985 (2010).
5. B. Alsina, T. Vu, S. Cohen-Cory, Visualizing synapse formation in arborizing optic axons in vivo: dynamics and modulation by BDNF. Nat Neurosci. 4, 1093–1101 (2001).
6. H. H.-W. Wong et al., RNA Docking and Local Translation Regulate Site-Specific Axon Remodeling In Vivo. Neuron. 95, 852–868.e8 (2017).
7. M. P. Meyer, S. J. Smith, Evidence from in vivo imaging that synaptogenesis guides the growth and branching of axonal arbors by two distinct mechanisms. Journal of Neuroscience. 26, 3604–3614 (2006).
8. E. S. Ruthazer, J. Li, H. T. Cline, Stabilization of axon branch dynamics by synaptic maturation. Journal of Neuroscience. 26, 3594–3603 (2006).
9. J. Courchet et al., Terminal Axon Branching Is Regulated by the LKB1-NUAK1 Kinase Pathway via Presynaptic Mitochondrial Capture. Cell. 153, 1510–1525 (2013).
10. W. D. Constance et al., Neurexin and Neuroligin-based adhesion complexes drive axonal arborisation growth independent of synaptic activity. Elife. 7, e31659 (2018).
11. B. J. Dickson, Molecular mechanisms of axon guidance. Science. 298, 1959–1964 (2002).

12. A. L. Kolodkin, M. Tessier-Lavigne, Mechanisms and molecules of neuronal wiring: a primer. Cold Spring Harb Perspect Biol. 3 (2011), doi:10.1101/cshperspect.a001727.

13. K. Shen, C. W. Cowan, Guidance molecules in synapse formation and plasticity. Cold Spring Harb Perspect Biol. 2, a001842 (2010).

14. O. Urwyler et al., Investigating CNS synaptogenesis at single-synapse resolution by combining reverse genetics with correlative light and electron microscopy. Development. 142, 394–405 (2015).

15. G. Dietzl et al., A genome-wide transgenic RNAi library for conditional gene inactivation in Drosophila. Nature. 448, 151–156 (2007).

16. P. Rios, X. Li, M. Köhn, Molecular mechanisms of the PRL phosphatases. FEBS J. 280, 505–524 (2013).

17. S. Saha et al., A phosphatase associated with metastasis of colorectal cancer. Science. 294, 1343–1346 (2001).

18. D. A. Wagh et al., Bruchpilot, a protein with homology to ELKS/CAST, is required for structural integrity and function of synaptic active zones in Drosophila. Neuron. 49, 833–844 (2006).

19. A. Schmid et al., Activity-dependent site-specific changes of glutamate receptor composition in vivo. Nat Neurosci. 11, 659–666 (2008).

20. J. Verdu, M. A. Buratovich, E. L. Wilder, M. J. Birnbaum, Cell-autonomous regulation of cell and organ growth in Drosophila by Akt/PKB. Nat Cell Biol. 1, 500–506 (1999).

21. A. A. Friedman et al., Proteomic and functional genomic landscape of receptor tyrosine kinase and ras to extracellular signal-regulated kinase signaling. Science signaling. 4, rs10–rs10 (2011).

22. H. Wang et al., PRL-3 down-regulates PTEN expression and signals through PI3K to promote epithelial-mesenchymal transition. Cancer Res. 67, 2922–2926 (2007).

23. Y. Jiang et al., Phosphatase PRL-3 is a direct regulatory target of TGFbeta in colon cancer metastasis. Cancer Res. 71, 234–244 (2011).

24. V. McParland et al., The metastasis-promoting phosphatase PRL-3 shows activity toward phosphoinositides. Biochemistry. 50, 7579–7590 (2011).

25. B. Vanhaesebroeck, L. Stephens, P. Hawkins, PI3K signalling: the path to discovery and understanding. Nat Rev Mol Cell Biol. 13, 195–203 (2012).

26. A. Klippel, W. M. Kavanaugh, D. Pot, L. T. Williams, A specific product of phosphatidylinositol 3-kinase directly activates the protein kinase Akt through its pleckstrin homology domain. Mol Cell Biol. 17, 338–344 (1997).

27. R. B. Campbell, F. Liu, A. H. Ross, Allosteric activation of PTEN phosphatase by phosphatidylinositol 4,5-bisphosphate. J Biol Chem. 278, 33617–33620 (2003).

28. S. Knirr, A. Santel, R. Renkawitz-Pohl, Expression of the PI4P 5-kinase Drosophila homologue skittles in the germline suggests a role in spermatogenesis and oogenesis. Dev. Genes Evol. 207, 127–130 (1997).

29. B. A. Hassan et al., skittles, a Drosophila phosphatidylinositol 4-phosphate 5-kinase, is required for cell viability, germline development and bristle morphology, but not for neurotransmitter release. Genetics. 150, 1527–1537 (1998).

30. S. Claret, J. Jouette, B. Benoit, K. Legent, A. Guichet, PI(4,5)P2 produced by the PI4P5K SKTL controls apical size by tethering PAR-3 in Drosophila epithelial cells. Curr Biol. 24, 1071–1079 (2014).

31. M. P. Myers et al., The lipid phosphatase activity of PTEN is critical for its tumor supressor function. Proc Natl Acad Sci USA. 95, 13513–13518 (1998).

32. P. Verstreken et al., Tweek, an evolutionarily conserved protein, is required for synaptic vesicle recycling. Neuron. 63, 203–215 (2009).

33. D. Raucher et al., Phosphatidylinositol 4,5-bisphosphate functions as a second messenger that regulates cytoskeleton-plasma membrane adhesion. Cell. 100, 221–228 (2000).

34. D. Dascenco et al., Slit and Receptor Tyrosine Phosphatase 69D Confer Spatial Specificity to Axon Branching via Dscam1. Cell. 162, 1140–1154 (2015).

35. J.-P. Sun et al., Structure and biochemical properties of PRL-1, a phosphatase implicated in cell growth, differentiation, and tumor invasion. Biochemistry. 44, 12009–12021 (2005).

36. J.-P. Sun et al., Phosphatase activity, trimerization, and the C-terminal polybasic region are all required for PRL1-mediated cell growth and migration. J Biol Chem. 282, 29043–29051 (2007).

37. X. M. Ma, J. Blenis, Molecular mechanisms of mTOR-mediated translational control. Nat Rev Mol Cell Biol. 10, 307–318 (2009).

38. Q. Zeng et al., PRL-3 and PRL-1 promote cell migration, invasion, and metastasis. Cancer Res. 63, 2716–2722 (2003).

39. A. Q. O. Al-Aidaroos, Q. Zeng, PRL-3 phosphatase and cancer metastasis. J. Cell. Biochem. 111, 1087–1098 (2010).

40. H. Wang et al., PCBP1 suppresses the translation of metastasis-associated PRL-3 phosphatase. Cancer Cell. 18, 52–62 (2010).

41. E. S. Lein et al., Genome-wide atlas of gene expression in the adult mouse brain. Nature. 445, 168–176 (2007).

42. W. Fouquet et al., Maturation of active zone assembly by Drosophila Bruchpilot. J Cell Biol. 186, 129–145 (2009).

43. J. Bischof, R. K. Maeda, M. Hediger, F. Karch, K. Basler, An optimized transgenesis system for Drosophila using germ-line-specific ϕC31 integrases. Proc Natl Acad Sci USA. 104, 3312–3317 (2007).

44. A. Couto, M. Alenius, B. J. Dickson, Molecular, anatomical, and functional organization of the Drosophila olfactory system. Curr Biol. 15, 1535–1547 (2005).

45. K. T. Pagarigan et al., Drosophila PRL-1 is a growth inhibitor that counteracts the function of the Src oncogene. PLoS ONE. 8, e61084 (2013).

46. I. Almudi, I. Poernbacher, E. Hafen, H. Stocker, The Lnk/SH2B adaptor provides a fail-safe mechanism to establish the Insulin receptor-Chico interaction. Cell Commun. Signal. 11, 26 (2013).

47. A. C. Groth, M. Fish, R. Nusse, M. P. Calos, Construction of transgenic Drosophila by using the site-specific integrase from phage phiC31. Genetics. 166, 1775–1782 (2004).

48. T. Lee, L. Luo, Mosaic analysis with a repressible cell marker for studies of gene function in neuronal morphogenesis. Neuron. 22, 451–461 (1999).

49. A. R. Bassett, C. Tibbit, C. P. Ponting, J.-L. Liu, Highly efficient targeted mutagenesis of Drosophila with the CRISPR/Cas9 system. Cell Rep. 4, 220–228 (2013).

50. L.-E. Jao, S. R. Wente, W. Chen, Efficient multiplex biallelic zebrafish genome editing using a CRISPR nuclease system. Proc Natl Acad Sci USA. 110, 13904–13909 (2013).

51. S. C. Fujita, S. L. Zipursky, S. Benzer, A. Ferrús, S. L. Shotwell, Monoclonal antibodies against the Drosophila nervous system. Proc Natl Acad Sci USA. 79, 7929–7933 (1982).

52. S. L. Zipursky, T. R. Venkatesh, D. B. Teplow, S. Benzer, Neuronal development in the Drosophila retina: monoclonal antibodies as molecular probes. Cell. 36, 15–26 (1984).

53. Y. Iwai et al., Axon patterning requires DN-cadherin, a novel neuronal adhesion receptor, in the Drosophila embryonic CNS. Neuron. 19, 77–89 (1997).

54. D. V. Vactor, H. Sink, D. Fambrough, R. Tsoo, C. S. Goodman, Genes that control neuromuscular specificity in Drosophila. Cell. 73, 1137–1153 (1993).

55. D. Riemer et al., Expression of Drosophila lamin C is developmentally regulated: analogies with vertebrate A-type lamins. J Cell Sci. 108 (Pt 10), 3189–3198 (1995).

56. H. He et al., Cell-intrinsic requirement of Dscam1 isoform diversity for axon collateral formation. Science. 344, 1182–1186 (2014).

57. D. Bishop et al., Near-infrared branding efficiently correlates light and electron microscopy. Nat Meth. 8, 568–570 (2011).

58. D. T. Chu, M. W. Klymkowsky, The appearance of acetylated alpha-tubulin during early development and cellular differentiation in Xenopus. Developmental biology. 136, 104–117 (1989).

59. D. Ray et al., A compendium of RNA-binding motifs for decoding gene regulation. Nature. 499, 172–177 (2013).

60. K. X. Zhang, L. Tan, M. Pellegrini, S. L. Zipursky, J. M. McEwen, Rapid Changes in the Translatome during the Conversion of Growth Cones to Synaptic Terminals. Cell Rep. 14, 1258–1271 (2016).

61. M. Calleja, E. Moreno, S. Pelaz, G. Morata, Visualization of gene expression in living adult Drosophila. Science. 274, 252–255 (1996).

62. M. D. Gordon, K. Scott, Motor Control in a Drosophila Taste Circuit. Neuron. 61, 373–384 (2009).

63. L. A. Perkins et al., The Transgenic RNAi Project at Harvard Medical School: Resources and Validation. Genetics. 201, 843–852 (2015).

Acknowledgments:

We thank Leslie Saucedo (University of Pudget Sound) for UAS-*prl-1* flies, Hugo Stocker (ETH Zurich) for UAS-*InR.CFP* flies, Patrik Verstreken (VIB KU Leuven) for UAS-PLCδPH.GFP flies, Katlijn Vints and Anneke Kremer (VIB BioImaging Core) for electron microscopy, Martijn Dirix, Bing Yan, Jiekun Yan and Zengjin Huang (VIB KU Leuven) for help with experiments, and Pierre Vanderhaeghen (VIB KU Leuven), Bassem Hassan (ICM Paris), Joris de Wit (VIB KU Leuven) and Matthew Holt (VIB KU Leuven) for critically reading the manuscript. Fly stocks obtained from the Bloomington Drosophila Stock Center (NIH P40OD018537) and from the Vienna Drosophila Resource Center (VDRC, www.vdrc.at) were used in this study. Some monoclonal antibodies were obtained from the Developmental Studies Hybridoma Bank (created by the NICHD of the NIH and maintained at The University of Iowa). **Funding:** This work was supported by VIB funds (D.S.), and project grants from Belgian FWO and EOS (30913351, SYNET) programs (D.S.) and from the Swiss National Science Foundation to O.U. (PBBEP3_130209 and PZ00P3_161448). **Author contributions:** Designed

experiments: O.U., D.S; performed experiments: O.U., A.I., S.V., S.S., A. M.; analyzed and interpreted the data: O.U., D.S.; wrote the manuscript: O.U., D.S.; acquired funding: O.U., D.S.; all authors read and commented on the manuscript. **Competing interests:** Authors declare no competing interests. **Data and materials availability:** All data are available in the manuscript or the supplementary material.

Supplementary Materials:

Materials and Methods

Figures S1-S22

Table S1

Movie S1

References (43 – 63)

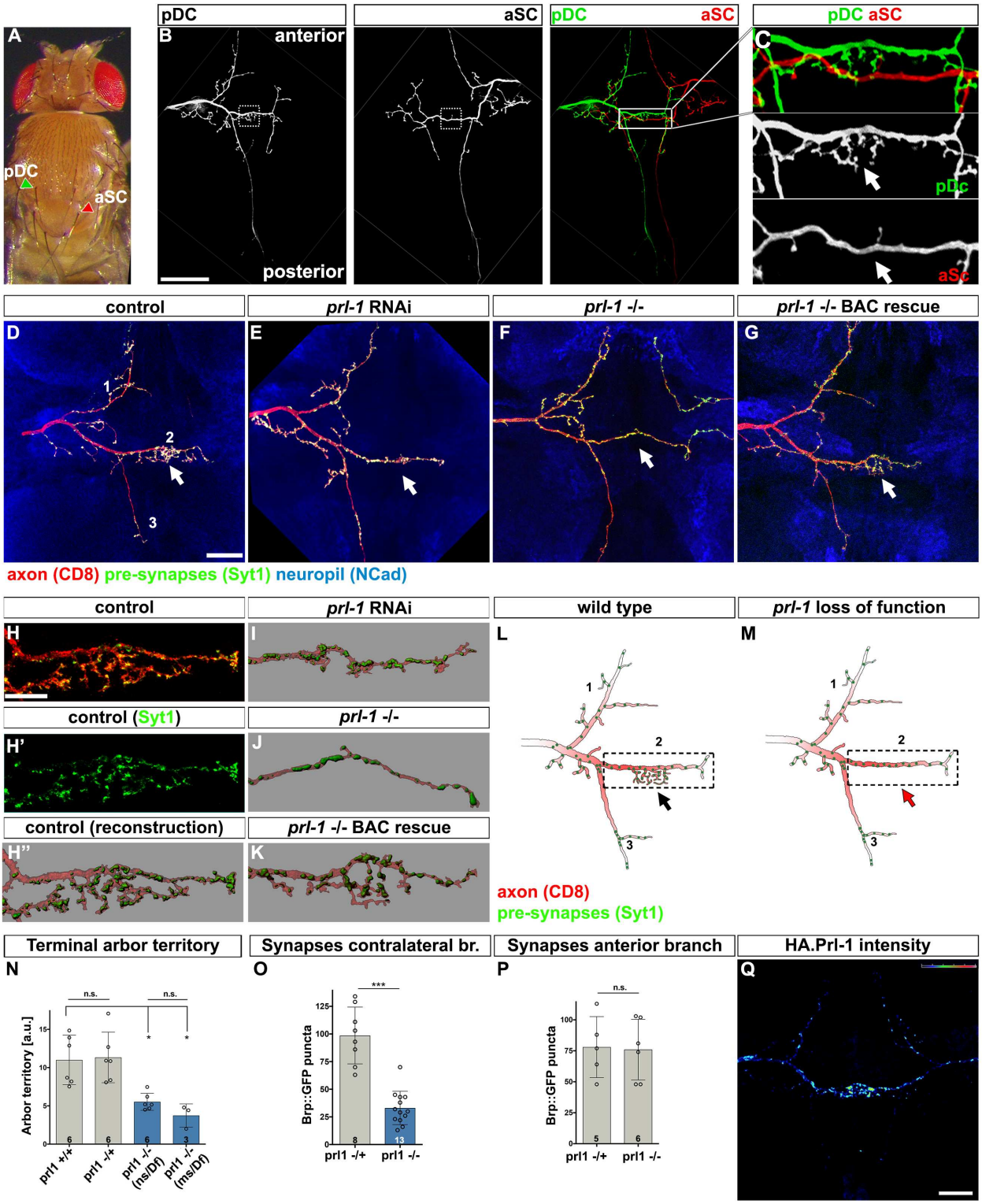

Figure 1. Loss of *prl-1* disrupts formation of synapse-dense terminal arbors specifically in one axon collateral. (**A**) Location of posterior Dorsocentral (pDC) and anterior Scutellar (aSC) large bristles on the

fly thorax. (**B**) Central axon projections of mechanosensory neurons innervating the pDC and aSC bristles, respectively, in the adult animal. Boxes indicate a central region of the contralateral collateral (see C). Top, anterior; bottom, posterior in this and all subsequent figures. (**C**) The DC axon collateral that projects to the contralateral side of the CNS has formed dense terminal arborizations, while the same axon collateral of the SC neuron has not (arrows). (**D**) Axon (CD8.GFP, red) and pre-synapse (Cherry.Syt1, Synaptotagmin-1, green) markers expressed in a single DC neuron and visualized by immunostaining. Neural Cadherin (NCad, blue) is used for neuropil staining. Three primary axon collaterals innervate distinct areas of the CNS (1, anterior; 2, contralateral; 3, posterior) with different amounts of synapses. Note the extensive Syt1 labelling in the terminal arbors of the contralateral axon branch (arrow). (**E**) DC neuron, in which *prl-1* was knocked down by RNAi. Terminal arbors are strongly reduced / virtually absent in the contralateral branch (arrow), while the two collaterals that innervate the other main target areas are unaffected. (**F**) Terminal arbors are completely lost from the contralateral branch in a whole-animal *prl-1* mutant (arrow), while the other target areas are unaffected. (**G**) The arbor loss phenotype is rescued by introduction of a transgenic bacterial artificial chromosome (BAC) containing *prl-1*. (**H-K**) Magnification of the DC neuron contralateral axon collateral in indicated genotypes, illustrating loss of terminal synaptic arborizations upon *prl-1* knockdown or loss-of-function (I, J). CD8.GFP and Cherry.Syt1 signals are reconstructed with Imaris software for panels H''-K. (**L,M**) Schematics illustrating the three target areas innervated by the main axon collaterals of mechanosensory neurons, the differential amounts and types of synapses formed, and the loss of synaptic arborizations in *prl-1* null animals (arrows). (**N**) The territory occupied by terminal arbors on the contralateral branch is strongly reduced in different whole-animal *prl-1* mutant combinations (ns/Df, nonsense mutation over deficiency; ms, missense mutation, see Fig. S1 for the mutations and Fig. S2 for the quantification method). a.u., arbitrary units; n.s., non significant. *, $p<0.05$, Kruskal-Wallis test with multiple comparisons. (**O**) Synapse numbers, as assessed by counting puncta of the Brp^{short}.GFP marker (*42*) expressed in single DC neurons are significantly decreased in the contralateral branch upon loss of *prl-1* (Mann-Whitney test, $p<0.0001$; see Fig. S5 for examples images of samples used for quantification). (**P**)

Synapse numbers are not altered in the anterior target area 1 upon loss of *prl-1* (Mann-Whitney test, n.s., non significant). (**Q**) HA-tagged Prl-1 protein is enriched in contralateral axon collaterals of DC neurons (false-color intensity display; blue, low levels; yellow-red, high levels). Scale bars: B, 50 μm; D & Q, 20 μm; H, 10 μm. In the graphs of this and all subsequent figures, individual measured values and mean are displayed, and error bars indicate standard deviation. Genotypes for all panels can be found in Table S1.

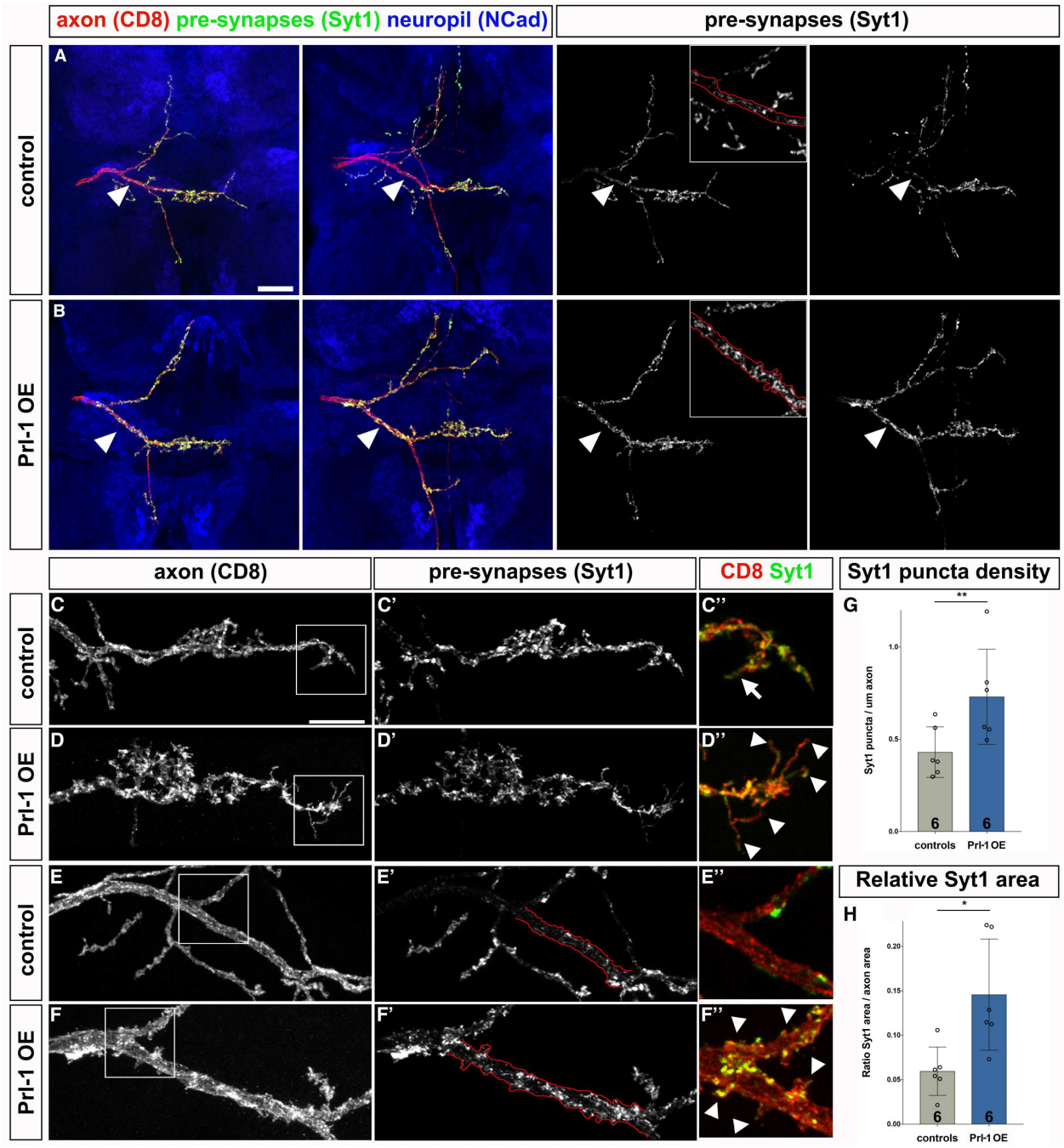

Figure 2. Prl-1 overexpression induces ectopic synaptic marker accumulation and immature axonal protrusions. (**A**) Proximal regions (arrowheads, magnified in inset) of central mechanosensory neuron projections contain few Syt1 marker puncta in control animals. (**B**) Syt1 marker accumulates in proximal axon projections in Prl-1 overexpressing (OE) animals (arrowheads; inset). (**C**) Morphology of a mature contralateral mechanosensory neuron projection in an adult control animal. Arrow in C'' (magnification)

indicates a terminal branch. (**D**) In adult animals overexpressing Prl-1 in mechanosensory neurons, the contralateral axon collateral has a less mature morphology, with small filopodial protrusions along the branch, and large protrusions at its distal end (arrowheads D''). (**E**) The proximal region of the central axonal projection contains only few Syt1 marker puncta in controls (see region outlined in red in E'). (**F**) Syt1 puncta are more numerous upon overexpression of Prl-1 in mechanosensory neurons (proximal axon projection region outlined in F'). Arrowheads in F'' indicate small immature protrusions from the main axon shaft. (**G**, **H**) Quantification of Syt1 puncta density (G) and area filled by Syt1 puncta (H) in the proximal axon projection of control and Prl-1-overexpressing (OE) mechanosensory neurons. *, $p<0.05$; **, $p<0.01$, Mann-Whitney test. Scale bars: A, 20 μm; C, 10 μm.

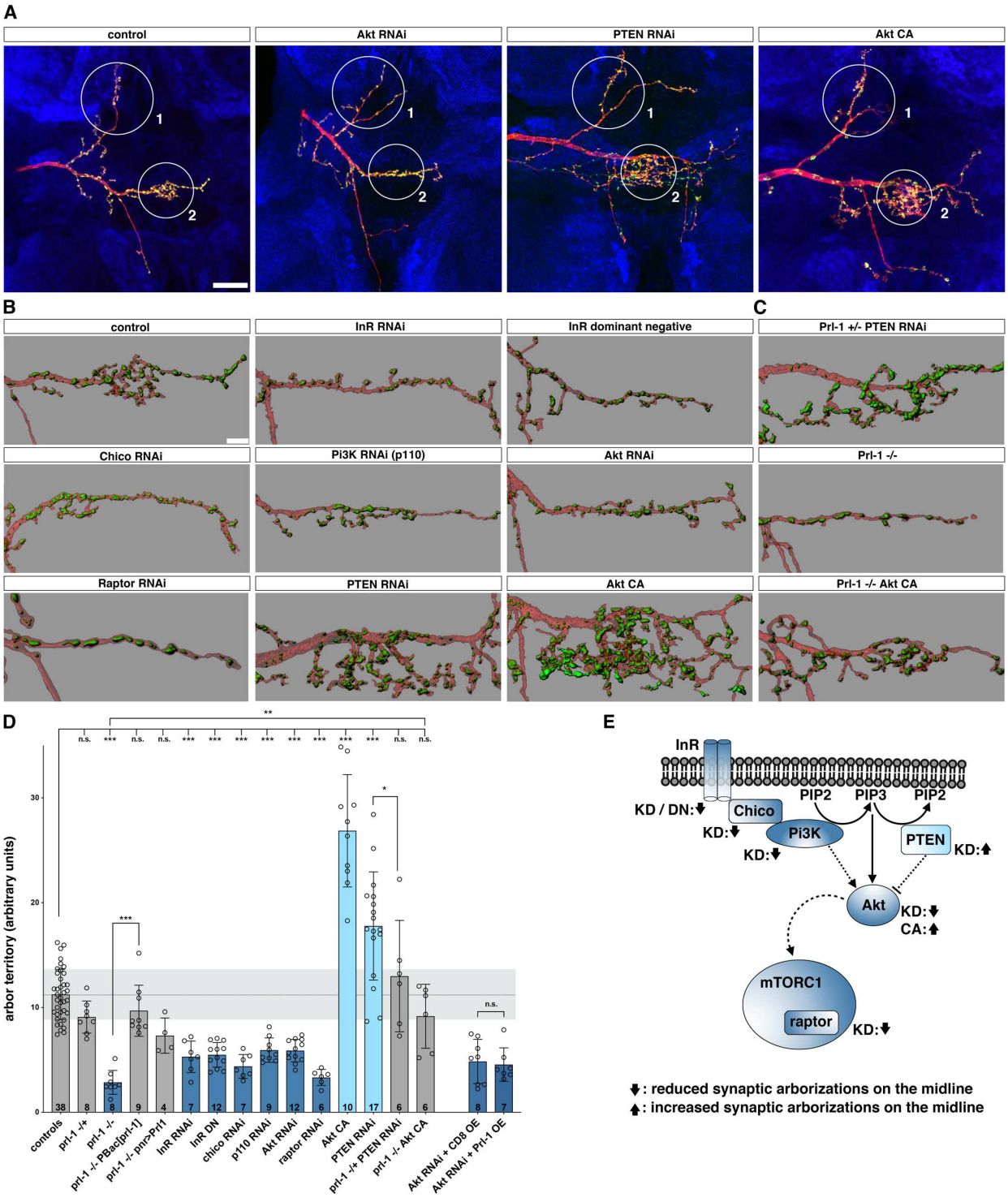

Figure 3. The Insulin Receptor signaling pathway controls formation of synapse-dense terminal arbors and interacts with *prl-1*. (**A**) Whole CNS projections of control DC neurons and DC neurons with reduced (Akt RNAi) or enhanced (PTEN RNAi; Akt constitutively active, CA) Akt signaling. Note drastic

reduction (Akt RNAi) and increase (PTEN RNAi; Akt CA), respectively, of synaptic terminal arbors in the contralateral branch (target area 2), while the other axon collaterals are unaffected (such as target area 1; note that the anterior contralateral projection, here present only in the RNAi samples, is variable also in wild-type flies). (**B**) Morphology of the contralateral axon branch upon indicated manipulations in mechanosensory neurons. Visualizations of the CD8.GFP axonal marker (red) and Cherry.Syt1 pre-synaptic marker (green) are shown. (**C**) Reduction of Prl-1 levels suppresses the PTEN phenotype (top), while activation of the Akt signaling pathway rescues the *prl-1* null phenotype (bottom, middle, respectively). Note that Akt CA was expressed only in mechanosensory neurons, which target into a small CNS (see Fig. S12). (**D**) Quantification of terminal arbor territory in the indicated genotypes. Standard deviation of controls is shaded in gray. Manipulations reducing activity of the InR/Akt signaling pathway are displayed in dark blue, manipulations enhancing the activity of the pathway are in light blue. Effects of co-expressing Akt RNAi with CD8.Cherry and Prl-1, respectively (last two columns of graph) were assessed by dye-fills and not with genetic labelling as for the rest of the genotypes. n.s., non significant; **, $p<0.01$; ***, $p<0.001$, ordinary one-way Anova with multiple comparisons. (**E**) Schematic of InR/Akt/mTORC1 signaling. Positive components are shaded in dark blue, the inhibitor PTEN is in light blue. Changes in mechanosensory neuron terminal arbor territory upon manipulation of the gene products are indicated by arrows. KD, knockdown; DN, dominant negative; CA, expression of constitutively active. PI, phosphatidylinositol; PIP2, PI(4,5)-bisphosphate; PIP3, PI(3,4,5)-trisphosphate. Scale bars: A, 20 μm; B, 5 μm.

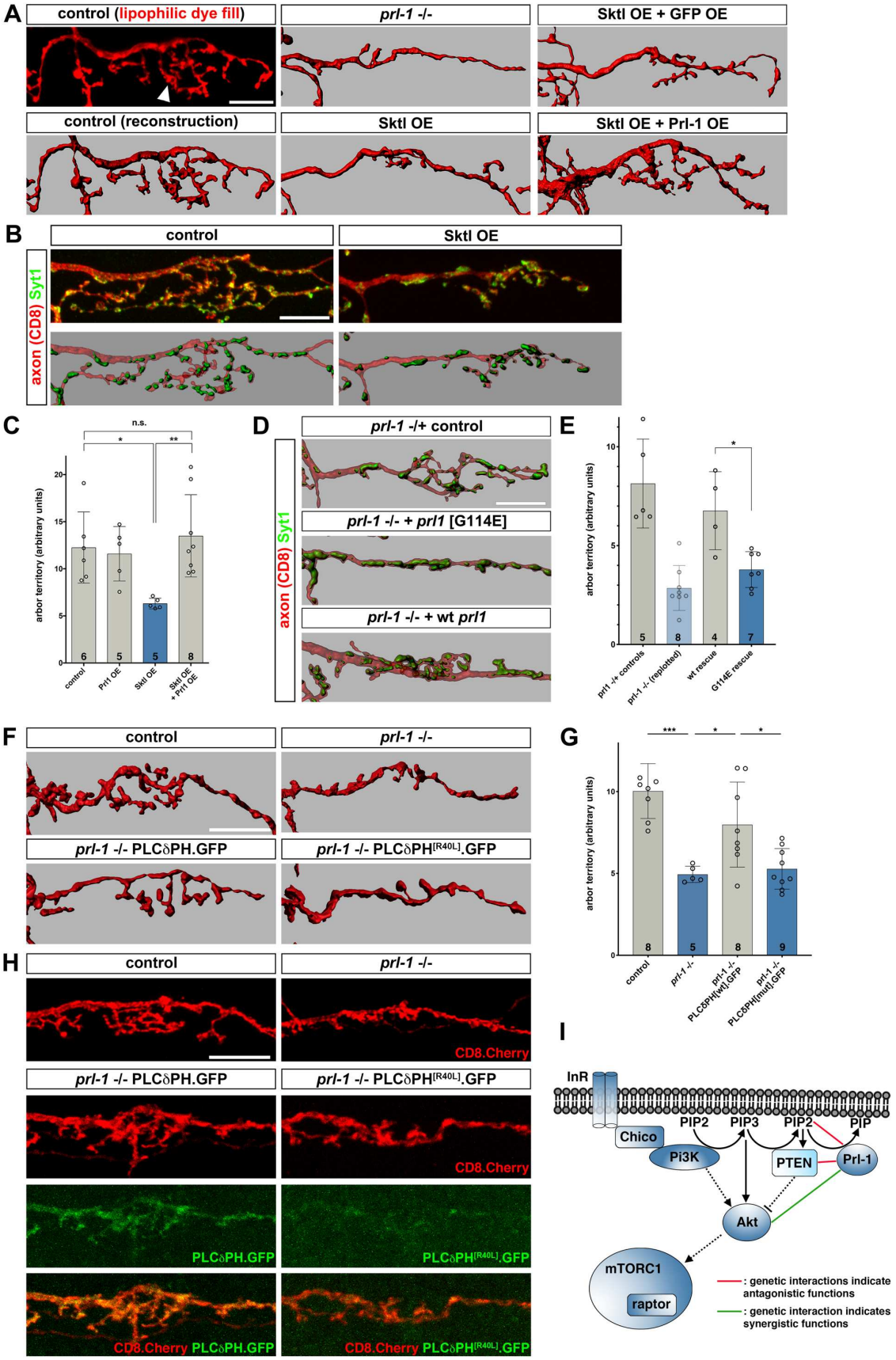
A
control (lipophilic dye fill)
prl-1 -/-
Sktl OE + GFP OE
control (reconstruction)
Sktl OE
Sktl OE + Prl-1 OE
B
control
Sktl OE
axon (CD8) Syt1
C
n.s.
*
**
arbor territory (arbitrary units)
control
Prl1 OE
Sktl OE
Sktl OE + Prl1 OE
D
prl-1 -/+ control
prl-1 -/- + prl1 [G114E]
prl-1 -/- + wt prl1
axon (CD8) Syt1
E
arbor territory (arbitrary units)
prl1 -/+ controls
prl-1 -/- (replotted)
wt rescue
G114E rescue
F
control
prl-1 -/-
prl-1 -/- PLCδPH.GFP
prl-1 -/- PLCδPH[R40L].GFP
G
***
*
*
arbor territory (arbitrary units)
control
prl-1 -/-
prl-1 -/- PLCδPH[wt].GFP
prl-1 -/- PLCδPH[mut].GFP
H
control
prl-1 -/-
CD8.Cherry
prl-1 -/- PLCδPH.GFP
prl-1 -/- PLCδPH[R40L].GFP
PLCδPH.GFP
CD8.Cherry PLCδPH.GFP
I
InR
Chico
Pi3K
PIP2
PIP3
PIP2
PIP
PTEN
Prl-1
Akt
mTORC1
raptor
: genetic interactions indicate antagonistic functions
: genetic interaction indicates synergistic functions

Figure 4. Genetically targeting phosphoinositide levels controls terminal arbor formation. (**A**) Original data and visualizations for examples of DC neuron contralateral branches in animals of the indicated genotypes. Axons were filled with a fluorescent lipophilic dye. Arrowhead points to terminal branches that are lost in *prl-1* null animals and upon overexpression (OE) of Sktl in mechanosensory neurons, but restored upon co-overexpression of Prl-1 with Sktl. (**B**) Sktl overexpression phenotype (right panels) in a mechanosensory neuron labelled genetically with CD8 axonal and Syt1 pre-synaptic markers. Note the reduction of terminal arbor synapses. (**C**) Quantification of terminal arbor territory for Sktl and Prl-1 overexpression. *, $p<0.05$; **, $p<0.01$; Kruskal-Wallis test. (**D**) Visualizations for examples of mechanosensory neuron contralateral collaterals in animals of the indicated genotypes. Expression in mechanosensory neurons of a wild-type (wt) *prl-1* transgene with 5'- and 3'-UTRs rescues terminal arbors, while expression of a UTR-containing *prl-1* transgene with the G114E mutation does not. Note that mechanosensory neurons project into a VNC of reduced size (Fig. S16). Defects in the target area are therefore likely preventing full rescue of terminal arborizations and synapses to wild-type levels (see also panels E, G and Fig. 6F). (**E**) Quantification of terminal arbor territory in *prl-1* null flies rescued with different *prl-1* transgenes as in D. See also Fig. 6 for more examples of rescue with a wild-type *prl-1* transgene. Data of *prl-1* -/- flies is replotted from Fig. 3D. *, $p<0.05$; Mann-Whitney test. (**F**) Visualizations of dye-filled contralateral axonal projections in animals of indicated genotypes. Expression of the PH domain of PLCδ (PLCδPH.GFP) in mechanosensory neurons rescues terminal arborization loss in *prl-1* mutant animals (see also Fig. S17 for PLCδPH.GFP expression in mechanosensory neurons). Expression of a mutant PLCδ PH domain (PLCδPH[R40L]) that does not bind to PI(4,5)P2 does not rescue the *prl-1* phenotype. (**G**) Quantification of terminal arbor territory of dye-filled contralateral collaterals in animals of genotypes as in F. *, $p<0.05$; ***, $p<0.0001$; ordinary one-way Anova with multiple comparisons. (**H**) Single-cell expression of PLCδPH.GFP wild-type and [R40L] mutant, respectively, in mechanosensory neurons. CD8.Cherry is co-expressed as an axon marker, and Cherry and GFP fluorescence were imaged. Expression of wild-type PLCδPH.GFP cell-autonomously rescues the

loss of terminal arborizations in *prl-1* null mutant animals, but PLCδPH.GFP [R40L] does not. Note that PLCδPH.GFP wild-type can be found at higher levels in the axon than the [R40L] mutant marker protein (see also Fig. S17 for PLCδPH.GFP wt localization in axons). (**I**) Schematic placing Prl-1 in the context of InR / Akt signaling and control of PIP levels based on the identified genetic interactions. All scale bars represent 10 μm.

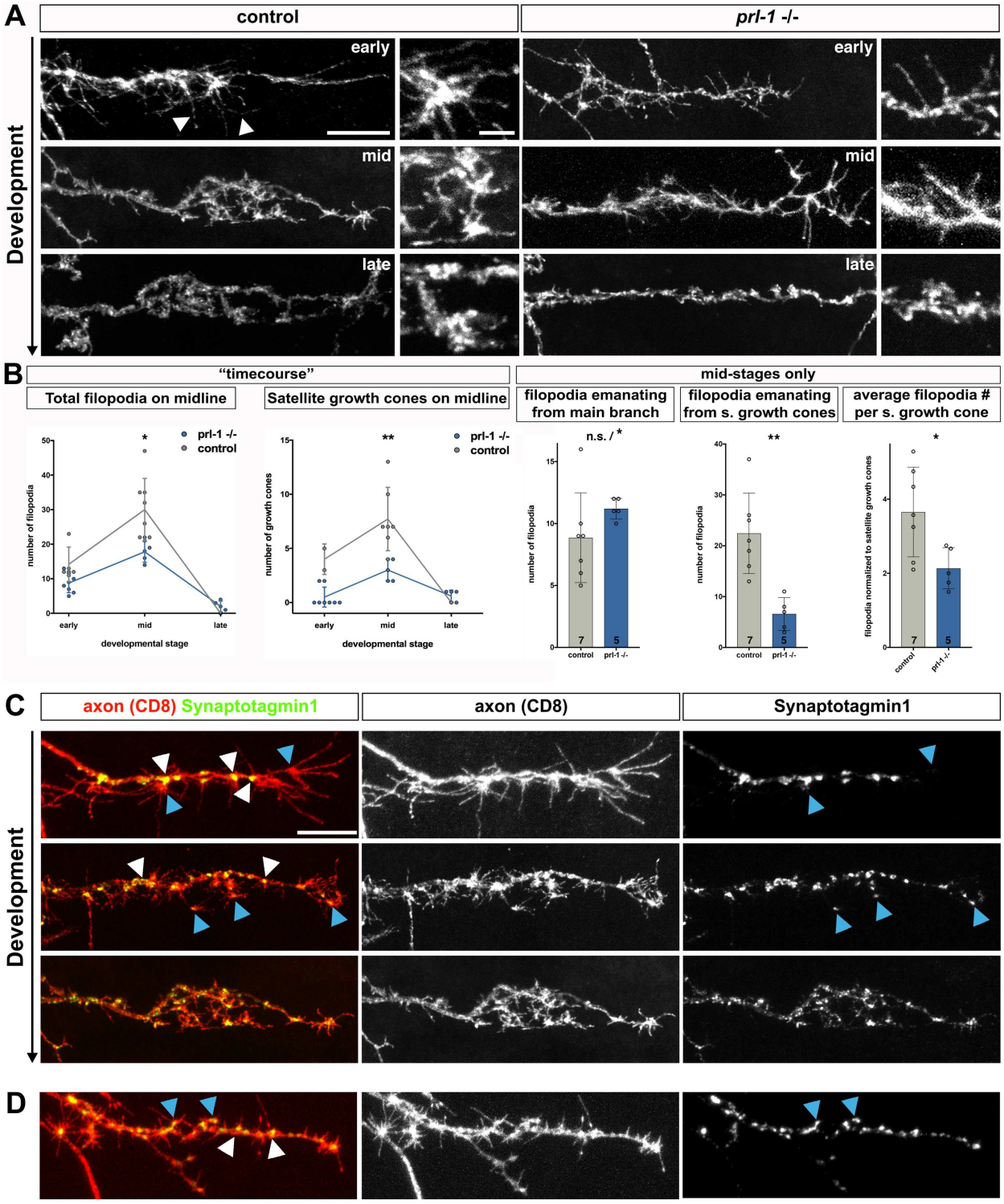

Figure 5. Prl-1 promotes consolidation of terminal arbors and nascent synapses. (**A**) Successive developmental stages of the contralateral DC neuron axon collateral in fixed control and *prl-1* null samples. In an early phase (top left, sample around 47 hrs after puparium formation, apf), developing

branches extend long filopodial protrusions (arrowheads) and grow towards the contralateral side of the CNS. At mid-stages (middle left, around 72 hrs apf), filopodia-rich satellite growth cones are visible (see C and also Fig. S18A, arrowheads). At late stages (bottom left, around 90 hrs apf), filopodia and satellite growth cones have disappeared, and terminal arbors have consolidated. In *prl-1* null animals (right panels), filopodia and satellite growth cones are initially formed, but fail to accumulate and be consolidated on the contralateral branch. Note that CNS development is delayed by approximately 5-10 hrs in the mutant at these stages. Corresponding developmental stages assessed by branch growth progression, rather than by absolute timing, are displayed. Magnified panels show examples of filopodia morphology. (**B**) Quantification of filopodia and satellite growth cones during different developmental stages (left panels) and at mid-stages of collateral branch formation (right panels). n.s., non significant, *, $p<0.05$, **, $p<0.01$, Mann-Whitney test. n.s./*: approximate p-value 0.06, computed exact p-value 0.048. (**C**) Co-labelling of axon and Synaptotagmin1 pre-synaptic marker in wild-type developing contralateral collaterals. White arrowheads indicate Syt1 accumulation on the main axon shaft, at sites where filopodia sprout. Blue arrowheads point to satellite growth cones, which are devoid of Syt1 signal at an early stage (top panels). Syt1 starts to localize to satellite growth cones at a slightly later developmental stage (middle panels). (**D**) *prl-1* mutant animal. Syt1 localizes to sites of filopodia sprouting (white arrowheads) and to satellite growth cones (blue arrowheads) at this early stage. Scale bars: 10 μm & 2.5 μm (insets).

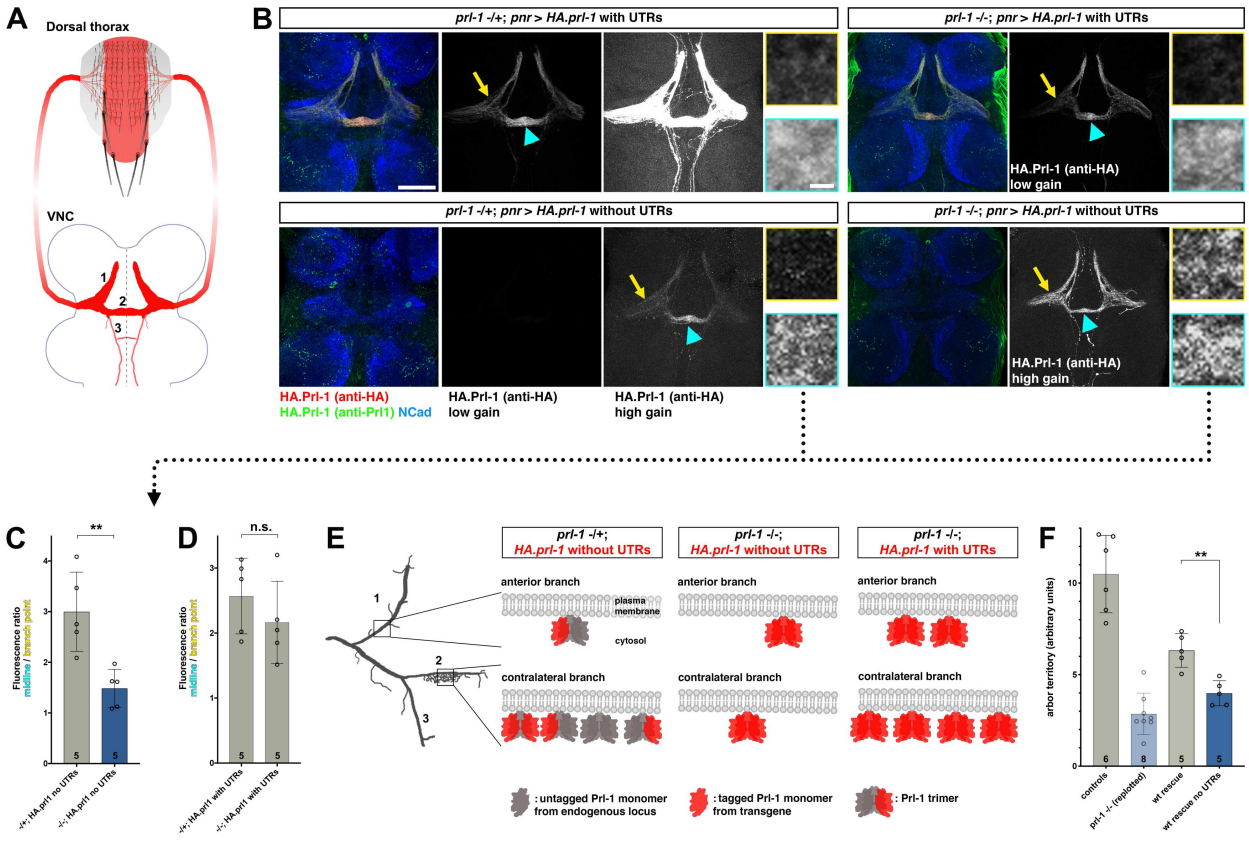

Figure 6. *prl-1* UTRs are essential for axon localization and function. (**A**) Schematic illustrating the expression pattern of *pnr-gal4* (red) in adult flies, which was used for driving UAS constructs in the experiment shown in (B). *pnr-gal4* is active in the mechanosensory neurons innervating the 8 large bristles (DC and SC macrochaetae) and all the small bristles (microchaetae) located in the central domain of the thorax (top, not to scale). The composite of the CNS axon projections of these neurons results in the bilateral symmetric pattern shown below; numbering of projections corresponds to the numbering at single-axon resolution in panel E and in Fig. 1D,L. (**B**) mechanosensory neuron expression of *prl-1* transgenes with and without UTRs, respectively, detected by antibodies against Prl-1 and against the HA epitope tag, respectively. Anti-Prl-1 staining is visible in CNS axon projections only when expressing Prl-1 from a transgene with UTRs. Prl-1 protein expressed from this transgene is readily detected by staining against the HA tag in mechanosensory neuron axon projections in the CNS (top panels; note panels showing data recorded with low and high gain, respectively, as labelled below), and is enriched in the

contralateral branches (blue arrowheads) both in presence (left panels) and absence (right panels) of endogenous Prl-1. In contrast, Prl-1 expressed from a transgene without UTRs (bottom panels) is expressed at much lower levels in mechanosensory neuron central axon projections (only visible when imaged with high gain), and its enrichment in the contralateral branch (blue arrowheads) strongly depends on endogenously expressed Prl-1. Yellow arrows point to proximal regions of the mechanosensory neuron central projections, for direct comparison between panels. Panels on the right show high magnification details of HA staining in the proximal regions (top, framed in yellow) and in the contralateral branches (bottom, framed in blue). Note that signal is stronger in contralateral regions for all genotypes except for HA.Prl-1 expression from a construct without UTRs in *prl-1* -/- animals. Scale bars: 50 µm main panels, 2 μm magnification panels. (**C**) Fluorescent signal quantification of HA.Prl-1 expressed from the transgene without UTRs, in a region of interest (ROI) on the contralateral branches (corresponding to magnification panels in B) relative to an ROI of the same size on a proximal CNS segment of the axons (magnification panels in B). The enrichment on the contralateral branches is strongly reduced in animals without endogenously expressed Prl-1. **, $p<0.01$, Mann-Whitney test. (**D**) Same fluorescent signal quantification as in C, for constructs with UTRs, reveals no significant (n.s., Mann-Whitney test) difference in the presence or absence of endogenously expressed Prl-1. Note that this construct is expressed at much higher levels than the construct without UTRs (see B), which is however not reflected here as relative values are displayed. See also Fig. S21 for quantification of the membrane marker CD8.Cherry in wild-type and *prl-1* -/- animals. (**E**) Schematic illustrating formation of heterotrimers between Prl-1 expressed from the endogenous locus and HA-tagged Prl-1 expressed from the transgene without UTRs, leading to enrichment of HA.Prl-1 in the contralateral branch (left). In the absence of endogenous Prl-1, HA.Prl-1 expressed from the transgene without UTRs is not enriched in the contralateral branch (middle). HA.Prl-1 expressed from a transgene with UTRs, however, is still enriched in the contralateral branch even in the absence of endogenous Prl-1 (right), albeit it also accumulates in the anterior branch, possibly due to over-expression of the protein. (**F**) Quantification of contralateral

projection arbor territory reveals that loss of arbors cannot be rescued by a *prl-1* transgene without UTRs (see also Fig. S16). *, $p<0.05$, Mann-Whitney test.

Science
AAAS

Supplementary Materials for

Prl-1 phosphatase directs compartmentalized control of InR/Akt signaling during CNS synapse formation

Olivier Urwyler, Azadeh Izadifar, Sofie Vandenbogaerde, Sonja Sachse, Anke Misbaer, Dietmar Schmucker

Correspondence to: dietmar.schmucker@kuleuven.vib.be
olivier.urwyler@uzh.ch

This PDF file includes:

Materials and Methods
Figs. S1 to S22
Caption for Movie S1

Other Supplementary Materials for this manuscript include the following:

Table S1

Materials and Methods

Cloning of constructs

For cloning the HA-tagged *prl-1* CDS construct without UTRs, the *prl-1* coding sequence was obtained from cDNA of Canton S wild-type flies as follows: RNA was extracted from 15 whole female adults using TRIzol™ Plus RNA Purification Kit (ThermoFisher Scientific, catalog #12183555) and reverse transcribed using iScript™ cDNA Synthesis Kit (Bio-Rad, catalog #1708890). The *prl-1* CDS was then PCR-amplified using the primers TGCTCTAGAGGAATGAGCATCACCATGCGTC and TGCTCTAGACTATTGCACAGAACATGAATTC, and cloned into pUASTattB (*43*) with XbaI. For insertion of a single HA-tag coding sequence at the 5'-end of the *prl-1* CDS, the plasmid was amplified using primers CGGGGTACCATGTACCCCTACGACGTGCCCGACTACGCCGGATC GGGAATGAGCATCACCATGCGTC and CGGCGGGGTACCCTCGAGCCGCGGC, followed by KpnI digestion and self-ligation of the amplification product. For cloning *prl-1* constructs with UTRs, the *prl-1* cDNA corresponding to the RB isoform (flybase.org) was obtained from the plasmid pFLC1-*prl-1*RB (clone #RE55984, the *Drosophila* Genomics Resource Center, Indiana University). *prl-1*RB was subcloned from pFLC1-*prl-1*RB into pUASTattB (*43*) as a NotI / KpnI fragment. For the constructs with HA-tag, insertion of a single HA-tag sequence at the 5' end of the *prl-1* coding sequence was done by PCR on the pFLC1-*prl-1*RB plasmid, using the primers CGACGTGCCCGACTACGCCGGATCG GGAATGAGCATCACCATGCGTC and CGGCGTAGTCGGGCACGTCGTAGGGGTAAAACAATT ACAAAAGCTGTTCTG. A start codon was created 6 nucleotides upstream of the beginning of the HA-tag sequence by mutagenesis with primers CAGAACAGCTTTTGTAATGTTTTACCCCTACGAC and GTCGTAGGGGTAAAACATTACAAAAGCTGTTCTG. Constructs with single point mutations in the *prl-1* coding sequence were generated by site-directed mutagenesis on the wild-type plasmid with following primers. GTGGCTGGTCTGGAACGAGCTCCTGTC and GACAGGAGCTCGTTCCAGACCAGCCAC were used for mutagenizing codon 114 to code for glutamic acid instead of glycine in the *prl-1*^{G114E} mutant. GGTCTGGGACGATCTCCTGTCCTTG and CAAGGACAGGAGATCGTCCCAGACC were used for mutagenizing codon 116 to code for serine instead of alanine in the *prl-1*^{A116S} mutant. For the transgene containing the *prl-1* genomic region, the BAC clone CH322-158N14 in attB-P[acman]-CmR-BW was obtained from BACPAC Resources (Children's Hospital Oakland Research Institute) and directly used for *Drosophila* embryo injections.

Fly stocks and genotypes

Genotypes for all figure panels are listed in Table S1. Single mechanosensory neuron labelling with axon and synaptic markers (Syt1 or Brp) was done as described in (*14*). Or83c-GFP (*44*) transgenic flies were obtained from the Bloomington stock center at Indiana University (stock #52639). The UAS-*sktl* line (*29*) was obtained from the group of Bassem Hassan (VIB and KU Leuven, Belgium / ICM, Paris, France). UAS-*prl-1* lines with UTRs but without tag were obtained from the group of Leslie Saucedo (University of Pudget Sound, USA) (*45*). The UAS-InR.CFP line was obtained from the group of Hugo Stocker (ETH Zurich, Switzerland) (*46*). The PLCδPH.GFP and PLCδPH[R40L].GFP lines were obtained from the group of Patrik Verstreken (VIB and KU Leuven, Belgium) (*32*). UAS-RNAi lines were obtained either from the Vienna *Drosophila* Rescource Center (Vienna, Austria) or from the Bloomington *Drosophila* stock center (Indiana University, USA). All other fly lines were obtained from the Bloomington *Drosophila* stock center.

DNA injection for generation of transgenic flies was done at Rainbow Transgenic Flies, Inc. (Camarillo, CA, USA). All newly generated *prl-1* UAS constructs were integrated site-specifically into landing platform P{CaryP}attP2 to allow for direct comparison between the transgenes, without possible differences in transcription levels (*47*). The new transgenes appear to express at lower levels than the transgenes described in (*45*), which were randomly integrated via P-element transformation. First, overexpression of the newly generated transgenes with a strong, ubiquitous *tub-gal4* (*48*) driver did not induce lethality as previously reported for Prl-1 overexpression (*45*) and confirmed by our own experiments (data not shown). Second, overexpression of the new transgenes in mechanosensory neurons with *pnr-gal4* did not cause synapse and axon phenotypes as strong as observed with the lines from (*45*) (data not shown). attB-P[acman]-CH322-158N14 (*prl-1* BAC) was also integrated into P{CaryP}attP2.

Generation of *prl-1* alleles by CRISPR/Cas9-mediated gene editing

Gene editing with CRISPR/Cas9 was essentially done as described in (*49*). The CRISPRF primer containing the T7 polymerase binding site and the *prl-1* target site (underlined) was as follows: GAAATTAATACGACTCACTATAGGTTATGTCTGATGGTCGATGTTTTAGAGCTAGAA ATAGC. This oligo was annealed to an oligo with the sequence AAAAGCACCGACTCGGTGCCACTTTTTCAA GTTGATAACGGACTAGCCTTATTTTAACTTGCTATTTCTAGCTCTAAAAC, which contains the rest of the synthetic guide RNA (sgRNAR, (*49*)), and overhangs were filled with KOD polymerase (Merck, catalog #71086). The double-stranded DNA template was then used as template for *in vitro* transcription with T7 RNA polymerase, using the TranscriptAid T7 High Yield Transcription Kit (ThermoFisher Scientific, catalog #K0441). The synthesized gRNA was purified by LiCl precipitation. Cas9 mRNA was produced using the plasmid pCS2-nCas9n (Addgene #47929, (*50*)). First, the plasmid was linearized by NotI digestion. Cas9 mRNA was then *in vitro* transcribed and 5' capped using the mMESSAGE mMACHINE™ SP6 Transcription Kit (ThermoFisher Scientific catalog #AM1340). Cas9 mRNA was purified by ethanol precipitation. The gRNA / Cas9 mRNA mix was prepared in water, at concentrations of 45 ng/µl for the gRNA and 910 ng/µl for the Cas9 mRNA. The mix was injected into syncytial blastoderm *y w* embryos under halocarbon oil according to standard procedures. F_0 animals were screened for mosaicism by PvuI digestion of a PCR product amplified from their genomic DNA (primer sequences CGTGTGACACTTAACAGGGAAC and CGTCAACGACTTGCTGAGG), spanning the target site. The PvuI recognition sequence overlaps with the predicted Cas9 cut site, and thus destruction of the PvuI site indicates small insertions / deletions induced by NHEJ-mediated repair of the DNA double-strand break. Mosaic F_0 animals were further crossed to a balancer line, and the F_1 progeny was again screened in the same way to recover heterozygous founder flies, which were used to establish stable stocks of the different *prl-1* alleles (see Figure S1A).

Generation of anti-Prl-1 antibodies

For full-length *Drosophila* Prl-1 protein production in bacteria, a PCR product of the *prl-1* coding sequence was cloned into pET28c vector with NotI / NheI, resulting in pET28c-*His::prl-1*. Prl-1 expressed from this plasmid is N-terminally tagged with 6x His. pET28c-*His::prl-1* was transformed into BL21DE3 competent cells (Agilent, catalog #200131). Prl-1 expression was induced in liquid LB medium cultures with an optical density between 0.6 and 0.8 by adding IPTG (Sigma catalog # I6758-1G) to a final concentration of 0.1 mM. Cells were grown for another 3-4 hrs at 25ºC, and subsequently lysed in 50 mM Tris HCl pH 7.5, 150 mM NaCl, 2 mM DTT (lysis buffer) with sonication. His-tagged Prl-1 protein in the lysate was bound to Ni-

NTA agarose beads (QIAGEN, catalog #30210) by gentle mixing for 2-3 hrs at 4ºC. Beads were pelleted by centrifugation and washed in 30mM imidazole in lysis buffer. Prl-1 protein was eluted with 300 mM imidazole in lysis buffer. The eluate was further purified on an Amicon Ultra 0.5 ml 3K UFC column (catalog #500396) according to the manufacturer protocol. Prl-1 protein was subsequently loaded onto a denaturing polyacrylamide gel, and stained with Coomassie Brilliant Blue R250 (Sigma-Aldrich, catalog # 27816). Gel bands containing Prl-1 protein were excised and used for immunization of guinea pigs. Polyclonal antibody production was done by Covance (Denver, PA, USA).

Immunostainings

Immunostainings on *Drosophila* CNS or peripheral tissue was done according to standard protocols. Briefly, VNCs, brains, or cuticles from the dorsal thorax were dissected from adult flies or pupae in 1x phosphate-buffered saline (PBS). CNS tissue and cuticles were fixed for 1.5 hrs at room temperature (r.t.) in 2% paraformaldehyde (PFA; Merck, catalog #8.18708.1000) in 1x PBS containing 0.1% Triton X-100 (Sigma-Aldrich, catalog #X100; PBST); body wall preparations of third instar wandering larvae for NMJ stainings were fixed for 25 min at r.t. in 3.5% PFA in PBST. After several washes in PBST, tissues were blocked in 5% non-fat dry milk (NFDM) in PBST ("block solution") for several hours or overnight (o.n.) at 4ºC. Incubation in primary antibodies was performed o.n. at 4ºC or for ≥2 hrs at r.t in block solution, followed by several washes in PBST, and incubation in secondary antibodies o.n. at 4ºC or for ≥2 hrs at r.t in block solution. After several washes in PBST, samples were mounted in SlowFade™ Diamond Antifade Mountant (Invitrogen, catalog #S36972) or Vectashield (Vector Laboratories, catalog #H-1000). Imaging was done on an LSM710 (Zeiss, Germany) confocal light scanning microscope. Images were processed using ImageJ / Fiji and Adobe Photoshop. Reconstructions of mechanosensory neuron axons and pre-synapses were done using the "Surfaces" function in Imaris (Bitplane, an Oxford Instruments company). Following antibodies were used at the indicated concentrations. 1:10 mouse monoclonal anti-Futsch 22C10 (obtained from the Developmental Studies Hybridoma Bank at the University of Iowa, DSHB, (*51*, *52*)); 1:20 rat monoclonal anti-NCad DN-Ex #8 (DSHB, (*53*)); 1:20 mouse monoclonal anti-Bruchpilot nc82 (DSHB, (*18*)), 1:20 mouse monoclonal anti-FasII 1D4 (DSHB, (*54*)), 1:50 mouse monoclonal anti-Lamin ADL67.10 (DSHB, (*55*)), 1:500 goat polyclonal anti-Horseradish Peroxidase, coupled to Alexa Fluor 488 (Jackson ImmunoResearch, catalog #123-545-021), 1:500 mouse monoclonal anti-HA epitope 16B12 (BioLegend, catalog #901501), 1:1000 mouse monoclonal anti-GFP (Abcam, catalog #ab1218), 1:1000 rabbit polyclonal anti-DsRed (Clontech, catalog #632496), 1:200 guinea pig polyclonal anti-Prl-1 (this study). Alexa Fluor-coupled secondary antibodies (ThermoFisher) were used at concentrations of 1:1000 - 1:500. TRITC-Phalloidin (Sigma-Aldrich, catalog #P1951) was used at a concentration of 1:200 for counterstaining muscles in preparations of larval NMJs. For DNA staining, DAPI (ThermoFisher Scientific catalog #D1306) was included in the penultimate wash step of the immunostaining protocol at a concentration of 100 ng/ml.

Dye labelling of mechanosensory neuron axons

Dye-fills were performed as described previously (*56*). Briefly, adult flies were glued to an insect pin (Fine Science Tools, catalog #26000-25), and large mechanosensory bristles on the dorsal thorax were plucked manually with forceps. Flies were subsequently beheaded and their abdomen ripped open, and fixed o.n. at 4ºC in 3.7% paraformaldehyde in 0.2 M sodium carbonate-bicarbonate ("carb-bicarb"). After washes in 0.2 M carb-bicarb, flies were briefly dried, and the lipophilic fluorescent dyes DiD (ThermoFisher, catalog #D7757, dissolved at 20

mg / ml in 100% ethanol) and DiI (ThermoFisher, catalog # D3911, dissolved at 20 mg/ ml in 1:1 dimethyl formamide : ethanol) were applied to the exposed bristle sockets with glass micropipettes (Sutter Instruments, catalog #BF100-50-10). Flies were incubated 48 hrs in humid chambers at r.t., VNCs dissected in 0.2 M carb-bicarb, and filled mechanosensory neurons imaged on an LSM710 (Zeiss) confocal microscope.

Quantification of active zones, synaptic boutons, nuclei and filopodia

Estimation of active zone numbers was done in Fiji / ImageJ on confocal microscopy image stacks of single DC neuron axons expressing Brp^{short}::GFP and CD8::Cherry (see Table S1 for full genotypes). First, a background image stack was generated by applying three filters (Gaussian Blur, Minimum and Maximum, each with a radius of 6 pixels). This background image stack was then subtracted from the original image stack. Next, an Otsu thresholding was performed, with 0.5 – 1% of pixels remaining, followed by image despeckling. A binary watershed was then applied to separate inaccurately fused objects. The 3D object counter function was then used with a threshold at 128 and a size filter of minimally 5 pixels to count segmented objects and get an estimate for active zone numbers in the anterior and the contralateral branch, respectively.

Syt1 bouton numbers were estimated by reconstruction of surfaces in Imaris (Bitplane, an Oxford Instruments company). A region of interest was defined on the contralateral collateral corresponding to the region in which terminal arbor territories were quantified for other figures (see Fig. S2). Boutons were then segmented using the "Surfaces" function of Imaris, allowing touching objects to be split (seed points diameter 0.4 µm).

Nuclei counting in Fiji / ImageJ was done in confocal microscopy image stacks of VNCs stained with DAPI for DNA and Lamin to visualize the nuclear envelope, in regions of interest in the VNC (anterior and posterior, respectively). First, contrast of both channels was optimized across the whole image stack with the "Enhance Contrast" function, so that 1% of pixels were saturated. Next, the Lamin channel was subtracted from the DAPI channel in the whole stack, to better separate the DAPI signal from individual nuclei, and avoid overlap where nuclei are very close to each other. Subsequently, an Otsu thresholding was performed, with 4% of pixels remaining in superficial sections and 15% remaining in sections deeper in the tissue, respectively. A binary watershed was then applied to separate inaccurately fused objects. Finally, segmented objects were counted with the 3D object counter function, using a threshold at 128 and a size filter of minimally 20 pixels.

Filopodia were counted manually in Fiji / ImageJ in confocal microscopy image stacks of developing *prl-1* null and control animals with single mechanosensory neurons labelled with CD8::GFP and Cherry::Syt1. A length threshold of 1.5 µm was set for considering a membrane protrusion as a filopodium.

Correlative light and electron microscopy

Correlative light and electron microscopy (CLEM) was done essentially as described in (*14*), except that the EM part was performed with a serial Block-Face Scanning electron microscope (SBF-SEM) and a transmission electron microscopy (TEM), and not block-face scanning electron microscopy with focused ion beam based milling (FIB-SEM). Fly thoraces were first fixed in 0.5% glutaraldehyde (Electron Microscopy Sciences, catalog #16019) and 2% paraformaldehyde (Electron Microscopy Sciences, catalog #157-8) in 0.15 M sodium cacodylate buffer. Single labelled mechanosensory neurons in *prl-1* null and control VNCs (see Table S1 for full genotypes) were marked by near-infrared branding (NIRB, (*57*)) with a MaiTai DeepSee two-photon laser on an LSM710 (Zeiss) confocal microscope as described in (*14*). After post-

fixation in 2% glutaraldehyde in cacodylate buffer, samples were processed for TEM as follows. Samples were rinsed in 0,1M sodium cacodylate buffer then osmicated in 1% osmium tetroxide (Electron Microscopy Sciences, catalog #RT19151) with 1,5% potassium ferrocyanide (Sigma Aldrich, catalog #P3289) in 0,1M sodium cacodylate buffer. Next, samples were stained with 0,2% tannic acid (Electron Microscopy Sciences, catalog #RT 21710) for 30 minutes and followed by 0,5% uranyl acetate (SPI-chem, catalog #02624-AB) in 25% methanol overnight. The next day, samples were stained *en bloc* with lead aspartate and dehydrated with graded series of ethanol followed by flat embedding in Agar 100 (Laborimpex). Then flat-embedded samples were mounted on aluminum pin stubs (Gatan, catalog #10-006002-50)) with conductive epoxy (Circuit Works, catalog #16043)). To approach the region of interest based on the branding marks, a Zeiss Sigma Variable pressure SBF-SEM with 3View technology (Gatan) was used. Imaging was done at 1,3 kV with a pixel size of 20 nm and sections of 200 nm thickness. After locating the region of interest, serial ultrathin sections of 70nm were cut using a Reichert Ultracut E ultramicrotome. All sections were collected on triple slot grids (Ted Pella, catalog #1816) and imaged with a JEOL JEM-1400-LaB6 Transmission Electron Microscope with a Olympus Quemesa 11Mpx camera at 80kV.

Western blotting

Polyacrylamide gels for separation of proteins, and western blotting to nitrocellulose membranes was done according to standard procedures. For the western blot shown in Fig. S1C, extracts were prepared from adult fly heads, and the equivalent of 5 heads was loaded per lane. The membrane was cut horizontally between the molecular weight marker bands corresponding to 25 and 50 kiloDaltons, respectively, and incubated in following primary antibodies: 1:1000 guinea pig polyclonal anti-Prl-1 (this study), 1:5000 mouse monoclonal anti-beta Tubulin E7 (DSHB, (*58*)). HRP-conjugated secondary antibodies against guinea pig and mouse, respectively (Jackson ImmunoResearch, catalog #106-035-003 and #115-035-003) were used at a concentration of 1:5000. Chemiluminescence was generated with Pierce™ ECL Western Blotting substrate (ThermoFisher Scientific, catalog #32209) and detected on a ChemiDoc-It 500 Imaging system (UVP).

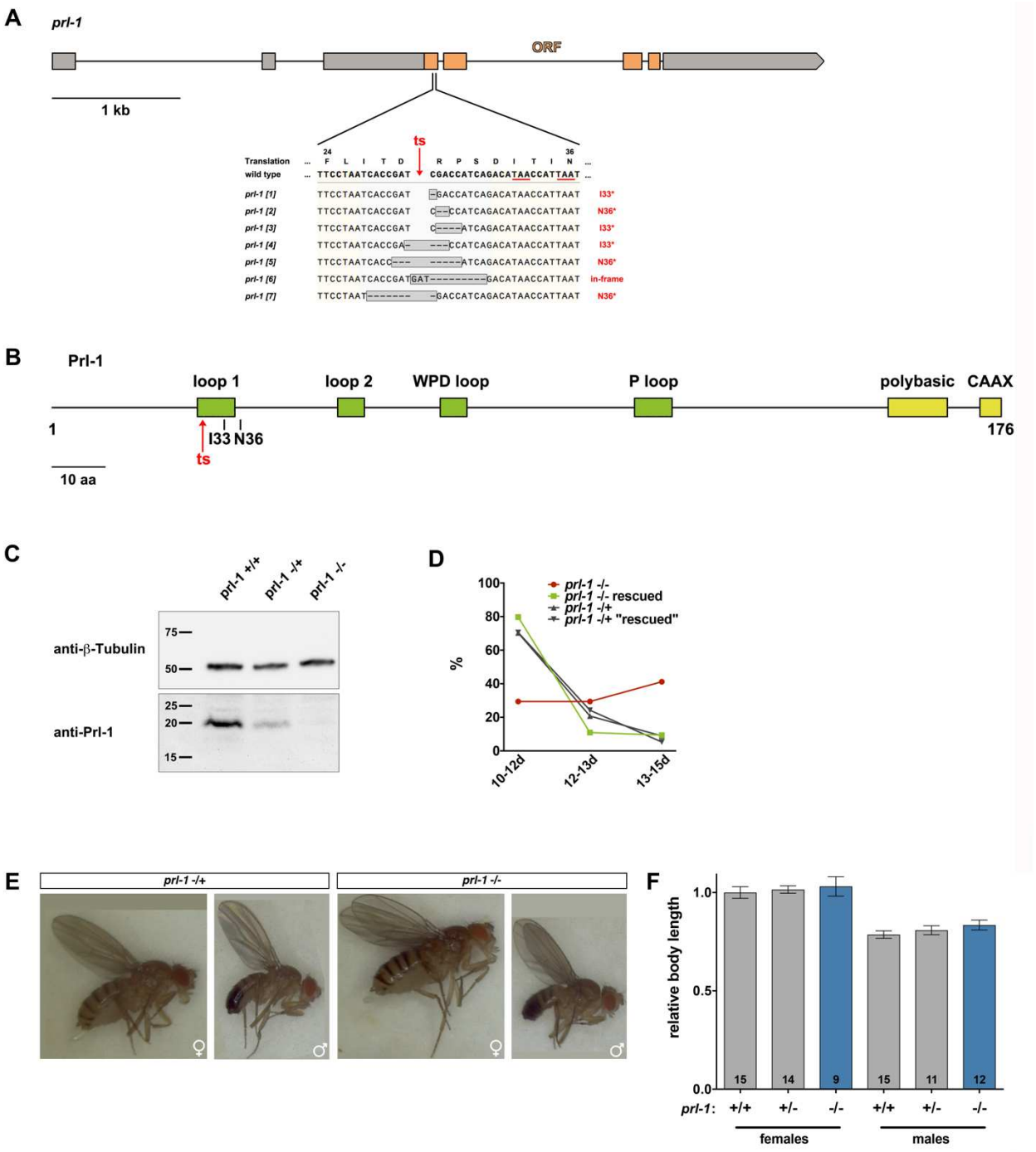

Figure S1. *prl-1* null mutants generated by CRISPR/Cas9-mediated gene editing. (**A**) Gene structure of the *Drosophila prl-1* RA isoform, according to flybase.org. Exons are depicted with boxes, introns with connecting lines. Open reading frame (ORF) is colored in orange. In the zoom-in on the sequence, amino acids are indicated above the coding sequence, from F at position 24 of the Prl-1 protein to N at position 36. "ts" denotes the target site for DNA cleavage by Cas9, directed to this site by the guide RNA used. The small insertions / deletions for the *prl-1* alleles 1-7 are indicated below. To the right of the sequence, amino acid positions are indicated, at which a premature termination codon is introduced through frame-shifts in alleles 1-5 and 7. "kb", kilobase. (**B**) Domain organization of the Prl-1 protein. Green boxes indicate

regions required for phosphatase activity, yellow boxes indicate sequences important for membrane localization (*16*). The target site for the guide RNA / Cas9-mediated DNA cleavage is indicated as in A. I33 and N36 correspond to the amino acids highlighted in A. “aa”, amino acid. (**C**) Detection of Prl-1 protein in head extracts from adult flies of the indicated genotypes. Tubulin was used as a loading control. (**D**) Quantification of adult fly hatching at different time periods (d, days) after egg laying. “rescued” denotes genotypes with one copy of the *prl-1* gene inserted into the genome as a bacterial artificial chromosome transgene. Note that for control genotypes, around 80% of all adults hatch 10-12 days after egg laying, while only around 30% of *prl-1* null flies hatch already at that time, and around 40% hatch only after 13-15 days. (**E, F**) External morphology and size of *prl-1* mutant animals are normal. Error bars in F represent standard deviation.

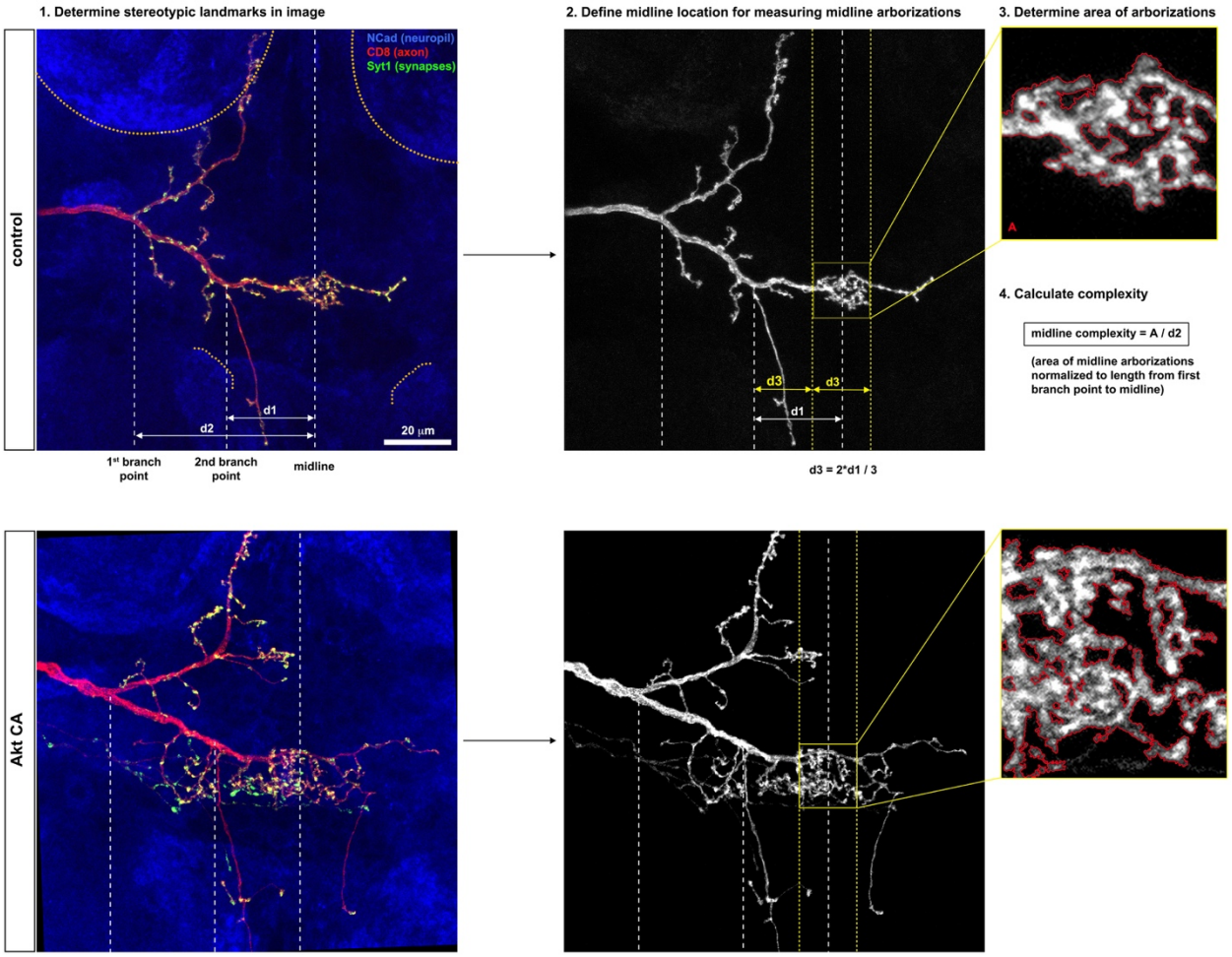

Figure S2. Quantification of contralateral branch arbor territory. Procedure followed to measure the branch arbor territory is exemplified for a control (top) and a DC neuron overexpressing constitutively active (CA) Akt (bottom), which forms exuberant arbors. As a first landmark, location of the CNS midline is determined with the help of the NCadherin neuropil staining (blue, note that the midline is located in the middle between prothoracic neuromeres and terminal projections of wing margin sensory neurons, outlined in orange in the top left panel). Location of the first and the second main branch points of DC neurons is determined with the axon staining (red). The distance between the second branch point and the midline (d1) is considered as half the length of the contralateral projection. The region for quantification of synaptic arborizations is defined as the central third (d3) of the contralateral projection. In this region, the area (A) filled by the axonal arborizations (CD8.GFP axon label channel) in a maximum projection of the 3D image stack is traced automatically in Adobe Photoshop. This area is then normalized to the distance between the first branch point and the midline to correct for variability in VNC size / flattening during mounting of the samples.

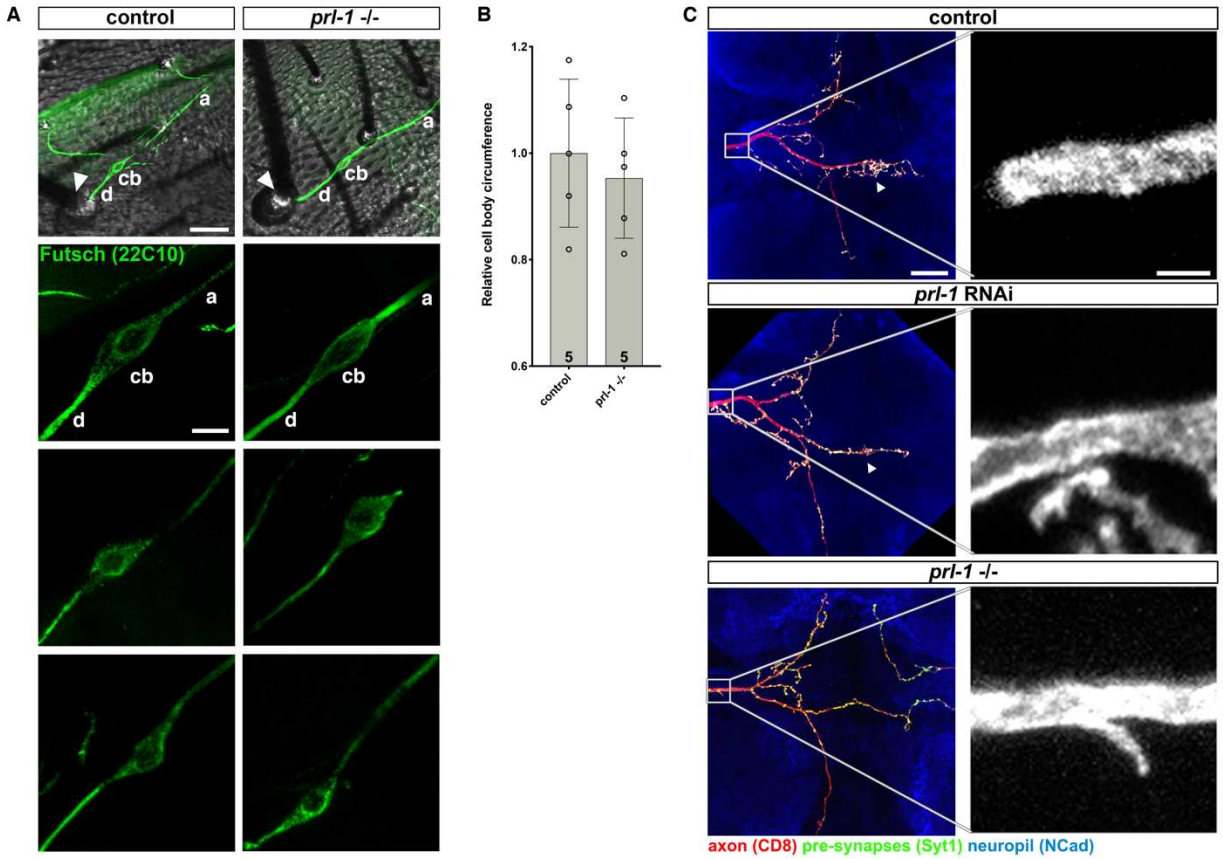

Figure S3. DC neuron cell body size and morphology, and axon caliber, are normal in *prl-1* null animals. (**A**) Immunostaining of DC neurons underneath the dorsal thorax cuticle, with an antibody against the microtubule-associated protein Futsch. Arrowheads point to the large DC bristles. "cb", cell body; "d", dendrite; "a", axon. Two additional examples for each genotype are indicated in the magnification panels. Scale bars: top panels, 20 µm; bottom panels, 5 µm. (**B**) Quantification of cell body circumference for 5 control and 5 *prl-1* null DC neurons, relative to the average of the controls. Error bars represent standard deviation. (**C**) Same samples as in Fig. 1D-F, with magnifications on an axon segment (stained for CD8.GFP) at the site of entry into the CNS. No differences in axon caliber are observed. Scale bars: left panels, 20 µm; right panels, 2.5 µm.

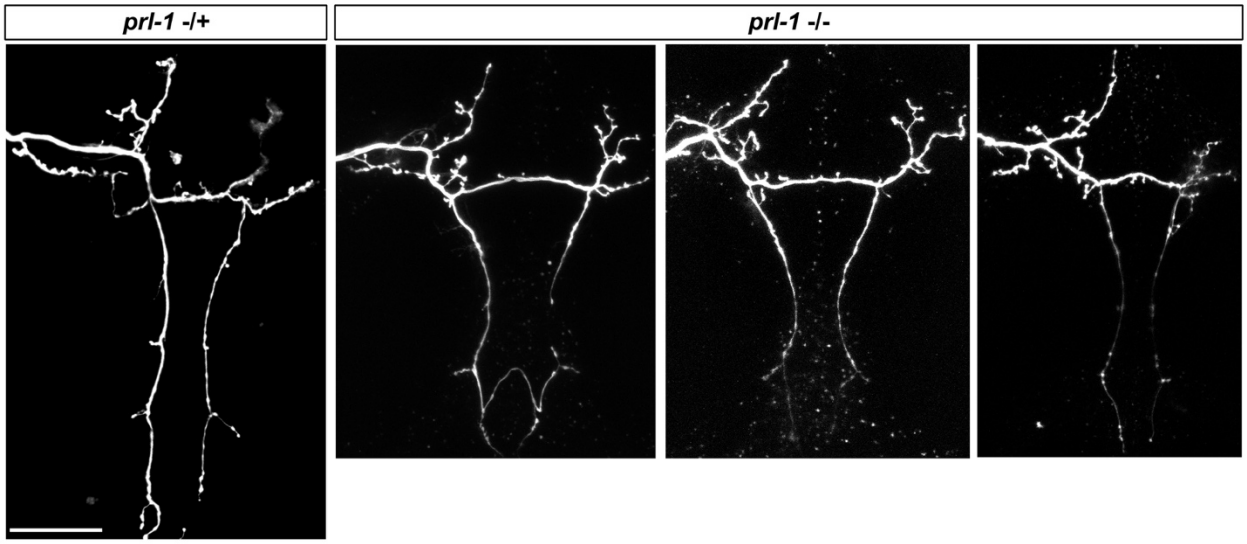

Figure S4. CNS axon projections of SC neurons are normal in *prl-1* null animals. Posterior scutellar (pSC) mechanosensory neurons were labelled with a lipophilic fluorescent dye in *prl-1* heterozygous and homozygous null animals. Except for slightly shorter posterior projections due to reduced VNC size, no defects were observed in *prl-1* null flies. Scale bar: 50 µm.

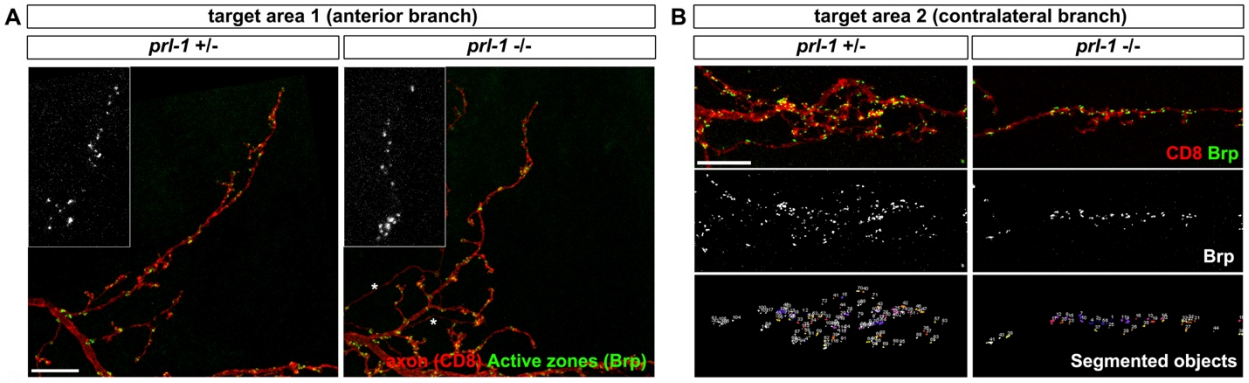

Figure S5. Estimation of presynaptic active zone numbers in anterior and contralateral branches, respectively. (**A**) Examples of the anterior projection of a DC neuron in a *prl-1* heterozygous and a homozygous null animal, respectively. Pre-synaptic active zones are stained with the marker Bruchpilot (Brp)^{short}.GFP (green), the axon is labelled with CD8.Cherry (red). Insets show a magnification on active zones of the distal branch segment. No differences are observed in appearance and distribution of active zones in the anterior branch. Asterisks indicate projections of another neuron (mechanosensory neuron innervating a small bristle on the central dorsal thorax). (**B**) Axon and pre-synaptic active zone labelling in the contralateral axon collateral (top and middle panels). Bottom panels show the result of segmentation of active zones using the 3D object counter plugin in Fiji / ImageJ (see Experimental Procedures). The counts of the segmented objects was used as the estimate of active zone numbers plotted in Fig. 1O,P. Active zone number is strongly reduced in the contralateral axon collateral in *prl-1* null animals. Scale bars: 10 µm.

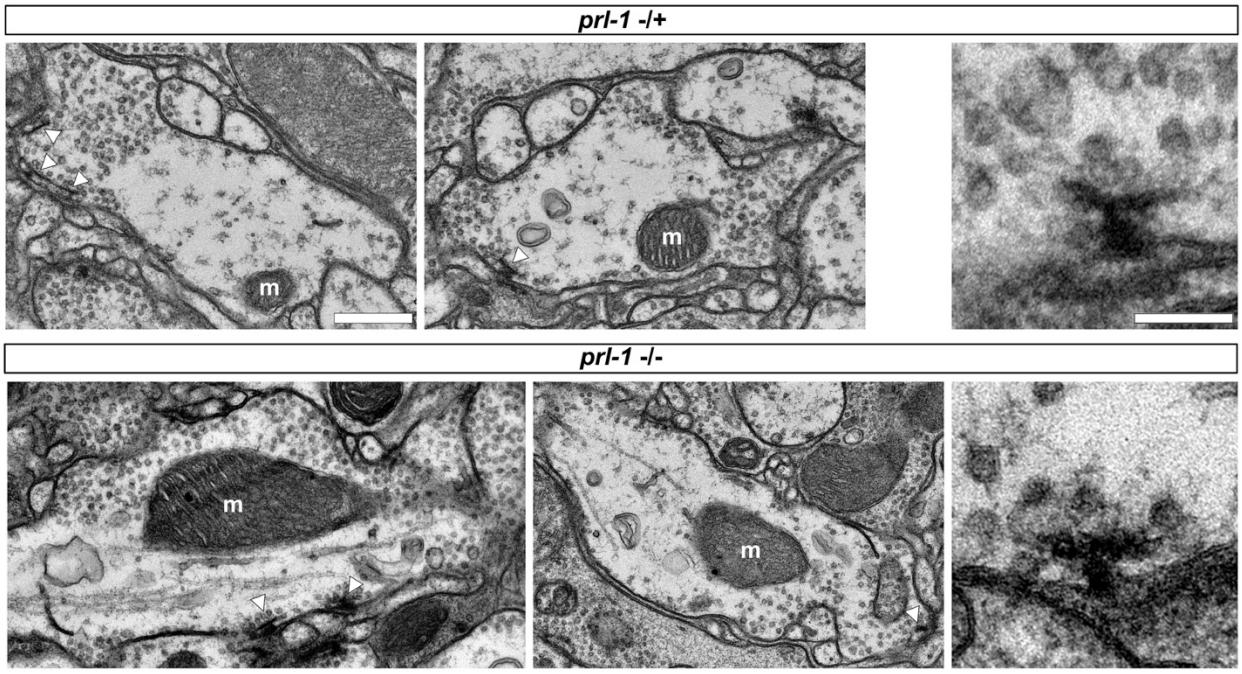

Figure S6. Ultrastructure of DC neuron active zones appears normal in *prl-1* null animals. Left and middle panels, overview transmission electron microscopy (TEM) images of cross-sections of the DC neuron axon contralateral branch. Individual DC neuron axons were labelled with the fluorescent marker CD8.Cherry and imaged with a confocal light microscope (not shown). At the same time, branding marks were introduced into the tissue by near-infrared branding (NIRB; (*14*, *57*)). The marks are recognizable after tissue processing for TEM and allow for identification and ultrastructural imaging of the DC neuron. Right panels show magnification of individual pre-synaptic active zones, with dense projections of characteristic shape ("T bars") and close-by synaptic vesicles. No striking differences are observed in the ultrastructure of synaptic components upon loss of *prl-1* (bottom panels). m, mitochondria. Scale bars: left panels, 500 nm; right panels, 125 nm.

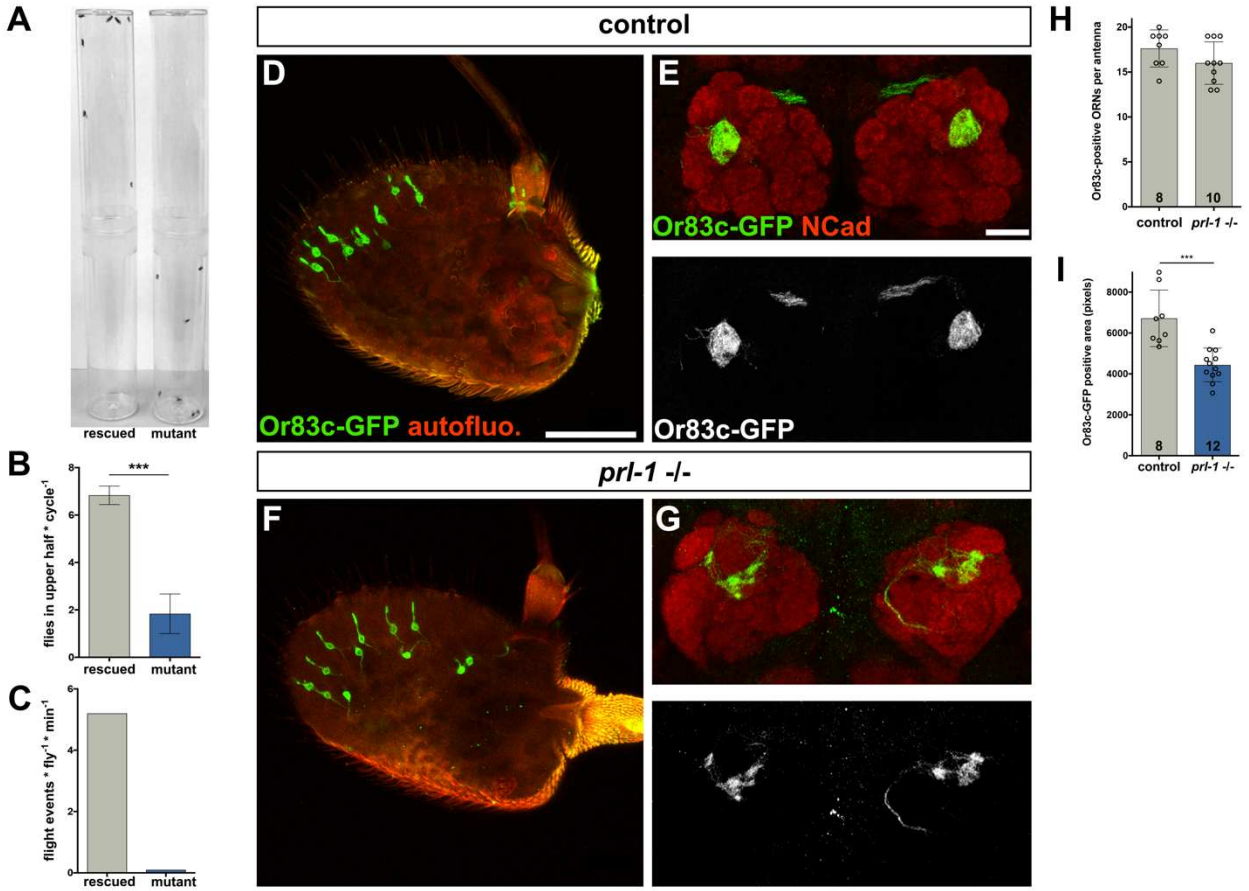

Figure S7. *prl-1* is broadly required for CNS development and function. (**A**) Example of a locomotor test setup with in each tube 7 female flies aged 7-10 days. Compared to *prl-1* hemizygous mutant flies rescued by a BAC transgene (left), non-rescued *prl-1* mutants tend to stay in the lower part of the test tube and have difficulties flying / climbing up the tube walls (right). See Movie S1. (**B**) Flies were tapped down every 30 sec and presence in the upper half of the test tube was quantified for each cycle. (**C**) Quantification of flight events in the same test setup. (**D-G**) GFP expressed in one class of odorant receptor neurons (ORNs) from an *or83c-gfp* transgene reveals defects in ORN targeting, but not cell numbers. D, F, visualization of ORN cell bodies in the antenna of control and *prl-1* null flies. E, control ORNs target to one specific glomerulus in the antennal lobe, and the target area appears homogenous in a maximum projection of a confocal microscopy image stack. G, ORN target area appears disrupted / less homogenous in *prl-1* mutants. (**H**) Numbers of ORN neurons (expressing or83c) are not reduced in *prl-1* null flies (P value 0.16 in a Mann-Whitney test). (**I**) Quantification of the target area of or83c ORNs in maximum intensity projections of control and *prl-1* null antennal lobes reveals a size reduction in the mutants (***, $p<0.001$, Mann-Whitney test). Scale bars: D, 50 µm; E, 20 µm.

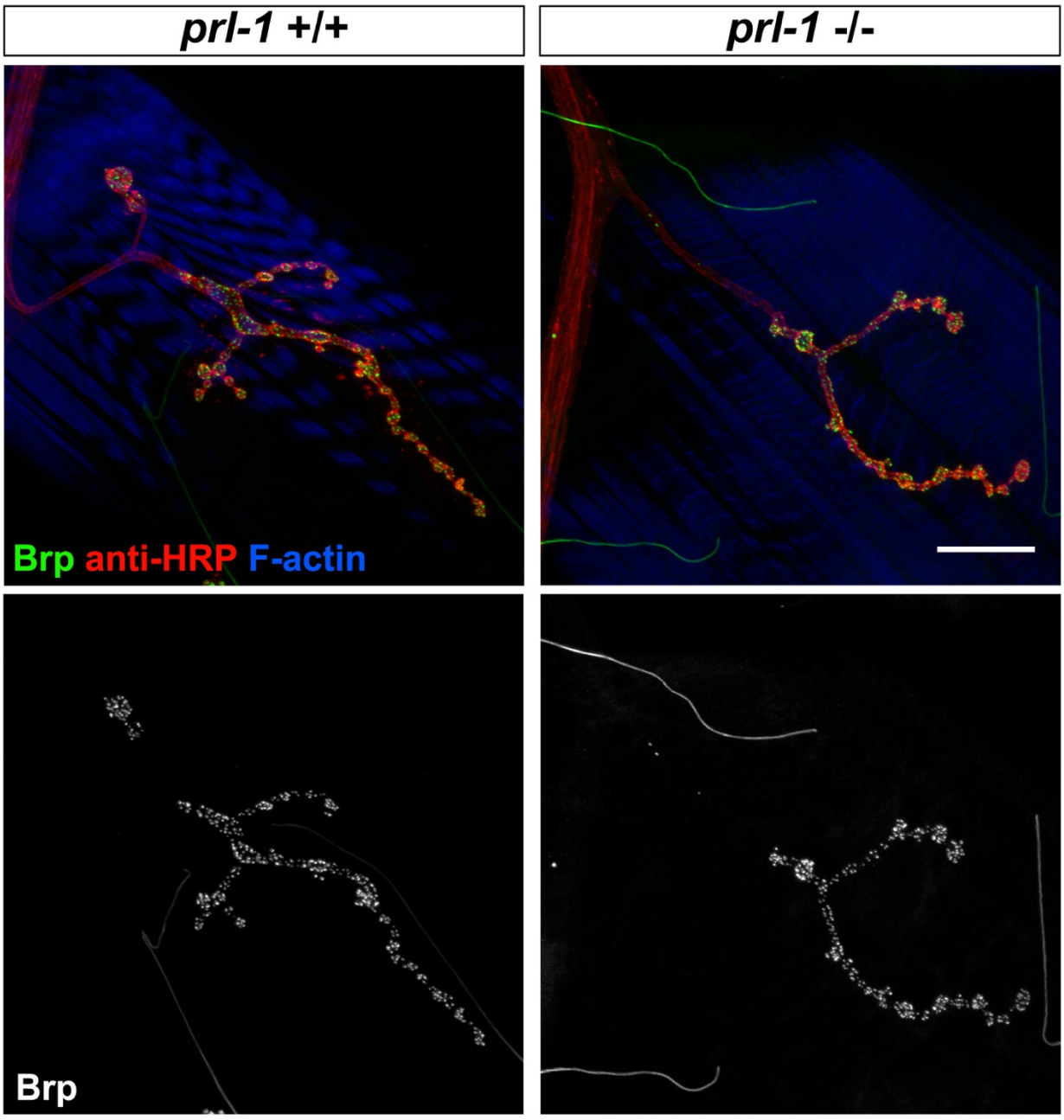

Figure S8. Neuromuscular junction (NMJ) morphology appears normal in *prl-1* null animals. NMJs of third-instar larvae were stained for the active zone component Bruchpilot (Brp, antibody nc82), anti-horseradish peroxidase (HRP), which labels the axon membrane, and F-actin (strongly visible in the post-synaptic muscle). Images show an example of an NMJ on muscle 4 in abdominal segment 4, each for wild-type and *prl-1* null animals. No gross morphology defects are observed upon loss of *prl-1*. Scale bar: 10 µm.

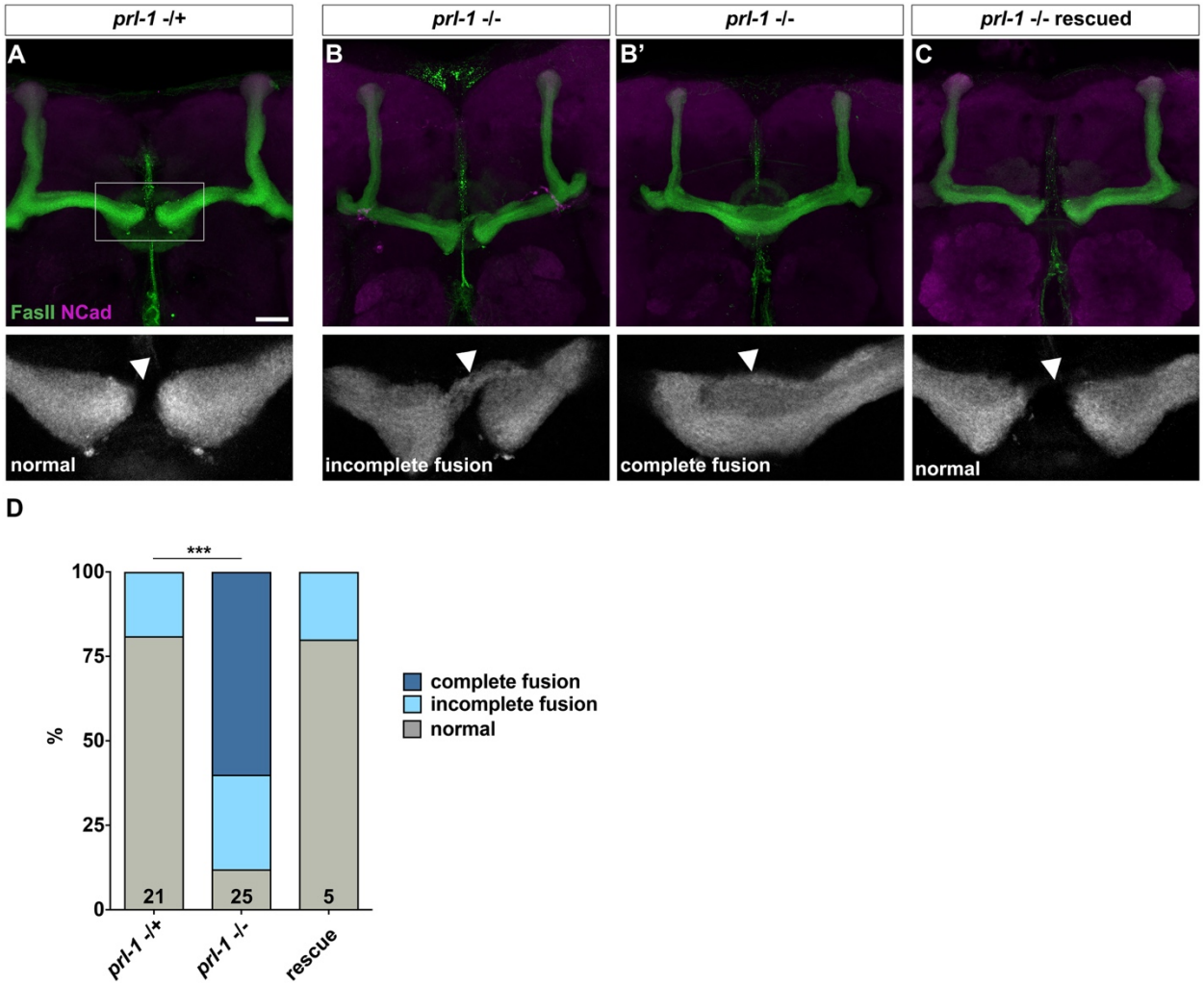

Figure S9. Mushroom body defects in *prl-1* null animals. (**A**) Brain of a control animal stained for Fasciclin II (FasII) and NCad. FasII staining prominently labels mushroom body axon projections. The mushroom body lobes that project centrally do not cross the midline (arrowhead in magnification panel). Scale bar: 20 µm. (**B**) Two examples of mushroom body axon defects in *prl-1* null animals, with midline crossing of some (B) or all (B') axons. (**C**) Example of a *prl-1* null animal rescued with a BAC transgene. (**D**) Quantification of mushroom body defects as exemplified in A-C. ***, $p<0.0001$, Chi-square test.

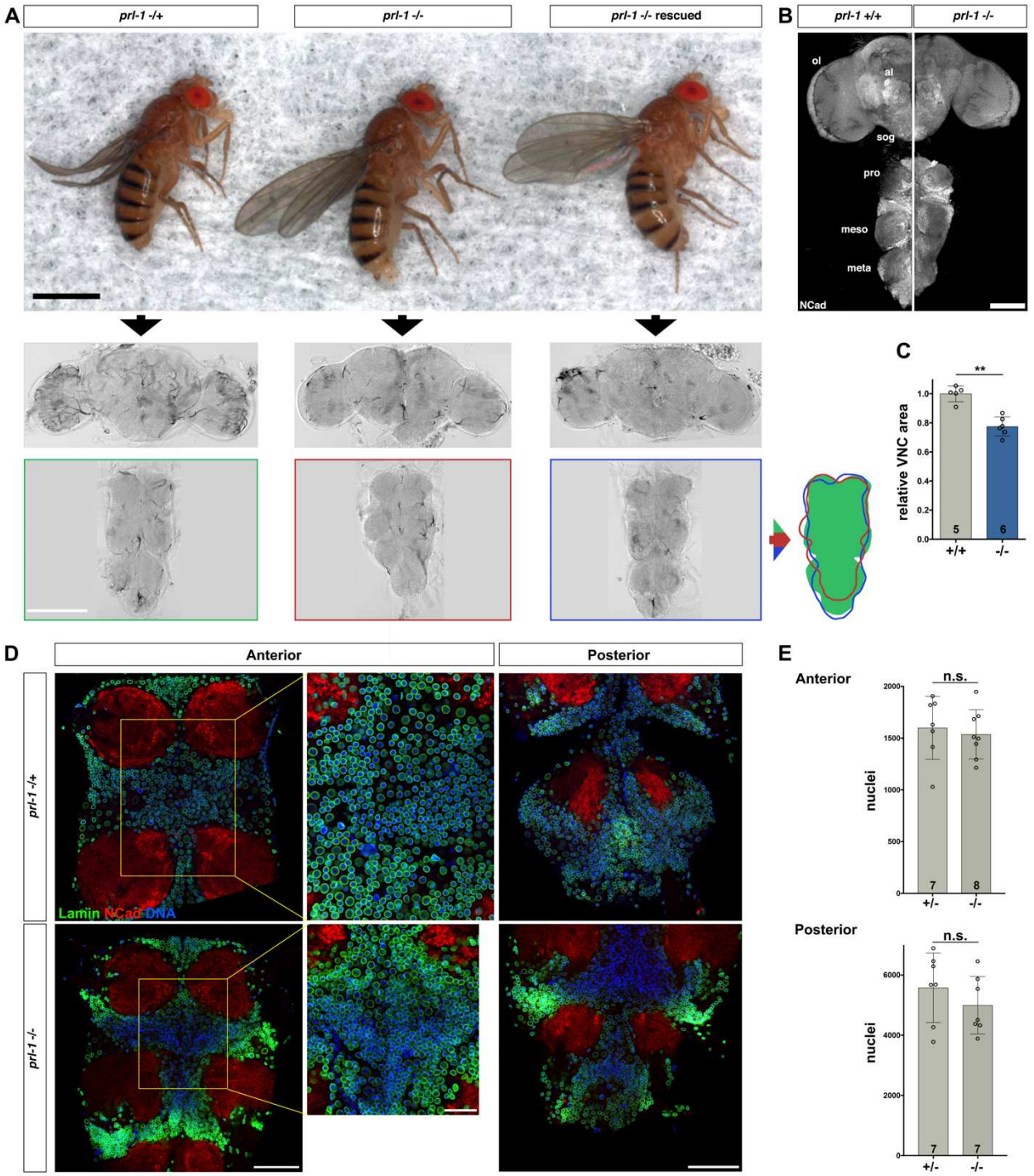

Figure S10. VNC neuropil size, but not cell numbers, is reduced upon loss of *prl-1*. (**A**) Adult flies (top) and their central nervous systems (brain and VNC; bottom) of the indicated genotypes. The *prl-1* null fly (middle) is of normal size, but particularly the VNC is smaller than in the heterozygous or the BAC-transgene rescued *prl-1* null fly. Cartoon on the right shows the outlines of the *prl-1* null VNC (red) and of the rescued VNC (blue) on top of the heterozygous VNC (green). (**B**) Side-to-side comparison of one half of a wild-type and of a *prl-1* null CNS, respectively. Note reduction in size of both brain and VNC neuropiles. (**C**) Quantification of the VNC area relative to controls, in maximum projections of confocal image stacks of VNCs

stained for NCad as in panel B. **, $p<0.005$, Mann-Whitney test. (**D**) Labelling of nuclear envelopes with anti-Lamin staining (green), DNA with DAPI stain (blue) and the neuropile with anti-NCad (red) allows estimation of cell numbers in different areas of the VNC. Examples show anterior and posterior VNC parts, respectively, of a heterozygous and of a homozygous *prl-1* null fly. Note that because the VNC size is reduced, nuclei appear more densely packed in the homozygous mutant (middle bottom panel). (**E**) Nuclei numbers were estimated with the 3D object counter plugin in Fiji / ImageJ (see Experimental Procedures). Despite a potential underestimation of nuclei numbers in the homozygous mutant samples due to dense packing, there are no significant differences between the genotypes (n.s.; unpaired t tests). Scale bars: A top, 1 mm; A bottom, 200 µm; B, 100 µm; D left and right, 50 µm; D center, 20 µm.

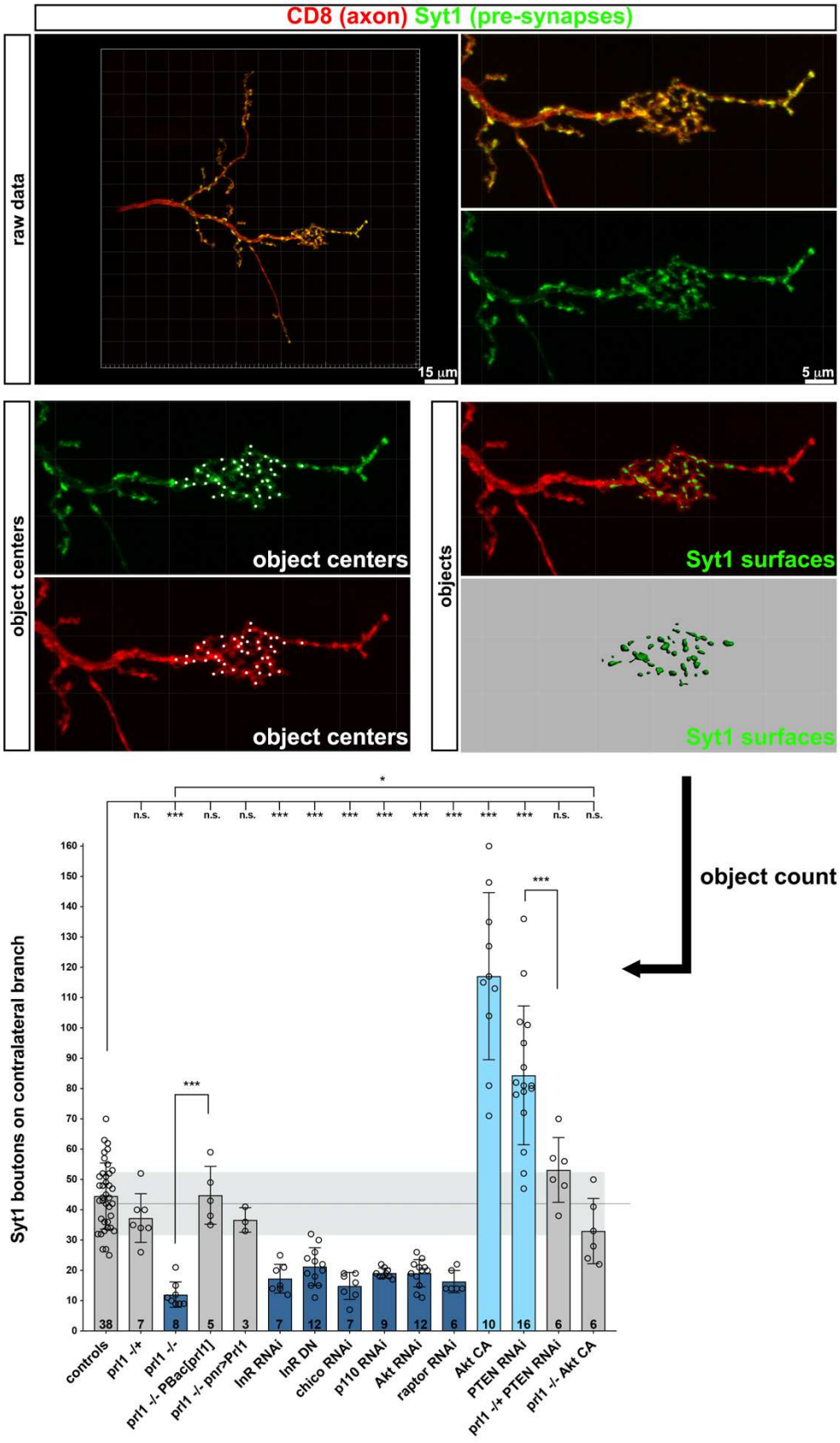
CD8 (axon) Syt1 (pre-synapses)
raw data
15 µm
5 µm
object centers
object centers
object centers
objects
Syt1 surfaces
Syt1 surfaces
object count
Syt1 boutons on contralateral branch
controls
prl1 -/+
prl1 -/-
prl1 -/- PBac[prl1]
prl1 -/- pnr>Prl1
InR RNAi
InR DN
chico RNAi
p110 RNAi
Akt RNAi
raptor RNAi
Akt CA
PTEN RNAi
prl1 -/+ PTEN RNAi
prl1 -/- Akt CA

Figure S11. Quantification of synaptic boutons based on Synaptotagmin1 (Syt1).Cherry marker expression. Top panels, example of a single mechanosensory neuron expressing CD8 axonal and Syt1 presynaptic markers, and magnification of the contralateral collateral. Middle panels, using Imaris software (Bitplane), boutons of Syt1 were reconstructed for the central part of the contralateral mechanosensory collateral, in the same region as terminal arbor complexity was quantified in Fig. 3D. Numbers of Syt1 boutons ("objects") are plotted in the bottom panel for the same genotypes as shown in Fig. 3D. n.s., non significant; *, $p<0.05$; ***, $p<0.001$, ordinary one-way Anova with multiple comparisons.

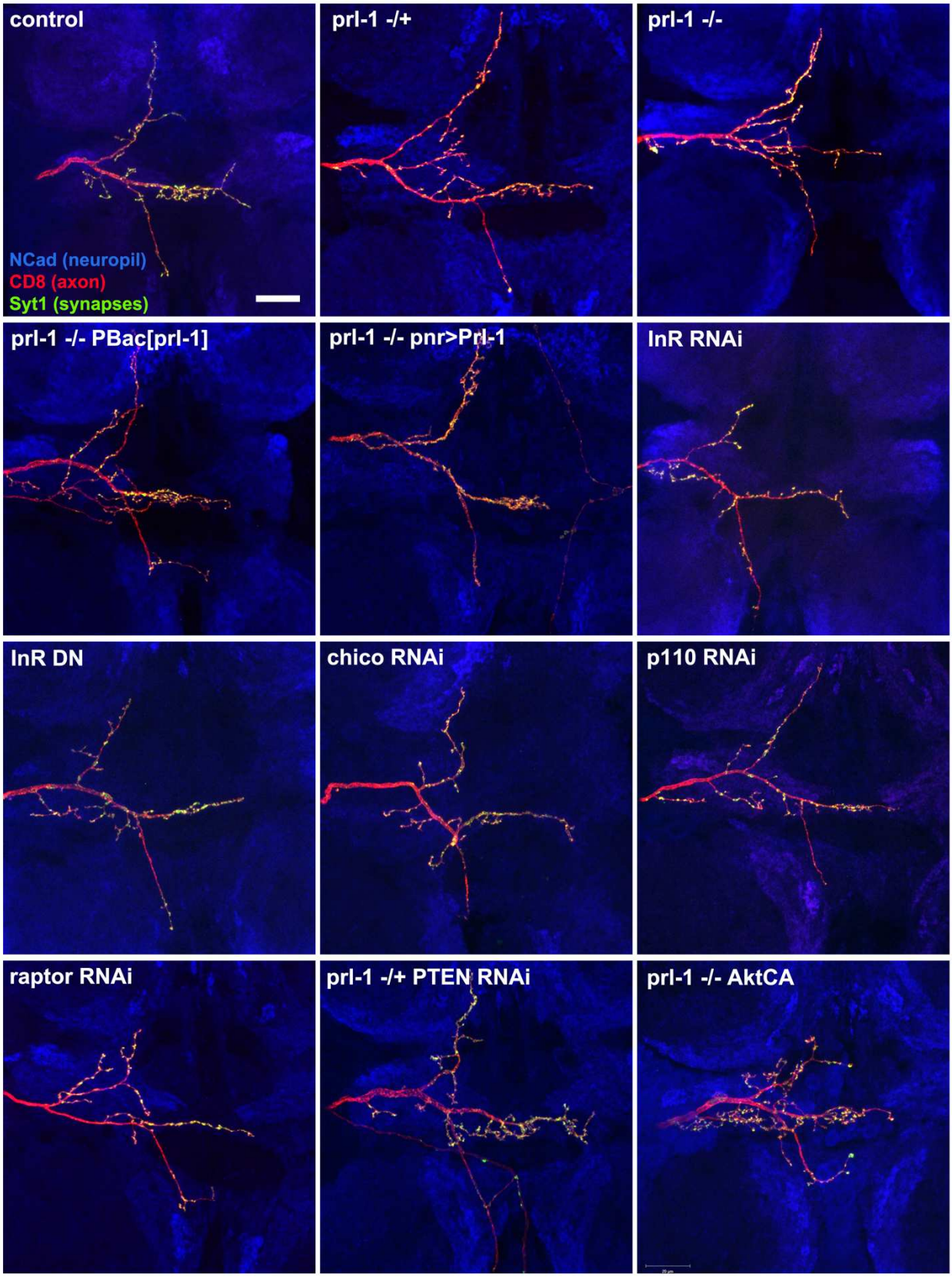

Figure S12. Full DC neuron projection patterns upon manipulation of the InR / Akt signaling

pathway. Genotypes correspond to the ones in Fig. 3. Note strong phenotypes in arborizations of the contralateral axon collateral, while the anterior and posterior branches, respectively, are all similar within a certain normal variability. Scale bar: 20 μm.

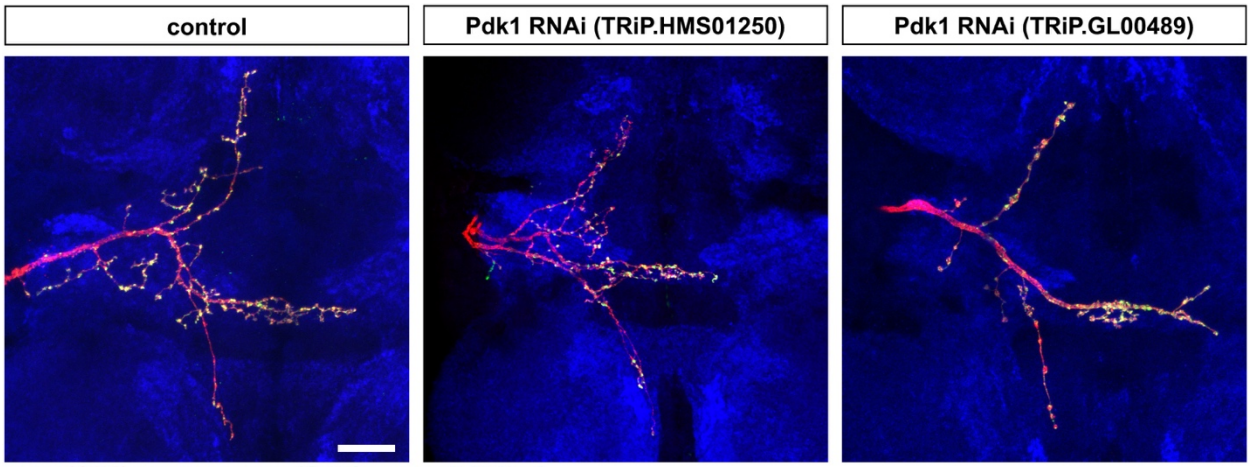

Figure S13. DC neuron projections are normal upon *pdk1* knockdown. Examples of *pdk1* knockdown in mechanosensory neurons, with two different RNAi lines (indicated in brackets), are shown. Projections appear normal, without changes in arborizations in the contralateral or other branches. Scale bar: 20 µm.

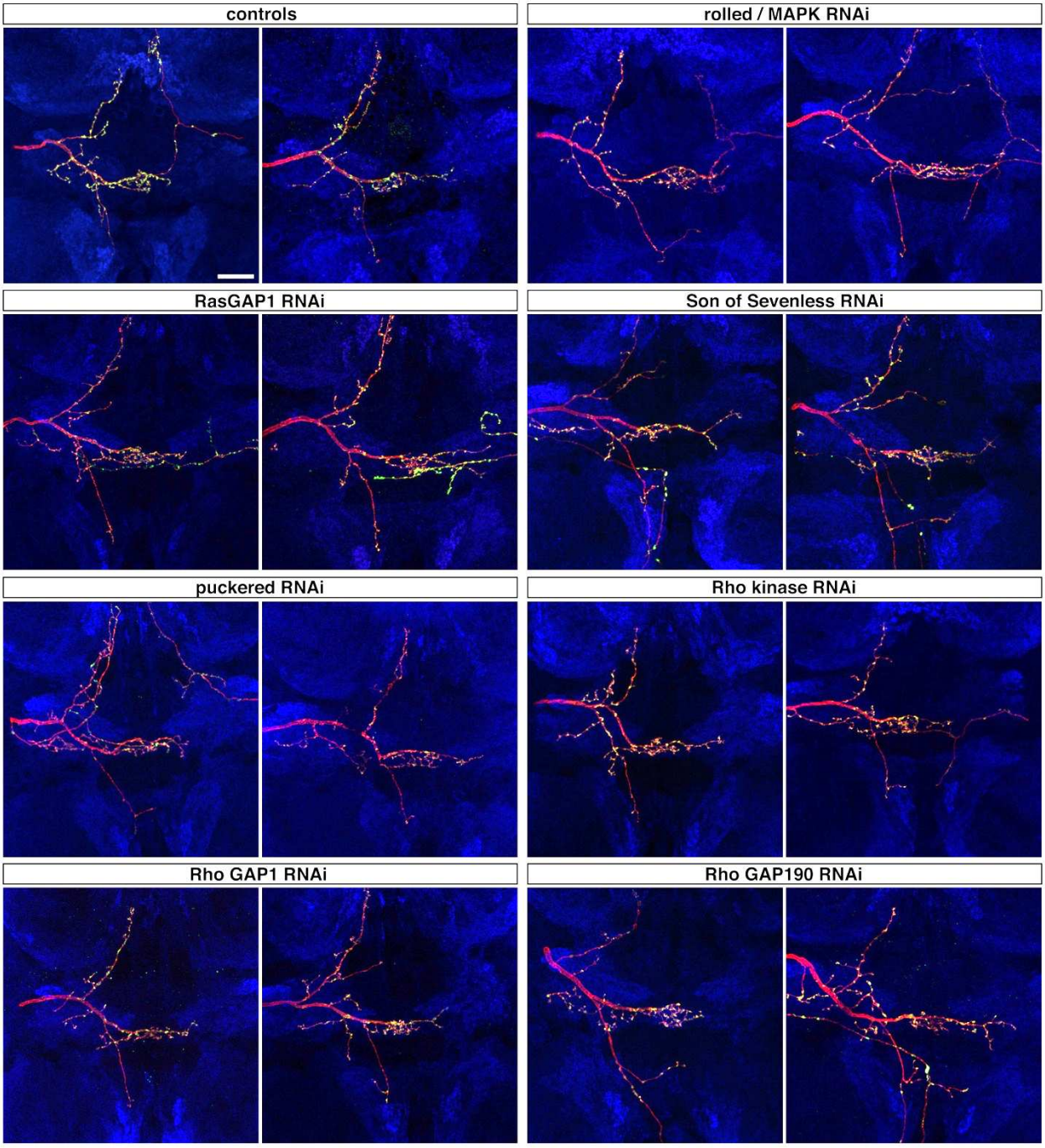

Figure S14. DC neuron projections appear normal upon knockdown of several suggested downstream Prl-1 protein targets. Two examples are shown for knockdown of each gene. No phenotype was observed in any of them. Scale bar: 20 μm.

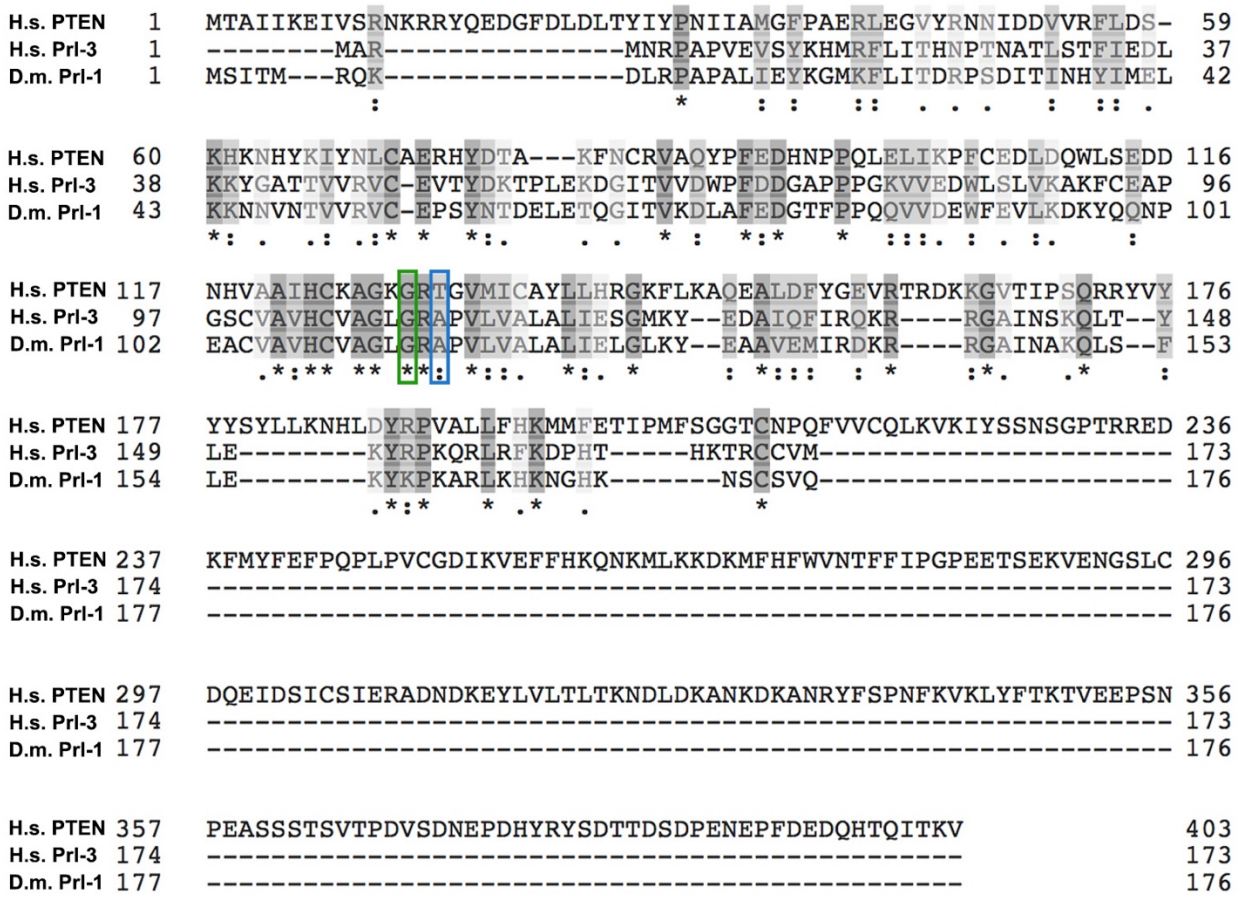

Figure S15. Amino acid alignment of *Drosophila* (D.m.) Prl-1 and human (H.s.) Prl-3 and PTEN proteins. Identical amino acids for all three proteins are indicated with asterisks, identities / similarities between some of the proteins with dots. The conserved glycine at position 114 of Prl-1 (green), and the alanine at position 116 of Prl-1 (blue) have been suggested to be essential for lipid phosphatase activity, but not for protein phosphatase activity, of human PTEN and Prl-3, respectively (*24*, *31*).

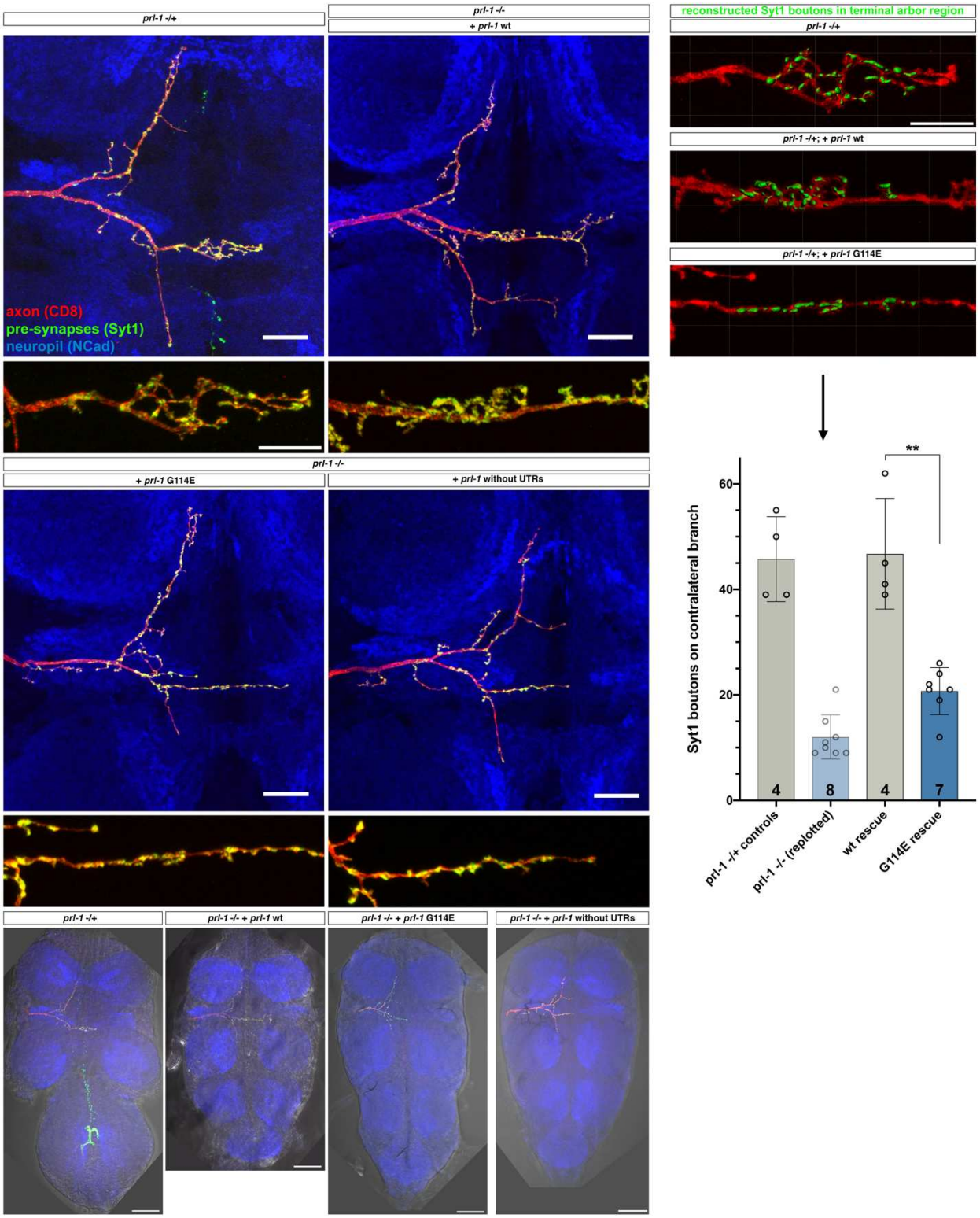

Figure S16. Full mechanosensory neuron projection patterns and Syt1 bouton quantification in *prl-1* null animals that express *prl-1* variants in mechanosensory neurons. Examples of the full DC neuron projection pattern are shown for each genotype. A magnification of the contralateral branch is also shown for one animal of each genotype. The whole VNC is shown in bottom panels, highlighting that in *prl-1* null flies, the DC neurons project into a smaller VNC. Only the

wild-type (wt) *prl-1* transgene expressed in mechanosensory neurons can rescue synaptic arborizations in the contralateral axon collateral. See text for details. Right panels, quantification of Syt1 boutons as in Fig. S11. Note that for the *prl-1* -/- genotype, the data from Fig. S11 is replotted. **, $p<0.01$; Mann-Whitney test. Scale bars: whole DC neuron projection panels, 20 μm; whole VNC panels, 50 μm; magnifications panels, 10 μm.

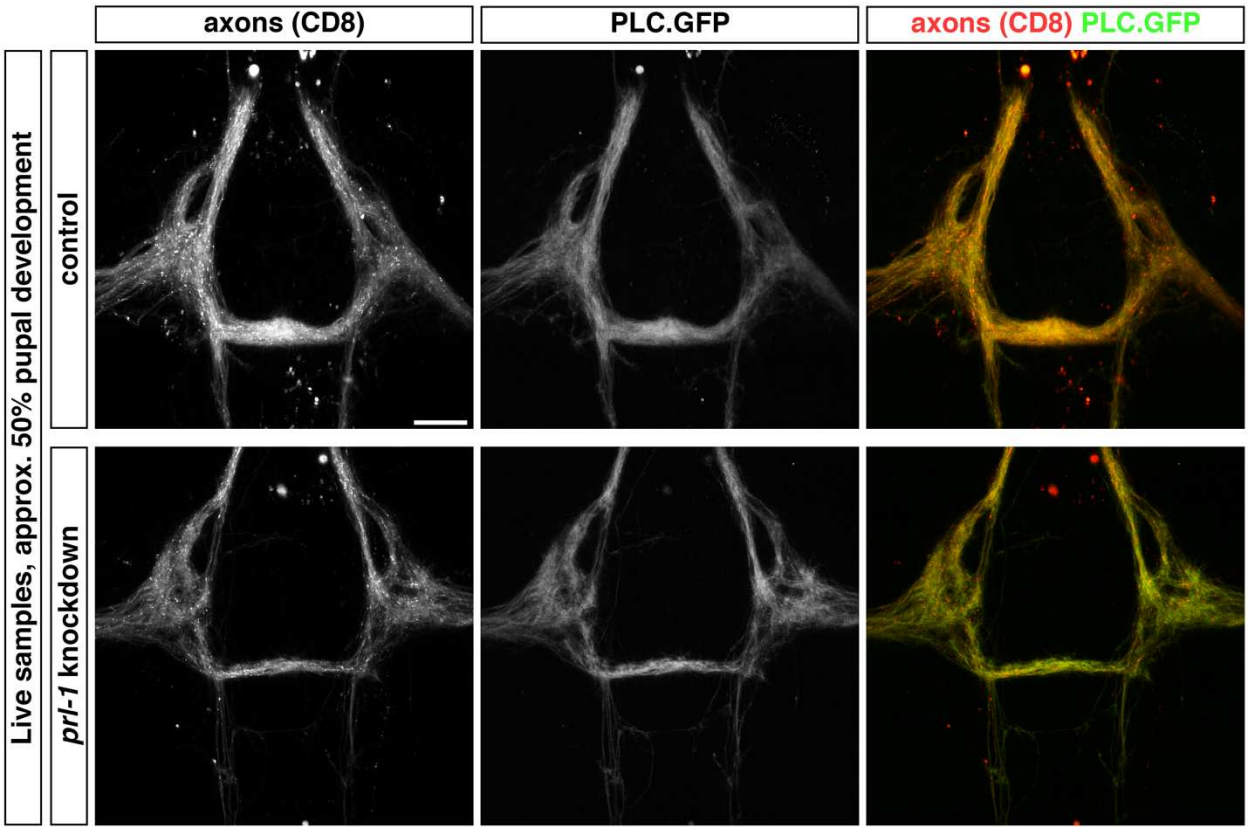

Figure S17. Localization of wild-type PLCδPH.GFP in a control and in an animal with knockdown of *prl-1* expression in mechanosensory neurons, at approximately 50% pupal development. CD8.Cherry axonal marker and PLCδPH.GFP, and in the bottom panels the RNAi construct targeting *prl-1*, were expressed in mechanosensory neurons innervating bristles of the central thorax with the *pnr-gal4* driver (see Fig. 6A). Ventral nerve cords were imaged without fixation. Scale bar, 20 µm.

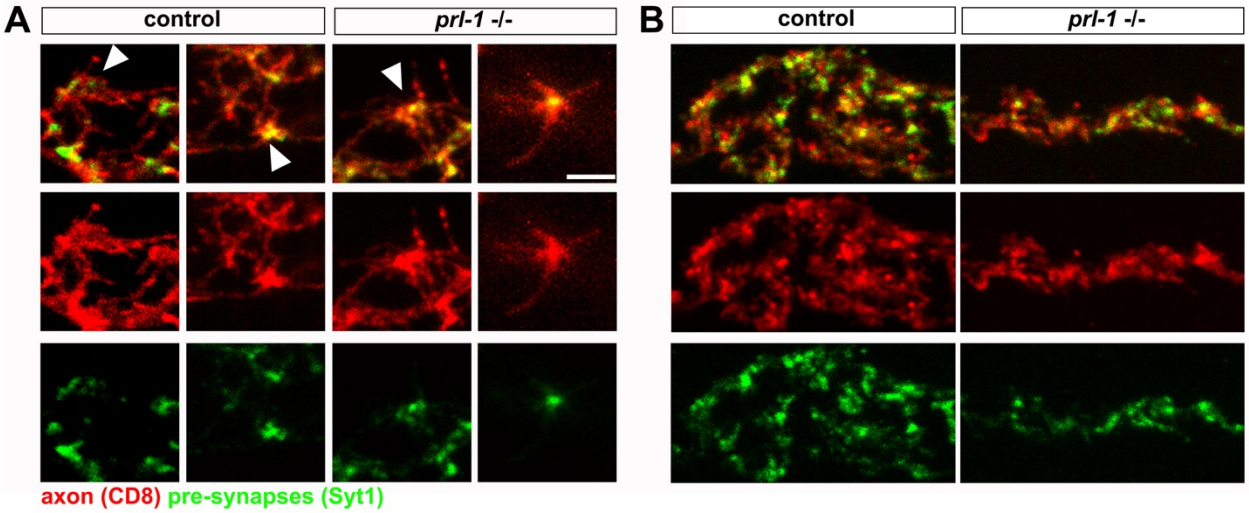

Figure S18. Filopodia, satellite growth cones and stabilized arborizations in developing DC neurons. (**A**) Examples of Cherry.Synaptotagmin1-containing satellite growth cones (arrowheads) in control and *prl-1* null animals at mid-stages of contralateral axon collateral development. (**B**) Morphology of stabilized contralateral axon collaterals at late stages of DC neuron development. Scale bar: 2.5 µm.

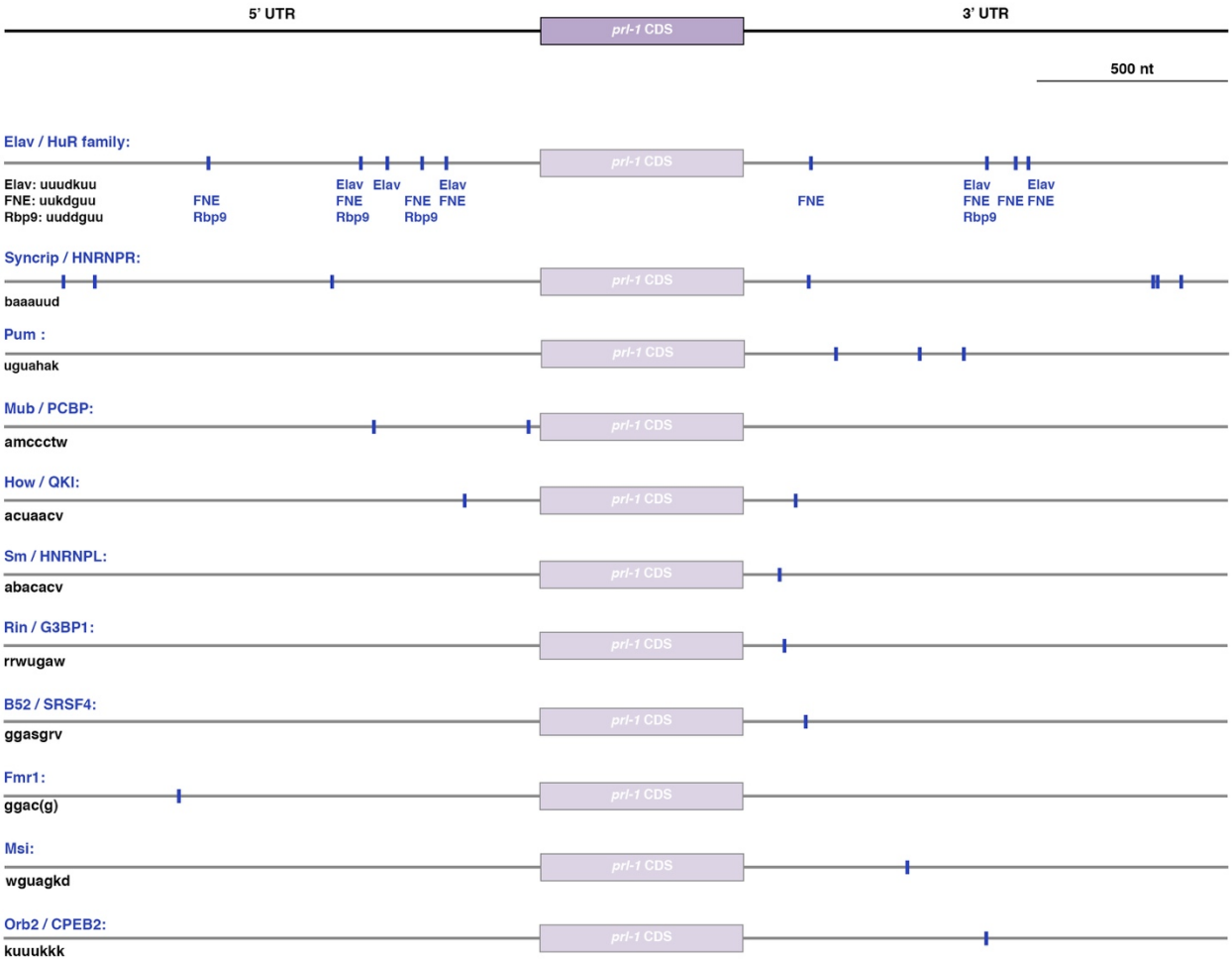

Figure S19. Predicted RNA binding proteins (RBP) binding motifs in the UTRs of the *prl-1* mRNA (isoform RB; flybase.org). The specific RBP is indicated in blue on the top left of each diagram of the *prl-1* mRNA. Consensus sequences for binding by the RBP are indicated by blue bars in the diagrams. The three members of the Elav family of RBPs are grouped into one diagram. Names of mammalian homologues of the RBPs are also indicated. The sequence consensus that was used for identifying motifs is indicated below each diagram. Where there is ambiguity for which nucleotide can be found at a particular position, following abbreviations are used: b, G or C or T; d, A or G or T; h, A or C or T; k, G or T; m, A or C; w, A or T; v, A or G or C; r, A or G; s, G or C. A non-optimal consensus sequence is shown for Fmr, with a G instead of an A at position 5. Motifs were searched for by a combination of the search tool RBPmap (http://rbpmap.technion.ac.il) and manual searching based on the consensus sequences provided in (*59*, *60*). CDS, coding sequence; nt, nucleotides.

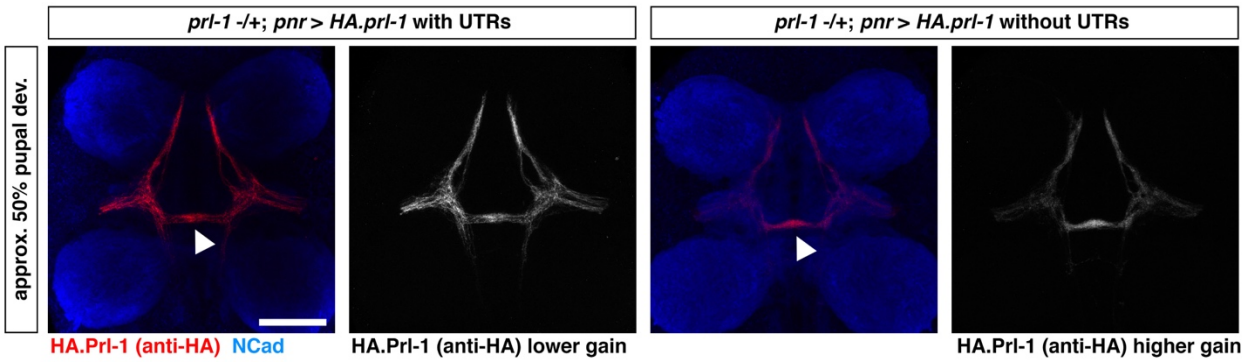

Figure S20. Tagged Prl-1 is enriched in the contralateral axon collateral of mechanosensory neurons during development. HA.Prl-1 was expressed from transgenes with and without UTRs, respectively, in all mechanosensory neurons innervating bristles in the central dorsal thorax (see Fig. 6A). Staining for the HA epitope was done in pupal VNCs at approximately 50% pupal development; note higher gain for imaging of HA.Prl-1 expressed from a transgene without UTRs (right). Particularly HA.Prl-1 expressed from the transgene without UTRs, which likely reflects distribution of endogenously expressed Prl-1 (see main text), is enriched in contralateral axon collaterals (arrowheads). Scale bar: 50 µm.

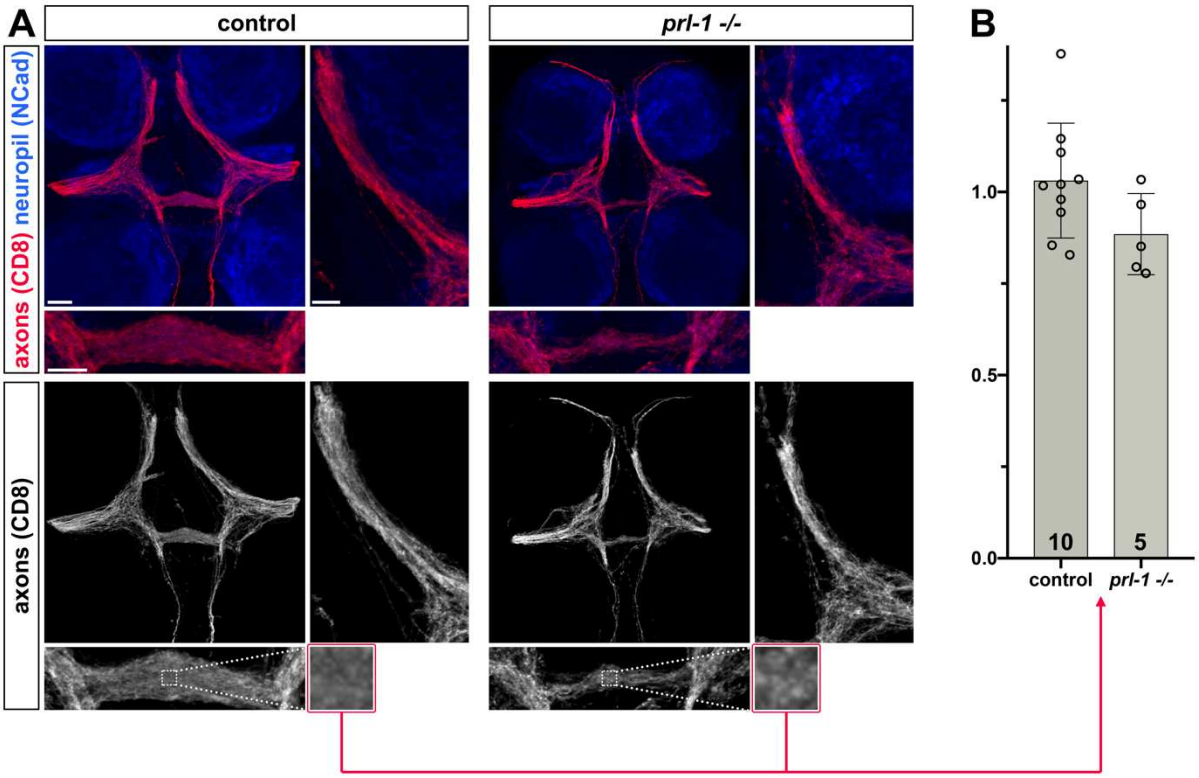

Figure S21. Localization of the general axon marker CD8.Cherry in mechanosensory neurons innervating bristles of the central thorax (see Fig. 6A). (**A**) CD8.Cherry is not enriched specifically in any axon collaterals, and reduction of contralateral collateral arbor complexity in *prl-1* null mutant animals (right panels) does not reduce CD8.Cherry signal significantly in these collaterals (see high magnification panel, analogous to high magnification panels in Fig. 6B). (**B**) Quantification of CD8.Cherry signal ratio between contralateral collaterals and anterior collaterals (analogous to Fig. 6C,D). Intensity density in regions of interest as shown in high magnification panels in A) was measured in Fiji software. Scale bars, 20 µm for low magnification panels, 10 µm for high magnification panels.

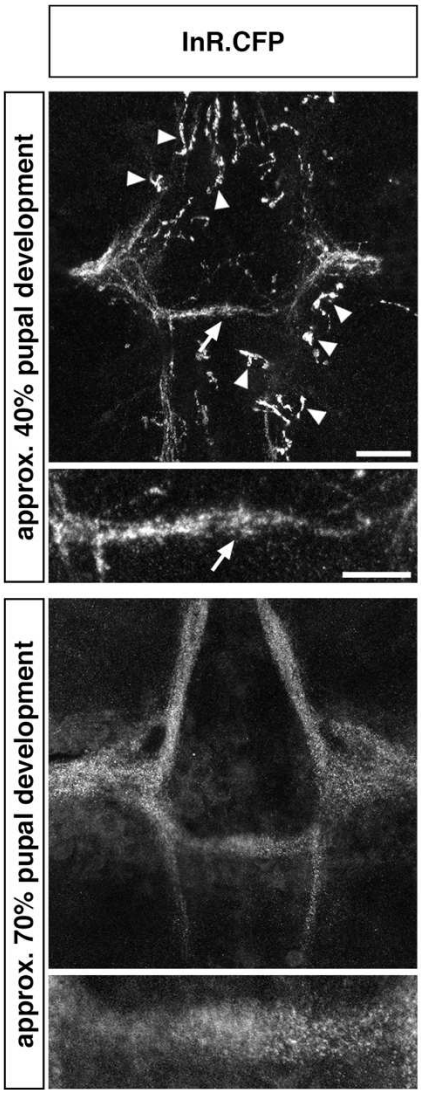

Figure S22. Localization of InR.CFP in mechanosensory neurons innervating bristles of the central thorax. InR.CFP was expressed using the *pnr-gal4* driver (see Fig. 6A), and its localization was assessed by immunostaining with an anti-GFP antibody at approximately 40% and 70% pupal development, respectively. Note unspecific expression of the InR.CFP construct in processes of other cells at the earlier stage (arrowheads). High magnification panels show the contralateral collateral projections. At 40% pupal development, InR.CFP is localized in the contralateral axon collateral of mechanosensory neurons (arrows). At later stages, InR.CFP appears distributed at similar levels across all collaterals (bottom panels). Scale bars, 20 µm for low magnification panels, 10 µm for high magnification panels.

Movie S1. Locomotor test with in each tube 7 female flies aged 7-10 days, see Fig. S7. Tube on the left contains *prl-1* null flies rescued with a *prl-1* BAC transgene, tube on the right contains *prl-1* null flies. Note that *prl-1* null flies do not fly, walk more slowly than rescued flies, frequently stay in the bottom of the tube, and have difficulties getting back to their legs when on the back. Note also the occasional held-up wing phenotype.

Table S1. List of all genotypes for all figure panels

Figure panel	Full genotype	References
1A-C	*w[*];* *+;* *+*	
1D	*y[*] w[*] / w[*];* *P{w[+mC] DC1.4-Flp} / +;* *p{w[+mC] UAS-FRT>STOP>FRT-CD8::GFP-2A-APEP-mCherry::Syt1}attp2 P{GawB}pnr^{MD237} /+*	(*14*) (*61*)
1E, I	*y[*] w[*];* *P{w[+mC] DC1.4-Flp} / P{KK108293}VIE-260B;* *p{w[+mC] UAS-FRT>STOP>FRT-CD8::GFP-2A-APEP-mCherry::Syt1}attp2 P{GawB}pnr^{MD237} / +*	(*15*)
1F, J	*w[*];* *P{w[+mC] DC1.4-Flp} prl-1[2] / prl-1[2];* *p{w[+mC] UAS-FRT>STOP>FRT-CD8::GFP-2A-APEP-mCherry::Syt1}attp2 P{GawB}pnr^{MD237} /+*	
1G, K	*w[*];* *P{w[+mC] DC1.4-Flp} prl-1[2] / prl-1[2];* *p{w[+mC] UAS-FRT>STOP>FRT-CD8::GFP-2A-APEP-mCherry::Syt1}attp2 P{GawB}pnr^{MD237} / P[acman]{w[+mC] prl-1}attP2*	
1O, P prl-1 -/+	*w[*] P{w[+mC] tub-FRT>Gal80>FRT} / w[*];* *prl-1[2 or 6] / CyO;* *P{w[+mC] DC1.4-Flp} P{GawB}pnr^{MD237} / P{UAS-Brp^{short}::GFP} P{UAS-CD8::Cherry}*	
1O, P prl-1 -/-	*w[*] P{w[+mC] tub-FRT>Gal80>FRT} / w[*];* *prl-1[2] / prl-1[6];* *P{w[+mC] DC1.4-Flp} P{GawB}pnr^{MD237} / P{UAS-Brp^{short}::GFP} P{UAS-CD8::Cherry}*	
1Q	*w[*] P{w[+mC] tub-FRT>Gal80>FRT} / Y;* *P{w[+mC] DC1.4-Flp} P{UAS-Brp^{short}::GFP} / +;* *P{GawB}pnr^{MD237} P{UAS-CD8::Cherry} / p{w[+mC] UAS-HA.prl-1^{noUTRs}}attP2*	(*62*) (*42*) F. Schnorrer, personal comm. to Flybase
2A, C, E	*w[*];* *+ / P{w[+mC] DC1.4-Flp};* *p{w[+mC] UAS-FRT>STOP>FRT-CD8::GFP-2A-APEP-mCherry::Syt1}attp2 P{GawB}pnr^{MD237} / +*	
2B, D, F	*w[*];* *P{w[+mC] UAS-Prl-1} / P{w[+mC] DC1.4-Flp};* *p{w[+mC] UAS-FRT>STOP>FRT-CD8::GFP-2A-APEP-mCherry::Syt1}attp2 P{GawB}pnr^{MD237} / +*	(*45*)
3 control	*w[*] / y w[*];* *+ / P{w[+mC] DC1.4-Flp};* *p{w[+mC] UAS-FRT>STOP>FRT-CD8::GFP-2A-APEP-mCherry::Syt1}attp2 P{GawB}pnr^{MD237} / +*	

3 Akt RNAi	*w[*] / y[1] v[1];* *+ / P{w[+mC] DC1.4-Flp};* *p{w[+mC] UAS-FRT>STOP>FRT-CD8::GFP-2A-APEP-mCherry::Syt1}attp2 P{GawB}pnr^{MD237} / P{y[+t7.7] v[+t1.8]=TRiP.HM04007}attP2*	(*63*)
3 PTEN RNAi	*w[*] / y[1] v[1];* *+ / P{w[+mC] DC1.4-Flp};* *p{w[+mC] UAS-FRT>STOP>FRT-CD8::GFP-2A-APEP-mCherry::Syt1}attp2 P{GawB}pnr^{MD237} / P{y[+t7.7] v[+t1.8]=TRiP.HMS00044}attP2*	
3 Akt CA	*w[*] / y[1] v[1];* *+ / P{w[+mC] DC1.4-Flp};* *p{w[+mC] UAS-FRT>STOP>FRT-CD8::GFP-2A-APEP-mCherry::Syt1}attp2 P{GawB}pnr^{MD237} / P{w[+mC]=UAS-myr-Akt1.V}3*	(*20*)
3 InR RNAi	*w[*] / y[1] v[1];* *P{y[+t7.7] v[+t1.8]=TRiP.HMS03166}attP40 / P{w[+mC] DC1.4-Flp};* *p{w[+mC] UAS-FRT>STOP>FRT-CD8::GFP-2A-APEP-mCherry::Syt1}attp2 P{GawB}pnr^{MD237} / +*	
3 InR dominant negative	*w[*] / y[1] v[1];* *+ / P{w[+mC] DC1.4-Flp};* *p{w[+mC] UAS-FRT>STOP>FRT-CD8::GFP-2A-APEP-mCherry::Syt1}attp2 P{GawB}pnr^{MD237} / P{w[+mC]=UAS-InR.K1409A}3*	A. Parks, personal comm. to Flybase
3 Chico RNAi	*w[*] / y[1] v[1];* *+ / P{w[+mC] DC1.4-Flp};* *p{w[+mC] UAS-FRT>STOP>FRT-CD8::GFP-2A-APEP-mCherry::Syt1}attp2 P{GawB}pnr^{MD237} / P{y[+t7.7] v[+t1.8]=TRiP.HMS01553}attP2*	
3 Pi3K RNAi	*w[*] / y[1] v[1];* *+ / P{w[+mC] DC1.4-Flp};* *p{w[+mC] UAS-FRT>STOP>FRT-CD8::GFP-2A-APEP-mCherry::Syt1}attp2 P{GawB}pnr^{MD237} / P{y[+t7.7] v[+t1.8]=TRiP.JF02770}attP2*	
3 Raptor RNAi	*w[*] / y[1] v[1];* *+ / P{w[+mC] DC1.4-Flp};* *p{w[+mC] UAS-FRT>STOP>FRT-CD8::GFP-2A-APEP-mCherry::Syt1}attp2 P{GawB}pnr^{MD237} / P{y[+t7.7] v[+t1.8]=TRiP.HMS00124}attP2*	
3 Prl-1 +/- PTEN RNAi	*w[*] / y[1] v[1];* *+ / P{w[+mC] DC1.4-Flp} prl-1[2];* *p{w[+mC] UAS-FRT>STOP>FRT-CD8::GFP-2A-APEP-mCherry::Syt1}attp2 P{GawB}pnr^{MD237} / P{y[+t7.7] v[+t1.8]=TRiP.HMS00044}attP2*	
3 Prl-1 -/-	*w[*];* *prl-1[2] / prl-1[2];* *p{w[+mC] UAS-FRT>STOP>FRT-CD8::GFP-2A-APEP-mCherry::Syt1}attp2 / P{GawB}pnr^{MD237} P{w[+mC] DC1.4-Flp};*	
3 Prl-1 -/- Akt CA	*w[*] / y[1] v[1];* *prl-1[2] / P{w[+mC] DC1.4-Flp} prl-1[2];* *p{w[+mC] UAS-FRT>STOP>FRT-CD8::GFP-2A-APEP-mCherry::Syt1}attp2 P{GawB}pnr^{MD237} / P{w[+mC]=UAS-myr-Akt1.V}3*	
3 Akt RNAi + CD8 OE	*w[*] / y[1] v[1];* *+ / P{UAS-CD8::Cherry};* *P{GawB}pnr^{MD237} / P{y[+t7.7] v[+t1.8]=TRiP.HM04007}attP2*	
3 Akt RNAi + Prl-1 OE	*w[*] / y[1] v[1];* *+ / P{w[+mC] UAS-Prl-1};* *P{GawB}pnr^{MD237} / P{y[+t7.7] v[+t1.8]=TRiP.HM04007}attP2*	(*45*)

4A, C control	*w[*];* *P{w[+mC] DC1.4-Flp};* *p{w[+mC] UAS-FRT>STOP>FRT-CD8::GFP-2A-APEP-mCherry::Syt1}attp2 P{GawB}pnr^{MD237} / TM6B Tb*	
4A prl-1 -/-	*w[*];* *prl-1[4] / prl-1[4];* *+*	
4A, C Sktl OE	*w[*] / P{w[+mC]=UAS-sktl.H}1, w[*];* *+ / P{w[+mC] DC1.4-Flp};* *p{w[+mC] UAS-FRT>STOP>FRT-CD8::GFP-2A-APEP-mCherry::Syt1}attp2 P{GawB}pnr^{MD237} / +*	(*29*)
4A Sktl OE + GFP OE	*w[*] / P{w[+mC]=UAS-sktl.H}1, w[*];* *P{w[+mC] DC1.4-Flp} P{UAS-Brp^{short}::GFP} / +;* *P{GawB}pnr^{MD237} P{UAS-CD8::Cherry} / +*	
4A, C Sktl OE + Prl-1 OE	*w[*] / P{w[+mC]=UAS-sktl.H}1, w[*];* *P{w[+mC] UAS-Prl-1} / +;* *P{GawB}pnr^{MD237} P{UAS-CD8::Cherry} / +*	(*45*)
4B control	*w[*] / y w;* *+ / P{w[+mC] DC1.4-Flp};* *p{w[+mC] UAS-FRT>STOP>FRT-CD8::GFP-2A-APEP-mCherry::Syt1}attp2 P{GawB}pnr^{MD237} / +*	
4B Sktl OE	*w[*] / P{w[+mC]=UAS-sktl.H}1, w[*];* *+ / P{w[+mC] DC1.4-Flp};* *p{w[+mC] UAS-FRT>STOP>FRT-CD8::GFP-2A-APEP-mCherry::Syt1}attp2 P{GawB}pnr^{MD237} / +*	
4D,E prl-1 -/+ control	*w[*];* *P{w[+mC] DC1.4-Flp} prl-1[2] / CyO;* *p{w[+mC] UAS-FRT>STOP>FRT-CD8::GFP-2A-APEP-mCherry::Syt1}attp2 P{GawB}pnr^{MD237} / TM2*	
4D,E prl-1 -/- + prl-1 [G114E]	*w[*];* *P{w[+mC] DC1.4-Flp} prl-1[2] / prl-1[2];* *p{w[+mC] UAS-FRT>STOP>FRT-CD8::GFP-2A-APEP-mCherry::Syt1}attp2 P{GawB}pnr^{MD237} / p{w[+mC] UAS-HA.prl-1[G114E]^{withUTRs}}attP2*	
4D, E prl-1 -/- + wt prl-1	*w[*];* *P{w[+mC] DC1.4-Flp} prl-1[2] / prl-1[2];* *p{w[+mC] UAS-FRT>STOP>FRT-CD8::GFP-2A-APEP-mCherry::Syt1}attp2 P{GawB}pnr^{MD237} / p{w[+mC] UAS-HA.prl-1[wt]^{withUTRs}}attP2*	
4F, G control	*w[*];* *prl-1[2] /CyO;* *P{GawB}pnr^{MD237} P{UAS-CD8::Cherry} / TM6*	
4F, G prl-1 -/-	*w[*];* *P{w[+mC] DC1.4-Flp} prl-1[2] / prl-1[6];* *P{GawB}pnr^{MD237} P{UAS-CD8::Cherry} / TM6*	

4F, G prl-1 -/- PLCδPH.GFP	*w[*];* *P{w[+mC] DC1.4-Flp} prl-1[2] / prl-1[6];* *P{GawB}pnr^{MD237} P{UAS-CD8::Cherry} / P{w+UAS-PLCδ-PH-EGFP}*	(*32*)
4F, G prl-1 -/- PLCδPH$^{[R40L]}$.GFP	*w[*];* *P{w[+mC] DC1.4-Flp} prl-1[2] / prl-1[6];* *P{GawB}pnr^{MD237} P{UAS-CD8::Cherry} / P{w+UAS-PLCδ-PH[R40L]-EGFP}*	
4H control	*w[*] P{w[+mC] tub-FRT>Gal80>FRT} / w[*];* *P{w[+mC] DC1.4-Flp} prl-1[2] / CyO;* *P{GawB}pnr^{MD237} P{UAS-CD8::Cherry} / P{w+UAS-PLCδ-PH-EGFP}*	
4H prl-1 -/-	*w[*] P{w[+mC] tub-FRT>Gal80>FRT} / w[*];* *P{w[+mC] DC1.4-Flp} prl-1[2] / prl-1[6];* *P{GawB}pnr^{MD237} P{UAS-CD8::Cherry} / TM2*	
4H prl-1 -/- PLCδPH.GFP	*w[*] P{w[+mC] tub-FRT>Gal80>FRT} / w[*];* *P{w[+mC] DC1.4-Flp} prl-1[2] / prl-1[6];* *P{GawB}pnr^{MD237} P{UAS-CD8::Cherry} / P{w+UAS-PLCδ-PH-EGFP}*	
4H prl-1 -/- PLCδPH$^{[R40L]}$.GFP	*w[*] P{w[+mC] tub-FRT>Gal80>FRT} / w[*];* *P{w[+mC] DC1.4-Flp} prl-1[2] / prl-1[6];* *P{GawB}pnr^{MD237} P{UAS-CD8::Cherry} / P{w+UAS-PLCδ-PH[R40L]-EGFP}*	
5 control	Either *prl-1* heterozygous mutant or +/+ animals were used as controls, with same results: *w[*];* *+ / prl-1[2];* *p{w[+mC] UAS-FRT>STOP>FRT-CD8::GFP-2A-APEP-mCherry::Syt1}attp2 / P{w[+mC] DC1.4-Flp} P{GawB}pnr^{MD237}* or *y[*] w[*] / w[*];* *P{w[+mC] DC1.4-Flp} / +;* *p{w[+mC] UAS-FRT>STOP>FRT-CD8::GFP-2A-APEP-mCherry::Syt1}attp2 P{GawB}pnr^{MD237} / +*	
5 prl-1 -/-	*w[*];* *prl-1[2] / prl-1[2];* *p{w[+mC] UAS-FRT>STOP>FRT-CD8::GFP-2A-APEP-mCherry::Syt1}attp2 / P{w[+mC] DC1.4-Flp} P{GawB}pnr^{MD237}*	
6B prl-1 -/+; pnr> HA.prl-1 with UTRs	*w[*];* *P{w[+mC] DC1.4-Flp} prl-1[2] / CyO;* *p{w[+mC] UAS-FRT>STOP>FRT-CD8::GFP-2A-APEP-mCherry::Syt1}attp2 P{GawB}pnr^{MD237} / p{w[+mC] UAS-HA.prl-1[wt]^{withUTRs}}attP2*	
6B prl-1 -/-; pnr> HA.prl-1 with UTRs	*w[*];* *P{w[+mC] DC1.4-Flp} prl-1[2] / prl-1[2];* *p{w[+mC] UAS-FRT>STOP>FRT-CD8::GFP-2A-APEP-mCherry::Syt1}attp2 P{GawB}pnr^{MD237} / p{w[+mC] UAS-HA.prl-1[wt]^{withUTRs}}attP2*	
6B prl-1 -/+; pnr> HA.prl-1 without UTRs	*w[*];* *P{w[+mC] DC1.4-Flp} prl-1[2] / CyO;* *p{w[+mC] UAS-FRT>STOP>FRT-CD8::GFP-2A-APEP-mCherry::Syt1}attp2 P{GawB}pnr^{MD237} / p{w[+mC] UAS-HA.prl-1[wt]^{noUTRs}}attP2*	

6B prl-1 -/-; pnr> HA.prl-1 without UTRs	*w[*];* *P{w[+mC] DC1.4-Flp} prl-1[2] / prl-1[2];* *p{w[+mC] UAS-FRT>STOP>FRT-CD8::GFP-2A-APEP-mCherry::Syt1}attp2 P{GawB}pnr^{MD237} / p{w[+mC] UAS-HA.prl-1[wt]^{noUTRs}}attP2*	
6F controls	*w[*];* *P{w[+mC] DC1.4-Flp};* *p{w[+mC] UAS-FRT>STOP>FRT-CD8::GFP-2A-APEP-mCherry::Syt1}attp2 P{GawB}pnr^{MD237} / TM6B Tb*	
6F wt rescue	*w[*];* *P{w[+mC] DC1.4-Flp} prl-1[2] / prl-1[2];* *p{w[+mC] UAS-FRT>STOP>FRT-CD8::GFP-2A-APEP-mCherry::Syt1}attp2 P{GawB}pnr^{MD237} / p{w[+mC] UAS-HA.prl-1[wt]^{withUTRs}}attP2*	
6F rescue no UTRs	*w[*];* *P{w[+mC] DC1.4-Flp} prl-1[2] / prl-1[2];* *p{w[+mC] UAS-FRT>STOP>FRT-CD8::GFP-2A-APEP-mCherry::Syt1}attp2 P{GawB}pnr^{MD237} / p{w[+mC] UAS-HA.prl-1[wt]^{noUTRs}}attP2*	
S1 C	prl-1 +/+: *y[*] w[*]* prl-1 -/+: *prl-1[2] / CyO* prl-1 -/-: *prl-1[2] / prl-1[2]*	
S1 D prl-1 -/-	*w[*] / +;* *prl-1[2] / Df(2L)r10;* *TM2 / +*	
S1 D prl-1 -/- rescued	*w[*] / +;* *prl-1[2] / Df(2L)r10;* *P[acman]{w[+mC] prl-1}attP2 / +*	
S1 D prl-1 -/+	*w[*] / +;* *prl-1[2] or Df(2L)r10 / CyO;* *TM2 / +*	
S1 D prl-1 -/+ “rescued”	*w[*] / +;* *prl-1[2] or Df(2L)r10 / CyO;* *P[acman]{w[+mC] prl-1}attP2 / +*	
S1 E prl-1 -/+	*w[*];* *Bl / prl-1[2];* *p{w[+mC] UAS-FRT>STOP>FRT-CD8::GFP-2A-APEP-mCherry::Syt1}attp2 / P{w[+mC] DC1.4-Flp} P{GawB}pnr^{MD237}*	
S1 E prl-1 -/-	*w[*];* *prl-1[2] / prl-1[2];* *p{w[+mC] UAS-FRT>STOP>FRT-CD8::GFP-2A-APEP-mCherry::Syt1}attp2 / P{w[+mC] DC1.4-Flp} P{GawB}pnr^{MD237}*	
S2 control	*y[*] w[*] / w[*];* *P{w[+mC] DC1.4-Flp} / +;* *p{w[+mC] UAS-FRT>STOP>FRT-CD8::GFP-2A-APEP-mCherry::Syt1}attp2 P{GawB}pnr^{MD237} /+*	

S2 Akt CA	*w[*] / y[1] v[1];* *+ / P{w[+mC] DC1.4-Flp};* *p{w[+mC] UAS-FRT>STOP>FRT-CD8::GFP-2A-APEP-mCherry::Syt1}attp2 P{GawB}pnr^{MD237} / P{w[+mC]=UAS-myr-Akt1.V}3*	
S3A,B control	*w[*] / +;* *prl-1[2] / Df(2L)r10;* *P[acman]{w[+mC] prl-1}attP2 / +*	
S3A, B prl-1 -/-	*w[*] / +;* *prl-1[2] / Df(2L)r10;* *TM2 / +*	
S3C control	*y[*] w[*] / w[*];* *P{w[+mC] DC1.4-Flp} / +;* *p{w[+mC] UAS-FRT>STOP>FRT-CD8::GFP-2A-APEP-mCherry::Syt1}attp2 P{GawB}pnr^{MD237} /+*	
S3C prl-1 RNAi	*y[*] w[*];* *P{w[+mC] DC1.4-Flp} / P{KK108293}VIE-260B;* *p{w[+mC] UAS-FRT>STOP>FRT-CD8::GFP-2A-APEP-mCherry::Syt1}attp2 P{GawB}pnr^{MD237} / +*	
S3C prl-1 -/-	*w[*];* *P{w[+mC] DC1.4-Flp} prl-1[2] / prl-1[2];* *p{w[+mC] UAS-FRT>STOP>FRT-CD8::GFP-2A-APEP-mCherry::Syt1}attp2 P{GawB}pnr^{MD237} /+*	
S4 prl-1 -/+	*w[*] / +;* *prl-1[2] or Df(2L)r10 / CyO;* *+*	
S4 prl-1 -/-	*w[*] / +;* *prl-1[2] / Df(2L)r10;* *+*	
S5 prl-1 +/-	*w[*] P{w[+mC] tub-FRT>Gal80>FRT} / w[*];* *prl-1[2 or 6] / CyO;* *P{w[+mC] DC1.4-Flp} P{GawB}pnr^{MD237} / P{UAS-Brp^{short}::GFP} P{UAS-CD8::Cherry}*	
S5 prl-1 -/-	*w[*] P{w[+mC] tub-FRT>Gal80>FRT} / w[*];* *prl-1[2] / prl-1[6];* *P{w[+mC] DC1.4-Flp} P{GawB}pnr^{MD237} / P{UAS-Brp^{short}::GFP} P{UAS-CD8::Cherry}*	
S6 prl-1 -/+	*w[*] P{w[+mC] tub-FRT>Gal80>FRT} / w[*];* *prl-1[2] or prl-1[4] / CyO;* *P{w[+mC] DC1.4-Flp} P{GawB}pnr^{MD237} / P{UAS-Brp^{short}::GFP} P{UAS-CD8::Cherry}*	
S6 prl-1 -/-	*w[*] P{w[+mC] tub-FRT>Gal80>FRT} / w[*];* *prl-1[2] / prl-1[4];* *P{w[+mC] DC1.4-Flp} P{GawB}pnr^{MD237} / P{UAS-Brp^{short}::GFP} P{UAS-CD8::Cherry}*	

S7A-C rescue	*w[*];* *prl-1[2] / Df(2L)r10;* *+ / P[acman]{w[+mC] prl-1}attP2*	
S7A-C mutant	*w[*];* *prl-1[2] / Df(2L)r10;* *+ / TM2*	
S7D-I, control	*w[*];* *prl-1[2] / CyO;* *Or83c-CD8::GFP / TM2*	(*44*)
S7D-I, prl-1 -/-	*w[*];* *prl-1[2] / prl-1[2];* *Or83c-CD8::GFP / TM2*	
S8 prl-1 +/+	*+;* *+;* *+ (CantonS)*	
S8 prl-1 -/-	*w;* *prl-1[2] / prl-1[2];* *+*	
S9A	*w[*];* *prl-1[2] / CyO;* *Or83c-CD8::GFP / TM2*	
S9B	*w[*];* *prl-1[2] / prl-1[2];* *Or83c-CD8::GFP / TM2*	
S9C	*w[*];* *prl-1[2] / prl-1[2];* *Or83c-CD8::GFP / P[acman]{w[+mC] prl-1}attP2*	
S10A prl-1 -/+	*w[*] / +;* *prl-1[2] or Df(2L)r10 / CyO;* + / TM2	
S10A prl-1 -/-	*w[*] / +;* *prl-1[2] / Df(2L)r10;* + / TM2	
S10A prl-1 -/- rescued	*w[*] / +;* *prl-1[2] / Df(2L)r10;* *+ / P[acman]{w[+mC] prl-1}attP2*	

S10B, C prl-1 +/+	*y[*] w[*];* *+;* *+*	
S10B, C prl-1 -/-	*w[*];* *prl-1[4] / prl-1[4];* *+*	
S10D, E prl-1 -/+	*w[*];* *prl-1[4] or prl-1[2] / CyO;* *+*	
S10D, E prl-1 -/-	*w[*];* *prl-1[4] / prl-1[2];* *+*	
S11 example (same as in Fig. 3A)	*w[*] / y w[*];* *+ / P{w[+mC] DC1.4-Flp};* *p{w[+mC] UAS-FRT>STOP>FRT-CD8::GFP-2A-APEP-mCherry::Syt1}attp2 P{GawB}pnr^{MD237} / +*	
S12 control	*y[*] w[*] / w[*];* *P{w[+mC] DC1.4-Flp} / +;* *p{w[+mC] UAS-FRT>STOP>FRT-CD8::GFP-2A-APEP-mCherry::Syt1}attp2 P{GawB}pnr^{MD237} /+*	
S12 prl-1 -/+	*w[*];* *+ / prl-1[2];* *p{w[+mC] UAS-FRT>STOP>FRT-CD8::GFP-2A-APEP-mCherry::Syt1}attp2 / P{w[+mC] DC1.4-Flp} P{GawB}pnr^{MD237}*	
S12 prl-1 -/-	*w[*];* *P{w[+mC] DC1.4-Flp} prl-1[2] / prl-1[2];* *p{w[+mC] UAS-FRT>STOP>FRT-CD8::GFP-2A-APEP-mCherry::Syt1}attp2 P{GawB}pnr^{MD237} /+*	
S12 prl-1 -/- PBAC[prl-1]	*w[*];* *P{w[+mC] DC1.4-Flp} prl-1[2] / prl-1[2];* *p{w[+mC] UAS-FRT>STOP>FRT-CD8::GFP-2A-APEP-mCherry::Syt1}attp2 P{GawB}pnr^{MD237} / P[acman]{w[+mC] prl-1}attP2*	
S12 prl-1 -/- pnr > Prl-1	*w[*];* *P{w[+mC] DC1.4-Flp} prl-1[2] / prl-1[4];* *p{w[+mC] UAS-FRT>STOP>FRT-CD8::GFP-2A-APEP-mCherry::Syt1}attp2 P{GawB}pnr^{MD237} / P{w[+mC] UAS-Prl-1}*	(*45*)
S12 InR RNAi	*w[*] / y[1] v[1];* *P{y[+t7.7] v[+t1.8]=TRiP.HMS03166}attP40 / P{w[+mC] DC1.4-Flp};* *p{w[+mC] UAS-FRT>STOP>FRT-CD8::GFP-2A-APEP-mCherry::Syt1}attp2 P{GawB}pnr^{MD237} / +*	
S12 InR DN	*w[*] / y[1] v[1];* *+ / P{w[+mC] DC1.4-Flp};* *p{w[+mC] UAS-FRT>STOP>FRT-CD8::GFP-2A-APEP-mCherry::Syt1}attp2 P{GawB}pnr^{MD237} / P{w[+mC]=UAS-InR.K1409A}3*	

S12 chico RNAi	*w[*] / y[1] v[1];* *+ / P{w[+mC] DC1.4-Flp};* *p{w[+mC] UAS-FRT>STOP>FRT-CD8::GFP-2A-APEP-mCherry::Syt1}attp2 P{GawB}pnr^{MD237} / P{y[+t7.7] v[+t1.8]=TRiP.HMS01553}attP2*	
S12 p110 RNAi	*w[*] / y[1] v[1];* *+ / P{w[+mC] DC1.4-Flp};* *p{w[+mC] UAS-FRT>STOP>FRT-CD8::GFP-2A-APEP-mCherry::Syt1}attp2 P{GawB}pnr^{MD237} / P{y[+t7.7] v[+t1.8]=TRiP.JF02770}attP2*	
S12 raptor RNAi	*w[*] / y[1] v[1];* *+ / P{w[+mC] DC1.4-Flp};* *p{w[+mC] UAS-FRT>STOP>FRT-CD8::GFP-2A-APEP-mCherry::Syt1}attp2 P{GawB}pnr^{MD237} / P{y[+t7.7] v[+t1.8]=TRiP.HMS00124}attP2*	
S12 prl-1 -/+ PTEN RNAi	*w[*] / y[1] v[1];* *+ / P{w[+mC] DC1.4-Flp} prl-1[2];* *p{w[+mC] UAS-FRT>STOP>FRT-CD8::GFP-2A-APEP-mCherry::Syt1}attp2 P{GawB}pnr^{MD237} / P{y[+t7.7] v[+t1.8]=TRiP.HMS00044}attP2*	
S12 prl-1 -/- AktCA	*w[*] / y[1] v[1];* *prl-1[2] / P{w[+mC] DC1.4-Flp} prl-1[2];* *p{w[+mC] UAS-FRT>STOP>FRT-CD8::GFP-2A-APEP-mCherry::Syt1}attp2 P{GawB}pnr^{MD237} / P{w[+mC]=UAS-myr-Akt1.V}3*	
S13 control	*y[*] w[*] / w[*];* *P{w[+mC] DC1.4-Flp} / +;* *p{w[+mC] UAS-FRT>STOP>FRT-CD8::GFP-2A-APEP-mCherry::Syt1}attp2 P{GawB}pnr^{MD237} /+*	
S13 Pdk1 RNAi (TRiP.HMS01250)	*w[*] / y[1] v[1];* *+ / P{w[+mC] DC1.4-Flp} prl-1[2];* *p{w[+mC] UAS-FRT>STOP>FRT-CD8::GFP-2A-APEP-mCherry::Syt1}attp2 P{GawB}pnr^{MD237} / P{y[+t7.7] v[+t1.8]=TRiP.HMS01250}attP2*	
S13 Pdk1 RNAi (TRiP.GL00489)	*w[*] / y[1] v[1];* *+ / P{w[+mC] DC1.4-Flp} prl-1[2];* *p{w[+mC] UAS-FRT>STOP>FRT-CD8::GFP-2A-APEP-mCherry::Syt1}attp2 P{GawB}pnr^{MD237} / P{y[+t7.7] v[+t1.8]=TRiP.GL00489}attP2*	
S14 controls	*y[*] w[*] / w[*];* *P{w[+mC] DC1.4-Flp} / +;* *p{w[+mC] UAS-FRT>STOP>FRT-CD8::GFP-2A-APEP-mCherry::Syt1}attp2 P{GawB}pnr^{MD237} /+*	
S14 rolled / MAPK RNAi	*w[*] / y[1] v[1];* *+ / P{w[+mC] DC1.4-Flp} prl-1[2];* *p{w[+mC] UAS-FRT>STOP>FRT-CD8::GFP-2A-APEP-mCherry::Syt1}attp2 P{GawB}pnr^{MD237}* / P{y[+t7.7] v[+t1.8]=TRiP.HMS00173}attP2	
S14 RasGAP1 RNAi	*w[*] / y[1] v[1];* *+ / P{w[+mC] DC1.4-Flp} prl-1[2];* *p{w[+mC] UAS-FRT>STOP>FRT-CD8::GFP-2A-APEP-mCherry::Syt1}attp2 P{GawB}pnr^{MD237}* / P{y[+t7.7] v[+t1.8]=TRiP.GL01258}attP2	
S14 Son of Sevenless RNAi	*w[*] / y[1] v[1];* *+ / P{w[+mC] DC1.4-Flp} prl-1[2];* *p{w[+mC] UAS-FRT>STOP>FRT-CD8::GFP-2A-APEP-mCherry::Syt1}attp2 P{GawB}pnr^{MD237}* / P{y[+t7.7] v[+t1.8]=TRiP.HMS00149}attP2	

S14 puckered RNAi	*w[*] / y[1] v[1];* *+ / P{w[+mC] DC1.4-Flp} prl-1[2];* *p{w[+mC] UAS-FRT>STOP>FRT-CD8::GFP-2A-APEP-mCherry::Syt1}attp2 P{GawB}pnr^{MD237}* / P{y[+t7.7] v[+t1.8]=TRiP.HMS01386}attP2	
S14 Rho kinase RNAi	*w[*] / y[1] v[1];* *+ / P{w[+mC] DC1.4-Flp} prl-1[2];* *p{w[+mC] UAS-FRT>STOP>FRT-CD8::GFP-2A-APEP-mCherry::Syt1}attp2 P{GawB}pnr^{MD237}* / P{y[+t7.7] v[+t1.8]=TRiP.HMS01311}attP2	
S14 Rho GAP1A RNAi	*w[*] / y[1] v[1];* *+ / P{w[+mC] DC1.4-Flp} prl-1[2];* *p{w[+mC] UAS-FRT>STOP>FRT-CD8::GFP-2A-APEP-mCherry::Syt1}attp2 P{GawB}pnr^{MD237}* / P{y[+t7.7] v[+t1.8]=TRiP.HMS00267}attP2	
S14 Rho GAP190 RNAi	*w[*] / y[1] v[1];* P{y[+t7.7] v[+t1.8]=TRiP.HMJ02052}attP40 / *P{w[+mC] DC1.4-Flp} prl-1[2];* *p{w[+mC] UAS-FRT>STOP>FRT-CD8::GFP-2A-APEP-mCherry::Syt1}attp2 P{GawB}pnr^{MD237} / +*	
S16 prl-1 -/+	*w[*];* *P{w[+mC] DC1.4-Flp} prl-1[2] / CyO;* *p{w[+mC] UAS-FRT>STOP>FRT-CD8::GFP-2A-APEP-mCherry::Syt1}attp2 P{GawB}pnr^{MD237} / TM2*	
S16 prl-1 -/- + wt	*w[*];* *P{w[+mC] DC1.4-Flp} prl-1[2] / prl-1[2];* *p{w[+mC] UAS-FRT>STOP>FRT-CD8::GFP-2A-APEP-mCherry::Syt1}attp2 P{GawB}pnr^{MD237} / p{w[+mC] UAS-HA.prl-1[wt]^{withUTRs}}attP2*	
S16 prl-1 -/- + prl-1 G114E	*w[*];* *P{w[+mC] DC1.4-Flp} prl-1[2] / prl-1[2];* *p{w[+mC] UAS-FRT>STOP>FRT-CD8::GFP-2A-APEP-mCherry::Syt1}attp2 P{GawB}pnr^{MD237} / p{w[+mC] UAS-HA.prl-1[G114E]^{withUTRs}}attP2*	
S16 prl-1 -/- + prl-1 without UTRs	*w[*];* *P{w[+mC] DC1.4-Flp} prl-1[2] / prl-1[2];* *p{w[+mC] UAS-FRT>STOP>FRT-CD8::GFP-2A-APEP-mCherry::Syt1}attp2 P{GawB}pnr^{MD237} / p{w[+mC] UAS-HA.prl-1[wt]^{noUTRs}}attP2*	
S17 control	*w[*];* *+ / +;* *P{UAS-CD8::Cherry} P{GawB}pnr^{MD237} / P{w+UAS-PLCδ-PH-EGFP}*	
S17 *prl-1* knock-down	*w[*];* *+ / +;* *P{TRiP.HMS01826}attP2 P{UAS-CD8::Cherry} P{GawB}pnr^{MD237} / P{w+UAS-PLCδ-PH-EGFP}*	
S18 control	Either *prl-1* heterozygous mutant or +/+ animals were used as controls, with same results: *w[*];* *+ / prl-1[2];* *p{w[+mC] UAS-FRT>STOP>FRT-CD8::GFP-2A-APEP-mCherry::Syt1}attp2 / P{w[+mC] DC1.4-Flp} P{GawB}pnr^{MD237}* or *y[*] w[*] / w[*];* *P{w[+mC] DC1.4-Flp} / +;* *p{w[+mC] UAS-FRT>STOP>FRT-CD8::GFP-2A-APEP-mCherry::Syt1}attp2 P{GawB}pnr^{MD237} / +*	